

FINAL TECHNICAL REPORT

Project Title: Development of a Process to Continuously Melt, Refine, and Cast High Quality Steel

Award Number: DE-FC36-03ID14279

Project Period: May 1, 2003 – April 30, 2006

Date of Report: July 28, 2006

Principal Investigators: Kent D. Peaslee, 573-341-4714, kpeaslee@umr.edu
Von L. Richards, David G.C. Robertson and Jeffrey D. Smith

Recipient: University of Missouri – Rolla
Department of Materials Science & Engineering
218 McNutt Hall, 1870 Miner Circle
Rolla, MO 65409-0340

Subcontractors: University of Illinois at Urbana-Champaign
Department of Mechanical and Industrial Engineering
140 Mechanical Engineering Building, MC-244, 1206 West Green Street
Urbana, IL 61801
Point of Contract: Brian Thomas, 217-333-6919, bgthomas@uiuc.edu

Other Partners: Bayou Steel, Nucor Steel, Nucor-Yamato Steel, SMI-Steel, TXI-Chaparral, Gerdau Ameristeel, Core Furnace Systems, Proware-Metsim, Heraeus Electronite

Acknowledgment, Disclaimer and Proprietary Data Notice

Acknowledgement:

This report is based upon work supported by the U. S. Department of Energy under Award No. DE-FC36-03ID14279.

Disclaimer:

Any findings, opinions, and conclusions or recommendations expressed in this report are those of the authors and do not necessarily reflect the views of the Department of Energy.

Table of Contents

<u>Report Section</u>	<u>Page</u>
Executive Summary	1
Introduction and Background	2
Critical Literature Review of Continuous Steelmaking	4
Historic developments in continuous steelmaking research	5
Conclusions from the Literature	13
Use of Experimental and Theoretical Methods to Investigate Mixing in Gas Stirred Reactors	14
Experimental Procedure – Ladle Metallurgy Industrial Trials	14
Development of Computational Model	17
Development of Ferroalloy Model	20
Discussion of Ladle Metallurgy Experimental and Modeling Results	22
Ferroalloy Melting and Mixing	23
Summary of Findings from Gas-Stirred Reactor Mixing Studies	27
Use of Computational Fluid Dynamics to Simulate Continuous Steelmaking Vessels	28
Experimental Technique – Mathematical Formulations and Computational Conditions	28
Results – Fluid Flow and Particle Motions – No Argon Injection	31
Results – Fluid Flow and Particle Motions – With Argon Injection	32
Summary of Results from CFD Modeling of Continuous Steelmaking Vessels	40
Experimental Study of Steel Treatment to Model Continuous Steelmaking Kinetics	41
Experimental Procedure – Industrial Trials	41
Experimental Procedure – Metsim Thermodynamic and Kinetic Modeling	41
Discussion of Experimental Data and Simulation Results	44
Correlation Between the Mass Transfer Rate Constant and the Specific Stirring Power	47
Specific Steel Transport Rate	49
Thermodynamic Factors that Affect Reaction Rates	50
Apparent Reaction Order	52
Decarburization of the Steel During Argon Purging	53
Summary of Findings -Experimental Study of Reaction Kinetics in Industrial Reactors	55
Design of Novel, Scrap-Based, Fully Continuous Steelmaking Process	56
Description of Modified Consteel EAF (vessel 1)	58
Description of Oxidizer (vessel 2)	59
Description of Reducer (vessel 3)	61
Description of Finisher (vessel 4)	61
Steady State Operation of the Continuous Steelmaking Process	62
Procedure for Grade Changes	63
Procedure for Start-up	64

Table of Contents (continued)

<u>Report Section</u>	<u>Page</u>
Procedure for Shut Down	64
Simulation of Steady-state Operation	65
Steady-state Simulations of Upset Conditions	67
Summary of Continuous Steelmaking Process Design and Simulation Results	68
Accomplishments	70
Milestones and Tasks	70
Publications and Patents	71
Education of Students for the Steel Industry	72
Conclusions	73
References	74

Executive Summary

The purpose of this project was to conduct research and development targeted at developing a design for a steel making process that will revolutionize the way steel is made in the 21st century. The process to be developed was to be less capital and energy intensive to both build and maintain, significantly more productive, safer, environmentally friendly and cost effective to operate, and able to produce higher quality steel faster than traditional batch processes. The research was to investigate and design the delivery of high quality steel from scrap to the casting mold in one continuous process.

Historically, steel has always been made by batch processing which has a number of disadvantages including high labor requirements, major energy losses, production limitations based on heat size, inconsistency in quality between heats, difficulty in automation, environmental problems, yield losses, and safety. Continuous steelmaking will result in use of energy more efficiently, lower production costs, less environmental impacts, safer production, and better, more consistent quality than present processes. Major benefits will result from eliminating the need to transport steel between vessels using crude open-air tapping, tipping, and transport cranes.

Many different continuous steelmaking processes have been proposed over the last 40 years. Some of these processes have even reached the stage of a pilot plant, yet no process has reached full commercialization. There are numerous reasons for the previous failures. In particular, all of the previous processes used hot metal which makes it necessary to remove larger amounts of carbon, phosphorus, and sulfur. The proposed process is scrap-based improving the probability of success. In addition, much of the research in the past was done in the 1960's and 1970's, prior to the development of the process simulation, sensors, advanced refractories, slide gates, automation and control tools available today. Some previous continuous steelmaking processes used an insufficient number of vessels with conflicting functions that could not be achieved simultaneously. The current design clearly defines a reasonable function for each vessel, (each of which has been achieved in conventional batch processes) resulting in a new process much easier to operate and optimize.

The research was successful in developing a fully continuous steelmaking process allowing for continuous steel treatment in a process in which the steel never stops flowing from the time it is molten until it solidifies at the continuous caster. The new continuous steelmaking process design incorporates three continuous refining vessels that connect a Consteel® EAF with the tundish of the continuous caster. The steel treatment in the three refining vessels supports the EAF and tundish operations and replaces batch LMF refining. Details of the research have been summarized in a series of papers published at international steelmaking conferences and in steelmaking journals culminating in a provisional patent, "Process to Continuously Melt, Refine, and Cast High-Quality Steel," filed with the US Patent office on May 6, 2005. The provisional patent number was 60/678,833. The final patent application was filed on May 5, 2006. Commercialization is in the beginning stages.

The computer modeling and industrial research resulted in the conclusion that the new process will save 70 kWhr/t in energy from traditional steelmaking processes. These savings and a 4% yield increase as well as improved refining and increased efficiency could lead to a \$20/t cost reduction as compared to current EAF-LMF operations. The capital cost for the new process is estimated to be \$35 million for equipment producing one million tons of steel per year. The estimated payback period is 1.8 years, corresponding to a rate of return on investment of 57%.

Introduction and Background

The purpose of this project was to conduct a revolutionary research and development program targeted at developing a design for a steel making process that would revolutionize the way steel is made in the 21st century. The process is designed to require less capital to build, less energy to operate, and increases productivity while operating safer and more environmentally friendly than current steelmaking processes. This research was successful in designing a process for the delivery of high quality steel from scrap to the casting mold in one continuous process.

Today, steel is made by batch processing which results in a number of inherent technical problems and barriers that are improved by the continuous steelmaking process developed at UMR. Current batch steel operations result in energy losses, reduced alloy recoveries, yield losses, and quality problems associated with the transfer operations and batch processing. Batch processing limits the steel processed to specific heat sizes, results in inconsistent quality between different heats, and is difficult to automate because it is dynamic and not operating at steady state. In addition, batch processing requires a large labor force to operate and maintain the individual furnaces, vessels and cranes. During continuous steelmaking, metal is continuously fed and extracted from each vessel resulting in lower energy losses, improved alloy recovery and metallic yield, and higher and more consistent quality during operation. This allows the process to operate near chemical equilibrium and provides for much easier automation and control of the process with less labor and maintenance. In addition, major benefits will result from eliminating the need to transport steel between vessels using open-air tapping, tipping, and transport cranes.

This project used a combination of computer simulation and modeling, laboratory experiments, and industrial data and trials to develop the necessary details on the design and operation of the new continuous steelmaking process leading to eventual commercialization of the process. Project participants include representatives from two universities, several scrap-based steel makers, and engineering/equipment manufacturer. The university team members, four professors at UMR and one professor at UIUC) along with graduate and undergraduate students conducted the research at the laboratories of the two universities. Core Furnace Technologies, a major steel equipment designer and manufacturer helped provide engineering and equipment support for design and cost of installations. The participating steel companies (Nucor-Yamato Steel, Nuco, TXI-Chaparral Steel, SMI, Ameristeel, Bayou Steel, and TAMCO Steel) provided a team of operators and engineers with the necessary operating and cost data to keep the research focused and relevant to the industry. In addition, these partners allowed the researchers to do several trials at their plants to validate the modeling results. Two partners (Gerdau Ameristeel-Knoxville and Nucor-Hertford) operate Consteel furnaces and provided necessary design and operating data for a continuous operation based on semi-continuous operations. Computer modeling of batch LMF operations were validated by laboratory and industrial trials at two Nucor locations which helped lead to the improved understanding of ladle metallurgy required to model the design and operation of continuous steelmaking. These industrial trials helped provide validation of the computer simulation and modeling. By combining the theoretical and experimental capabilities of University of Missouri-Rolla and University of Illinois-Champaign Urbana with the engineering, technical and practical operating experience of the participating steel mills and engineering/equipment manufacturers, a realistic continuous steelmaking design with excellent prospects for commercialization was completed.

The new design continuously melts, refines, alloys and casts steel by continuously transporting liquid metal through four vessels. In the first vessel (melter), preheated scrap is continuously charged and melted. The melting is primarily accomplished through electrical energy but is supplemented with chemical energy which also accomplishes preliminary dephosphorization. The second vessel (oxidizer) continuously decarburizes and dephosphorizes the steel before discharging low carbon and low phosphorus steel to the third vessel. In the third vessel (reducer), steel is continuously deoxidized,

desulfurized and bulk alloyed to produce a generic semi-finished high quality liquid steel which continuously flows into the final vessel (finisher) where final alloying and inclusion flotation occurs before the steel is continuously discharged into the tundish of a continuous caster.

Energy is saved by eliminating the ladle metallurgy furnace, reducing the energy needed for auxiliary operations, increasing the yield, and reducing the tap temperature. A total of 10% energy savings is anticipated over current EAF operations. No electrical power will be required for the LMF (saving 30 kWhr/t) and yield will increase by 4% (saving 10 kWhr/t) in addition to 20 kWhr/t saving in auxiliary energy. However, these savings will only occur once the plant has been operating at full capacity and all start-up problems have been resolved which will take an estimated 3 years to resolve. The new continuous steelmaking designed to produce 1,000,000 tons per year can be built for an estimated 30% less capital than a traditional melt shop (\$35 million versus \$50 million) and will save 15% in operational costs (\$20 per ton) due to increased yield, 10% lower energy requirements and other associated cost savings.

Critical Literature Review of Continuous Steelmaking

Modern melt shops produce hundreds of thousands of tons of semi-finished steel year-around, in specialized reactors, and at high production rates. In principle, greater profits should be achieved with a continuous process as compared with a batch process under these types of manufacturing conditions.¹⁻⁴ Not surprisingly, the economic advantage of continuous steel production has provided the motivation to pursue new processes ever since the industrial revolution when steel started to be manufactured in large quantities.

Approximately 80 continuous steelmaking processes have been proposed since the mid 1800's. These different processes can be separated into seven categories based on the general type of process and the time period of their development as summarized in Table I. Many of the processes evolved from the predominant steelmaking processes of their time such as modified Open Hearth Furnaces in Period one, oxygen-based processes during the third and fourth period, and scrap-based processes of the fifth and seventh period.

Table I: Periods of continuous steelmaking research

Period	Title	Time	# of proc.
1	Continuous Open Hearth Furnaces	1860's – 1930's	3
2	Development of fundamental designs and principles	1930's – 50's	9
3	Experimental research on non-equilibrium CSTR's*	1950's – 60's	7
4	Experimental research on PFR's*	1960's – 70's	17
5	Experimental research on scrap-based processes	1970's – 80's	20
6	Hot metal refining including equilibrium CSTR's*	1980's – 90's	17
7	Scrap-based processes and commercialization	1990's – 2000's	7

* CSTR's are Completely Stirred Tank Reactors and PFR's are Plug Flow Reactors.

The term “continuous steelmaking” has been used for different types of operation over the years. The array of definitions includes operations that:

1. semi-continuously charge hot metal or scrap and deslag while *periodically tapping steel into ladles* [first: Siemens⁵ (1860's), last: CRISP/Hatch⁶ (2000's)];
2. continuously utilize vessels or systems of vessels while *continuously tapping steel into ladles* [first: Dobrokhoto⁷ (1930's), last: VAI concept⁸ (1990's)]; and
3. fully continuously process and transport steel from a smelting or melting unit, through refining units, to the mold of the continuous caster *without interrupting the flow of steel* [first: Elliott⁹ (1950's), last: Royzman¹⁰ (1980's)].

Although processes that fit any of these definitions are considered in this report, only the last definition describes a fully continuous production in which raw materials (scrap or ore) are continuously fed to the process and completely refined and alloyed steel continuously exits the process into the continuous caster. Only four concepts were proposed that used a fully continuous steelmaking design.

Continuous Reactors and Their General Performance

Reactors for continuously treating liquid steel can be categorized into two types, the ideal Completely Stirred Tank Reactor (CSTR) or the ideal Plug Flow Reactor (PFR). These reactors are theoretical models of real, operational reactors for limiting conditions. Simplified illustrations of a PFR, a CSTR, and their equivalent batch operations are shown in Figure 1.

The composition of slag and steel and the concentration gradient between them change along the channel in a PFR with concurrent flow. The concentration gradient can be kept at a large value throughout the PFR if the steel and slag flow counter-currently to each other. Similar to the PFR with concurrent flow, the composition and the concentration gradient change in batch reactors (ladle, BOF, EAF); however, in these reactors the changes are over time rather than position. In contrast, the composition and the concentration gradient in a CSTR and in its equivalent semi-continuous reactor stay constant during the entire operation, assuming constant composition and flow of the input. Usually, corrective actions have immediate results during the operation of a CSTR, its semi-continuous equivalent reactor, and during batch operations because these reactors are well mixed. As a result, it is possible to accurately control these three types of reactors. Corrective actions have delayed results in the PFR, reducing the degree of control in this reactor.

There are limitations for chemical conversions (defined as the change in concentration of a specific component) in PFR's and CSTR's. In general, the conversion is limited by backmixing in the PFR and by kinetics in the CSTR. Szekely¹² showed that conversion could only be increased in the CSTR for a given kinetics situation if the residence time of the steel is increased, which is only possible by increasing the size of the reactor or decreasing the throughput. In the PFR, backmixing must be reduced to increase conversion. Necessary changes to the PFR would either increase the heat loss, capital expenses and/or the complexity of this reactor, making it less attractive. Szekely¹² concluded that the best solution would be a series of CSTR's, which would provide necessary control and high overall chemical conversion at required production rates.

Historic developments of continuous steelmaking research

Eighty historic continuous steelmaking processes are listed and grouped in Table II. The processes were sorted according to their time (period) of introduction, the starting material (hot metal or scrap), the extent of research (proposed or tested in pilot plant or similar industrial setting), the principal reactor type (CSTR or PFR), and the major characteristic of the process. Developments during each of these periods will be discussed in the following sections.

Period 1: Continuous Open Hearth Furnaces (1860's – 1930's)

The idea of continuous steelmaking was developed during this period. Researchers realized that continuous steelmaking had the potential to decrease the cost of steelmaking. It was believed that modification of the then-new Open Hearth Furnace (OHF) technology could create a furnace for continuous steelmaking. Figure 2 shows a schematic of a modified OHF. Siemens⁵ pioneered the idea of continuous steelmaking and designed the first furnace that continuously produced steel in the 1860's. He modified a small Siemens-Martin furnace (OHF) to make steel directly from high-grade ore. The bath was continuously decarburized while the generated CO was used to continuously prereduce the ore. The ore descended through a shaft and fell into the bath during the operation of the furnace that was periodically tapped.

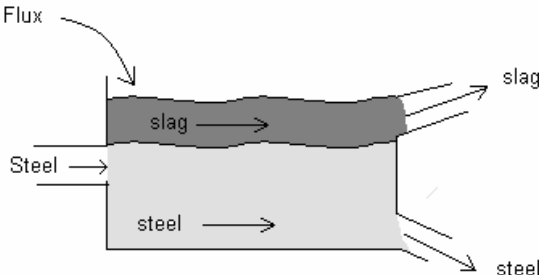
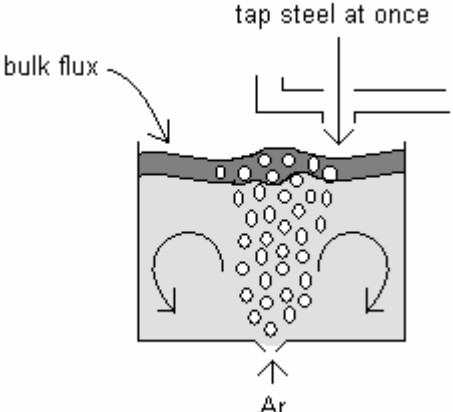
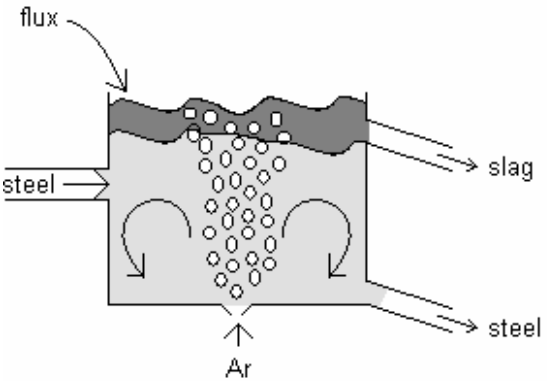
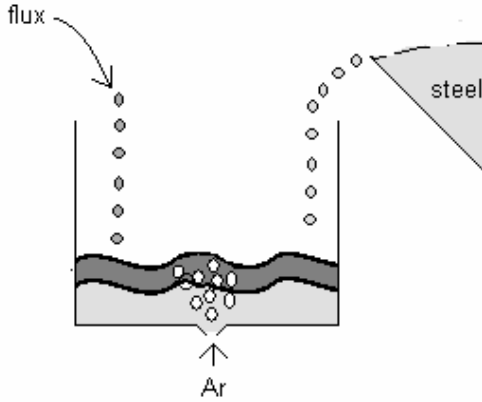
Principal Continuous Reactors	Equivalent Batch Operations
 <p>The composition and gradient between slag and steel change with respect to distance.</p> <p>PFR with concurrent flow</p>	 <p>The composition and gradient between slag and steel change with respect to time.</p> <p>Ladle, BOF, EAF</p>
 <p>The composition does not change with respect to time or distance and the gradient between the slag and the steel is small and constant.</p> <p>Near CSTR</p>	<p><u>Fill slowly</u></p>  <p>The composition does not change with respect to time or distance and the gradient between the slag and the steel is small and constant.</p> <p>Semi-continuous</p>

Figure 1: The principal continuous steelmaking reactors and their equivalent batch reactors are illustrated (based on reference 11)

Other researchers continued to pursue the idea of continuous steelmaking by modifying OHF's. In the 1900's, Talbot⁷ used a larger OHF than Siemens, trying to maintain a concentration gradient throughout the furnace. In the 1930's, Dobrokhotoy^{9,13} used two OHF's to refine steel stepwise. The literature implies that all three processes were used to produce steel for a limited amount of time.

Table II: Summarized list of 80 continuous steelmaking processes

<i>Period</i>	<i>Starting material</i>	<i>Extent of research</i>	<i>Principal reactor</i>	<i>Major characteristic</i>	<i># of proc.</i>	<i>References</i>	
1	Hot metal	Pilot plant	CSTR / PFR	Modified OHF's	3	5, 7, 9, 13	
2	Scrap	Pilot plant	PFR	Counter flow	1	9	
				Single vessel	1		
	Proposal	CSTR	Series of vessels	1			
			Fully continuous	1			
		PFR	Single vessel	2			
			Series of vessels	2			
		3	Hot metal	Pilot plant	CSTR		Spray refining
Emulsion	1					9, 13-18	
Proposal	Single vessel			2		9, 13, 14, 16	
	Series of vessels			1		19	
4	Hot metal	Pilot plant	PFR	Counter flow	9	9, 13-18, 20-27	
				Concurrent flow	3	9, 13, 14, 16-18	
		Proposal		Series of vessels	1	13, 14, 16-18	
					2	26, 28	
				Counter flow	2	29, 30	
5	Scrap	Pilot plant	CSTR	Semi-cont. EAF	6	16, 31-35	
				Series of vessels	4	13, 16, 36, 37	
		Proposal	PFR		2	16, 38, 39	
	Hot metal	Pilot plant		Fully continuous	1	13	
				Rotary furnace	1	16	
		Proposal		Concurrent flow	2	40, 41	
				Series of vessels	1	42	
		Proposal	CSTR		1	38, 39	
	Fully continuous			1	15, 43		
	Vacuum refining			1	44		
6	Hot metal	Pilot plant	CSTR	Series of vessels	2	16-18, 45-47	
			PFR	Counter flow	5	13, 16, 17, 48	
		Proposal			2	49, 50	
			CSTR	Series of vessels	4	16-18, 51, 52	
					2	16, 53	
			Fully continuous	1	10		
			Single vessel	1	54		
7	Scrap	In use	CSTR	Semi-cont. EAF	2	55, 56	
		Proposal			2	6, 57	
			PFR	Counter flow	2	8, 58	
	Scrap/Ore	Pilot plant	PFR	Induction furnace	1	18, 59	

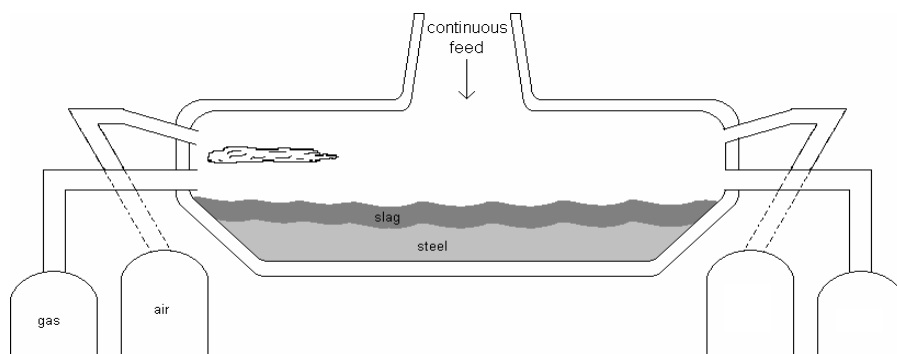


Figure 2: Schematic illustration of a typical modified Open Hearth Furnace from period 1

Period 2: Development of Fundamental Designs and Principles (1930's – 1950's)

The fundamental designs and principles for continuous steelmaking processes were developed during this period and are schematically summarized in Figure 3. Figure 3a illustrates processes that use either hot metal or scrap as starting material. Hot metal was already used during the first period; however, for the first time Thring⁹ and Schack⁹ developed three designs that continuously processed scrap. Two of these three designs actually operated commercially. For instance, one of Schack's⁹ processes melted scrap continuously for a foundry. Figure 3b illustrates the possibility to use a series of vessels or a single reactor. Another of Schack's⁹ designs and the designs of Waldron⁹, Elliott⁹, Grah⁹, and Gremaux⁹ included series of vessels while a single vessel process was introduced by Rochling and Johanssen⁹, Hudson⁹, Thring⁹, and Schack⁹. Overall, nine designs were introduced, resembling either a PFR (five designs) or a CSTR (four designs) as illustrated in Figure 3c. A fully continuous steelmaking process is illustrated in Figure 3d. Elliott⁹ proposed the first fully continuous design, which connected the continuously operating blast furnace with a continuous casting machine.

Period 3: Experimental Research on Non-Equilibrium CSTR's (1950's – 1960's)

The first BOF (LD) started operating in 1952⁶⁰, producing steel at high productivity due to the fast reaction rates during the oxygen blow. This development sparked new research on continuous steelmaking for hot metal processing. Blowing oxygen into the steel seemed to be the solution to provide the necessary kinetics for a continuous steelmaking process that would use a CSTR.

The French research institute IRSID^{9,13-18} developed a continuous steelmaking process that used an emulsion similar to that formed in the BOF. Emulsion refining together with spray refining is schematically illustrated in Figure 4. British (BISRA)^{9,13-16}, Austrian (VOEST)^{13,14,16}, and Soviet¹³ researchers tried to increase the kinetics even more by using a spraying process, blowing steel with oxygen and fluxes into a vessel. However, decarburization of the metal droplets was less efficient than expected and iron oxide formed on the suspended droplets while most decarburization occurred in the bath, defeating the idea of spray refining. In general, the advantage of control during a CSTR operation was not realized in the spraying and emulsion processes because these reactors operated at non-equilibrium conditions. One result of the lost control was varying final chemistry. Other general problems included low or varying iron yield, large amounts of slag, long settling times to separate the phases, and refractory problems. The research on these processes continued until the 1970's and 1980's when the IRSID process and a Soviet design were changed to use substantially larger quantities of scrap.

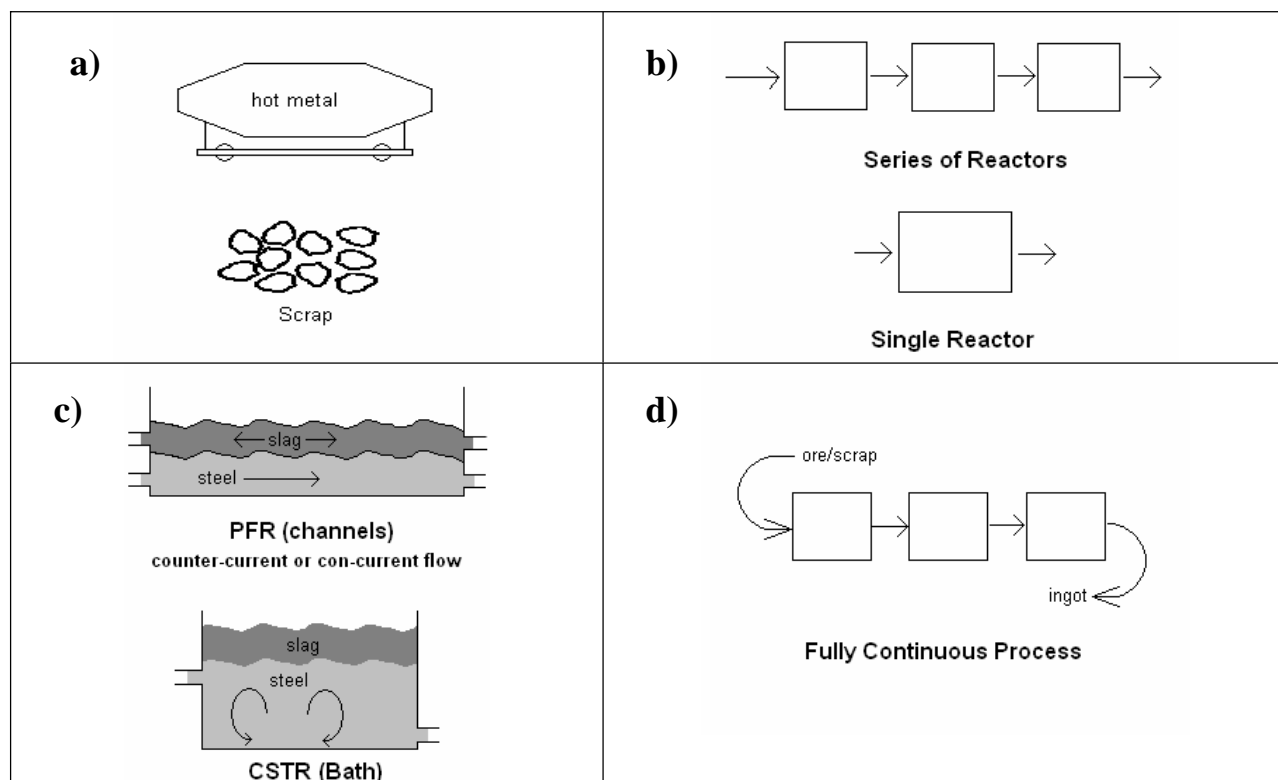


Figure 3: Schematic illustration of principal designs and fundamental ideas (period 2) a) hot metal or scrap as starting material b) series of reactors or single reactor c) PFR or CSTR d) fully continuous

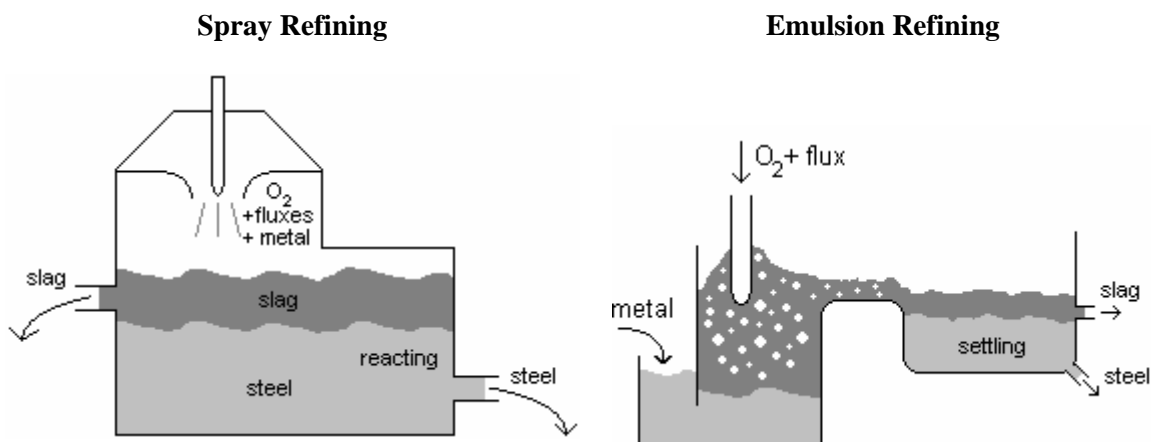


Figure 4: Schematic illustration of typical non-equilibrium CSTR's from period 3

In addition, continuous deslagging of the BOF was tried in Luxemburg⁹. A series of continuous refining reactors that operate near equilibrium was proposed in the Netherlands¹⁹ and other single-vessel processes were tested in the Soviet Union^{9,13,14,16}. None of the processes were capable of reliably producing steel at the rate, quality, and cost of the BOF.

Period 4: Experimental Research on PFR's (1960's – 1970's)

Seventeen new continuous steelmaking processes^{9,13-18,20-30} were proposed. At least thirteen of these processes were tested experimentally. Channel reactors (or PFR's) were used for all designs during this period as illustrated in Figure 5. Channel reactors closely resemble the familiar batch operations. In addition, a large driving force (concentration gradient) can be maintained throughout the channel if the steel flows countercurrently to slag, increasing the kinetics of the process and the overall conversion. Consequently, countercurrent channel reactors were the most common design during this period.

The largest challenge that channel reactors face is backmixing, which decreases the performance by loss of operational control, varying final chemistry, unsatisfactory productivity, varying steel temperature, and heat losses. Design changes that were aimed to reduce backmixing included increased length of the channel, insertion of baffles and dams, argon bubbling along the center of the channel, and electromagnetic uphill transportation of the steel while the slag flowed downhill due to gravity. These changes increased heat loss, capital cost, and/or complexity of the channel reactors and did not always work. The research on some of these processes continued for a long time. For instance, the WORCRA process was changed to exclusively process scrap in the 1970's and publications continued well into 1990's. Most of the Soviet designs were researched until the 1980's and some of them were changed to process scrap. As with the spray and emulsion reactors, none of the processes from this period could reliably produce steel at the rate, quality, and cost of the BOF.

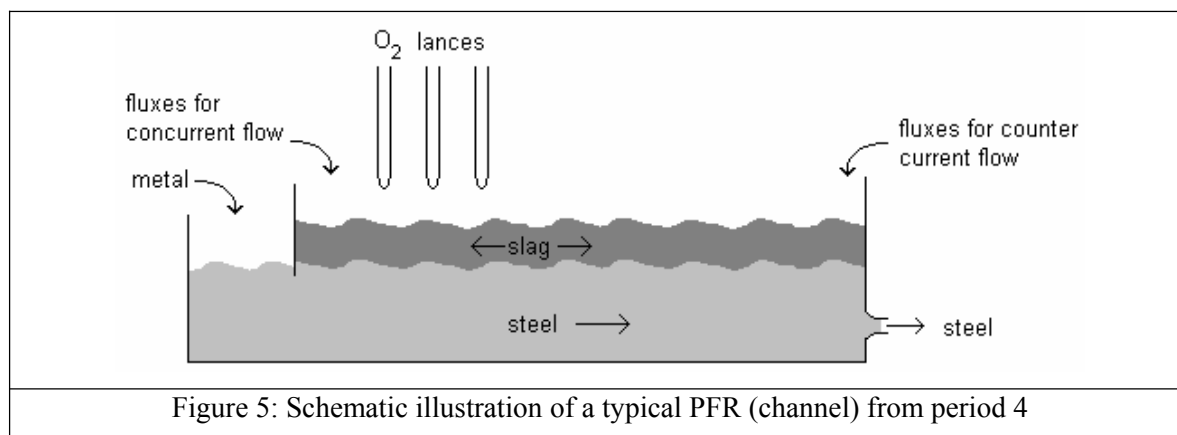


Figure 5: Schematic illustration of a typical PFR (channel) from period 4

Period 5: Experimental Research on Scrap-Based Processes (1970's – 1980's)

The increasing scrap supply and the reluctance of operators to implement continuous steelmaking processes that refine hot metal changed the focus of continuous steelmaking research from hot metal refining to scrap melting and refining. Fourteen scrap-based continuous steelmaking processes were proposed with ten proceeding to experimental tests. Figure 6 illustrates a typical scrap-based continuous steelmaking process of this period.

Scrap was either melted in an EAF or in a cupola and sometimes refined in one or more additional vessels before steel was tapped into a ladle. Six of the tested designs are simple and only include an EAF that is continuously charged^{16,31-35}. The other four tested designs included a series of reactors that resemble CSTR's^{13,16,36,37}. The four proposed scrap-processing designs used PFR's^{13,16,38,39}.

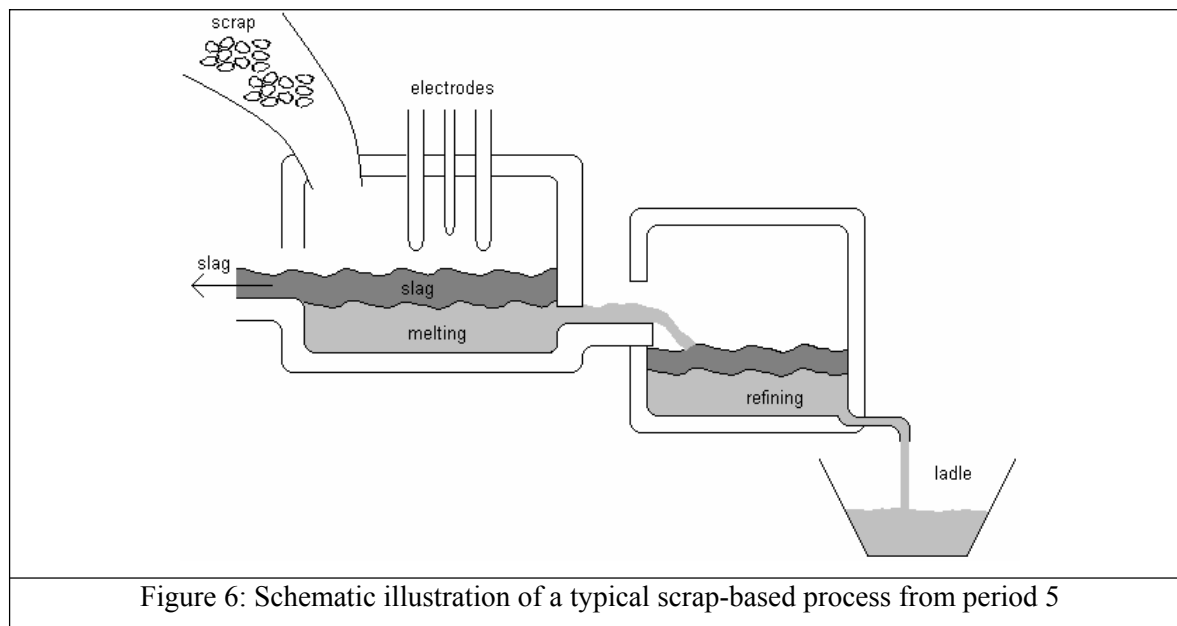


Figure 6: Schematic illustration of a typical scrap-based process from period 5

Although, some experimentally tested processes produced quality steel, the refining of the steel beyond the metallurgical operations in the EAF or cupola was usually not very successful. Some shortcomings were the requirement of small and/or clean scrap, low productivity, and/or low chemical conversions. In short, most of the scrap-based continuous steelmaking processes could not compete with EAF steelmaking, which was being significantly optimized during and after this period. For instance, the use of the LMF allowed for a single slag practice in the EAF.

Six additional processes for hot metal refining were proposed during this period. Three of them were channel reactors⁴⁰⁻⁴². These three reactors were experimentally tested and suffered similar problems to the PFR's from the previous period. A proposal from Taguchi⁴⁴ was a continuous vacuum refining process and a proposal from Krupp Stahl^{38,39} was a series of CSTR's. Two proposals (Eketorp^{15,43} for hot metal and NIRM¹³ for scrap) continued to pursue the idea of a fully continuous steelmaking process.

Period 6: Hot Metal Refining Including Equilibrium CSTR's (1980's – 1990's)

Research continued on continuous hot-metal refining processes although none of the scrap-based processes being developed in the previous period were successfully implemented in the industry. Seventeen new processes were proposed; however, only seven of them were experimentally tested. Five of the tested processes were counterflow channel reactors^{13,16,17,48}. Again, these processes suffered similar problems to PFR's from the fourth period. Two processes using near-equilibrium CSTR's were experimentally tested. Continuous steelmaking using two near-equilibrium CSTR's is schematically illustrated in Figure 7.

Pielet and Schlichting¹⁷ developed a post-hearth refining process, decarburizing steel in two steps. In addition, continuous decarburization and desulfurization of steel was researched within the AISI/DOE Direct steelmaking program^{16-18,45-47}. The research showed that continuous steelmaking (de-C & de-S) in a series of CSTR's (as proposed by Szekely⁷) is possible. However, conversion can be only as high as reaction rates are able to support. During the work of the AISI/DOE project, metal with 4% carbon was continuously decarburized to low carbon steel; however, the iron-yield losses were too high to make this process commercially successful.

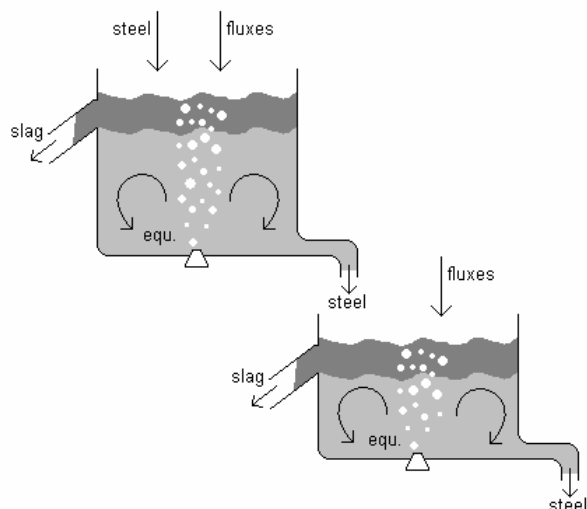


Figure 7: Schematic illustration of two equilibrium CSTR's in series (period 6)

Continuous steelmaking processes that were proposed but not tested during this period included ten processes, six utilizing PFR's^{16-18,49-52} and four using CSTR's^{10,16,53,54}. Royzman¹⁰ proposed an additional concept for fully continuous steelmaking, using a series of CSTR's including a spraying chamber. None of the processes proposed during this period have been commercialized.

Period 7: Scrap-based Processes and Commercialization (1990's – 2000's)

The first commercialization of a semi-continuous charging process was the Consteel EAF⁵⁵, which is illustrated in Figure 8. Consteel was designed in the early 1980's and operates successfully in several steelmills⁶¹. The process was developed to preheat steel; however, in contrast to many other preheating systems, the EAF of the Consteel process continuously works at near-equilibrium steady state conditions during its operation (melt, de-C, de-P), increasing the metallic yield. The tapping of the furnace periodically interrupts the steady state operation.

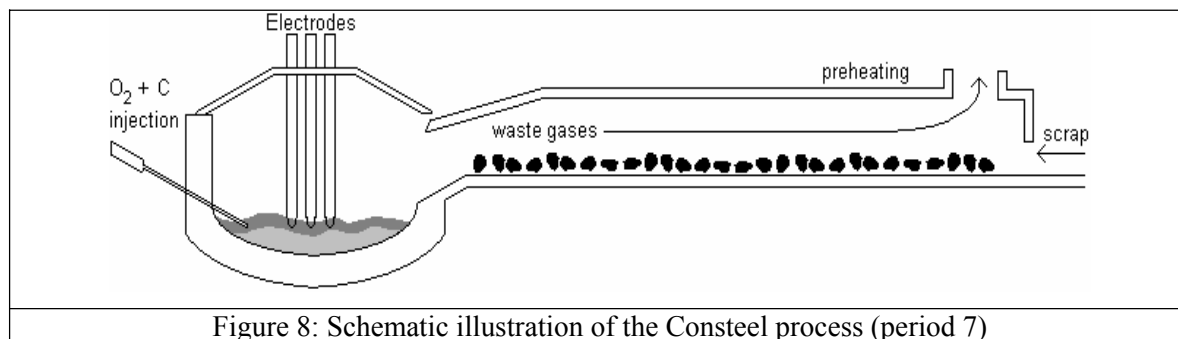


Figure 8: Schematic illustration of the Consteel process (period 7)

Contiarc⁵⁶ is a semi-continuously operating EAF developed by DEMAG and was installed in American Cast Iron Pipe Co. in 2001. It is a shaft furnace that continuously produces iron and is periodically tapped. ISCOR in South Africa operated an induction furnace developed by Fourie¹⁸ that could continuously reduce ore and produce steel in a vessel resembling a PFR. An Indian proposal (Contifur⁵⁹) used Fourie's concept and modified the furnace to continuously melt scrap.

Four additional scrap-based continuous steelmaking concepts were proposed by the Austrian supplier VAI⁸ and the Ukraine research institute NAN⁵⁸, using PFR's, and by NKK (Ecoarc⁵⁷) and Hatch (CRISP⁶), using EAF's.

Conclusions from the Literature

In general, numerous continuous steelmaking designs could not compete with conventional steelmaking technology. The frequent improvements of the BOF's and EAF's and the introduction of ladle metallurgy furnaces (LMF's) and other secondary metallurgy treatment facilities provided production and quality flexibility perceived as more profitable than commercialization of a new and risky continuous steelmaking process.

Specifically, non-equilibrium CSTR's (emulsion and spray processes) and PFR's were not successful despite extensive research and pilot plant tests that produced substantial amounts of steel. The lack of control and failure to substantially lower meltshop costs as compared to conventional batch operations are general reasons for their failure. Most of these processes were designed to continuously utilize the equipment and to perform only one major refining step (e.g. de-C) while tapping steel into a ladle as practiced during batch operations. Currently, the utilization of most batch reactors is close to one hundred percent, eliminating a key advantage of continuous processes that are not fully continuous and do not completely prepare the steel for casting.

Studies and tests have proven that near-equilibrium CSTR's could be successful if problems associated with kinetic limitations were solved. The reduction of the necessary chemical conversion by using scrap and the increase of possible chemical conversion by using a series of near-equilibrium CSTR's should help to overcome these limitations and to provide required reliability and control. Several plants are already operating EAF's at near-equilibrium conditions due to semi-continuous charging of scrap (Consteel).

The largest number (23) of continuous steelmaking processes was introduced during the 1960's just after the peak of the open hearth process and during the time of rapid BOF development and growth. The number of new continuous steelmaking processes per decade declined after the 1960's as BOF and EAF steelmaking were optimized and improved through the introduction of the ladle metallurgy furnace (LMF). Today, the BOF, EAF, and LMF are mature technologies and are operating close to optimum, allowing for only marginal improvements in these processes in the future. A major decrease in melt shop costs is only possible by installing a new, revolutionizing process.

In order to offset the risk of investing in a new technology, a new steelmaking process needs to have the potential of not only significantly reducing the meltshop costs but also of being reliable. Of all the continuous steelmaking processes reviewed in this article, only four are fully continuous, and these were only proposed in limited detail with none progressing to the point of being tested. However, it is believed that a fully continuous process, using a series of near-equilibrium CSTR's, could produce high quality steel at significant lower cost than current batch technology with sufficient reliability and benefits to justify further development. Today, Consteel, a semi-continuous scrap-based process, is being used successfully. The performance of this process could be improved when steel is continuously removed and further refined. At the same time, tundish operations could be improved with a continuous and steady supply of steel. Therefore, research at the University of Missouri-Rolla is aimed at developing a commercially viable fully continuous process, utilizing a continuous scrap charging system (Consteel) with a series of near-equilibrium CSTR's, which refine and alloy steel to result in a continuous stream of high quality steel that is supplied to the tundish.

Use of Experimental and Theoretical Methods to Investigate Mixing in Gas Stirred Reactors

Gas stirred ladle refining is widely used in steelmaking to homogenize temperature and chemical composition, as well as to remove inclusions. Accurate ability to predict the mixing time is important because it determines the operation time needed to ensure homogeneity. In addition, it can provide further insight into optimizing process parameters for developing new practices and vessel designs. For example, the development of a new process for continuous steelmaking needs computational models with sufficient accuracy to validate the process prior to full-scale pilot-plant trials and commercialization.

In this section of the report, a fundamental investigation is undertaken to quantify mixing in a gas-stirred ladle with off-centered bottom injection. Industrial trials in a Ladle Metallurgy Furnace (LMF) were performed to investigate the time-dependent change in concentration of various elements in the steel during the addition of a Silicomanganese (SiMn) ferroalloy into unkill steel. The measurements were used to validate a computational model featuring the simulation of the three-dimensional multi-phase fluid-flow, and the simulation of the ferroalloy addition, transport, melting, and mixing.

This work is a first step to quantify metallurgical phenomena during steel treatment at the LMF. In addition, the results of this study will be combined in future work with other experiments and simulations to design a fully continuous steelmaking process.

Experimental Procedure – Ladle Metallurgy Industrial Trials

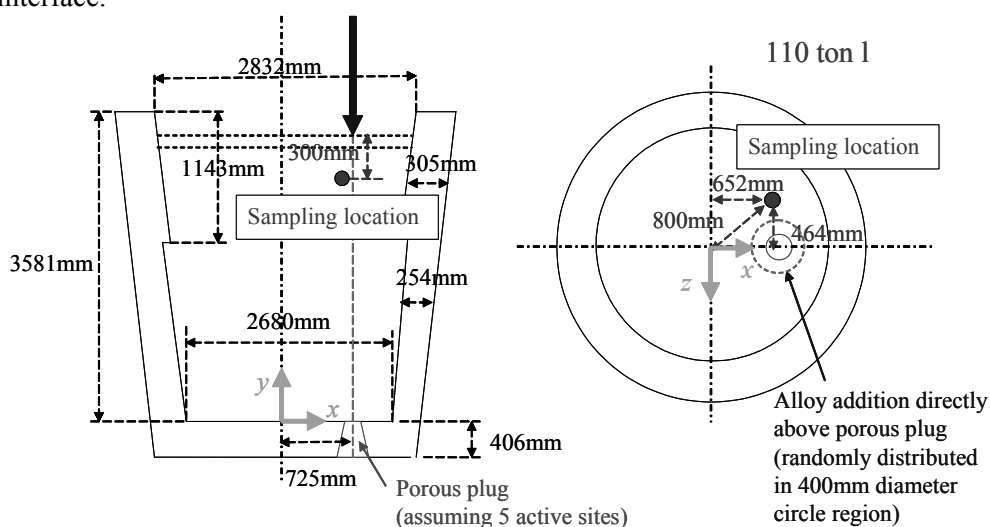
The first set of experiments included temperature and composition measurements during and after ferroalloy additions at a LMF station for eight heats of a common structural steel grade. The argon flow rate, the initial and final temperatures, the initial and final calculated oxygen concentrations and the manganese recovery are listed in Table III. The manganese recoveries of the eight heats ranged between 91% and 98% and the initial oxygen concentration of these heats ranged between 380 ppm and 1055 ppm. Heat 1 had the highest alloy recovery and the lowest initial oxygen concentration, and therefore was deemed the most accurate for comparing the industrial data and the computer-model predictions, described later. The detailed operational conditions for Heat 1 are described in this section. The results for Heat 2 were used to investigate the effect of superheat on alloy melting and mixing. The experimental conditions during Heat 2 were generally similar to Heat 1, except that the gas flow rate was lower, reducing the flow velocities.

Table III Operational conditions, oxygen change, and manganese recovery in the eight heats

Heat	Ar flow rate (Nm ³ /min)	Temperature (°C)		Oxygen (ppm)		Mn recovery (%)
		Initial	Final	Initial	Final	
1	0.170	1551	1516	380	20	97.8
2	0.113	1590	1557	909	30	93.0
3	0.113	1578	1541	415	25	96.6
4	0.113	1566	1529	1055	23	91.1
5	0.113	1605	1568	810	33	95.1
6	0.113	1586	1564	734	32	95.6
7	0.170	1577	1533	840	24	94.7
8	0.170	1577	1552	735	29	95.8

Possible reasons for the high alloy recovery of Heat 1 are the low slag reactivity and low initial oxygen content in the steel, owing to the low temperature of the steel and the high initial carbon content (0.051%). The temperature was 1551°C at the beginning of the measurements and decreased to 1516°C by the end of the trial, which was lower than steel temperatures of the other seven heats. The liquidus

The size and shape of the ladle, the location of the porous plug, the location of the ferroalloy addition, and the sampling location are illustrated in Figure 9. Heat 1 was the twenty-first heat of the ladle refractory campaign and the sixth heat on the alumina porous plug. The diameter of the porous plug at the steel/refractory interface was 113 mm. It was estimated that the slag layer on the ladle had an average thickness of approximately 35 mm, with a freeboard distance of ~ 0.3 m below the top of the ladle. The sampling location was approximately 300 mm below the slag/air surface, near the location of the ferroalloy addition (see Figure 9). Efforts were made to take the 24 composition samples and the two temperature measurements from the same location. On average, samples were taken every 22 seconds. The surface of the liquid was disturbed due to the stirring action of the argon gas with resulting surface waves of approximately 200 mm to 300 mm high. This was observed to mix the slag and the steel at the steel slag interface.



The argon flow rates were 0.17 and 0.113 Nm³/min at pressures of 448 and 269 kPa gage with an estimated maximum leakage of less than 5% for Heat 1 and 2 respectively. New couplings were recently installed and the connections were checked for tightness before sampling started. The stirring gas contained 99.99% argon, less than 20 ppm nitrogen, and less than 5 ppm oxygen.

It took 37 seconds to add the 1823.44 kg of SiMn ferroalloy to the steel. The ferroalloy entered the steel directly above the off-center porous plug where the slag layer is thinner than in the rest of the top surface (eye). It was estimated that the velocity of the ferroalloy pieces at the time of their entry into the liquid steel was similar to the velocity of pieces after a vertical free fall of approximately two meters (6 m/s). Ninety weight percent of the ferroalloy was between 13 mm and 64 mm in size, five weight percent between 64 mm and 76 mm, and the remaining 5 percent was fines. A normal size distribution of the ferroalloy was assumed. Furthermore, the ferroalloy particles did not contain foreign matter (e.g. dirt) and it was dense without any visible porosity. The chemical composition of the SiMn ferroalloy is detailed in Table IV.

Table IV Chemical composition of SiMn ferroalloy

Element	Mn	Si	C	P	S	Moisture	Fe
%	71.8	16.3	1.9	0.45	0.007	0.07	balance

The concentration changes of manganese, silicon, and carbon in the steel in response to the SiMn additions in Heat 1 and Heat 2 are plotted in Figure 10. Oscillating concentration variations were observed in all heats. However, the first small concentration drop at the end of the ferroalloy addition time seen in the left graph in Figure 2 was observed only in Heat 1. The steel samples were analyzed with a spectrometer. The phosphorus content of the steel increased from 0.010% to 0.020% during the experiment. The initial oxygen content was calculated based on the carbon concentration of the steel, and the final oxygen concentration was calculated based on the silicon concentration and the temperature of the steel. The slag samples were taken with a spoon and analyzed using X-ray Fluorescence. The initial and final slag compositions and slag masses in Heat 1 are reported in Table V. It should be noted that the power was off and the electrodes were raised during the entire experiment, eliminating the potential for carbon pick-up.

Table V Initial and final slag composition and calculated mass

Component	CaO	SiO ₂	Al ₂ O ₃	MgO	MnO	FeO	Mass
Initial wt%	44.0	21.9	1.3	13.5	3.4	14.2	570 kg
Final wt%	38.7	28.8	1.3	16.6	8.8	4.8	645 kg

(The balance to 100% is other slag components such as phosphates, sulfides, and titania.)

A mass balance was performed to calculate the initial and final steel and slag mass and to quantify the alloy loss. In addition, the amount of refractory loss due to slag line erosion during the time between the two slag samples was calculated. For Heat 1, the calculated steel mass was 110.1 tonnes (metric tons) before the ferroalloy additions and 111.9 tonnes after the ferroalloy additions, closely matching the average tap weight of 111 tonnes at this facility. The calculated slag mass increased from 570 kg before the additions to 645 kg after the final chemistry sample. These slag masses correlate well to the estimated observed average slag thickness of 35 mm. An estimated 33.6 kg of refractory was lost within 610 seconds between the two slag samples.

Table VI Alloy losses and resulting effects on steel composition, including effects from slag line erosion

	Alloy loss		Change in steel concentrations	
	Mass of element	Percent of element	due to Oxidation	due to Erosion
	kg	%	wt % steel	wt % steel
Mn	27	2.1	- 0.025	n/a
Si	27	9.1	- 0.025	n/a
C	2	5.8	- 0.002	+ 0.003
Total alloy	56	3.1	-	-

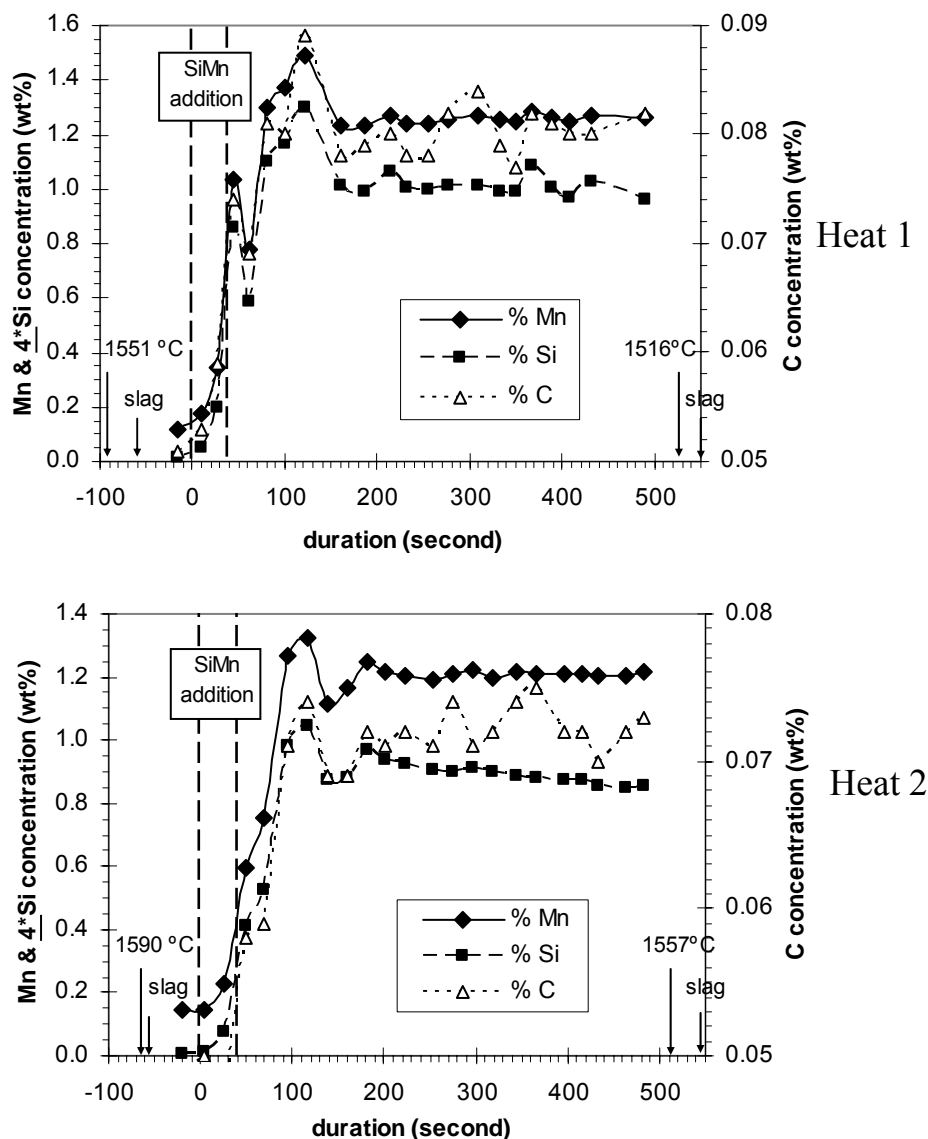


Figure 10 Steel concentrations of Mn, Si, and C during the experiment including times for temperature and slag samples

The mass balance calculations were based on the mass of the ferroalloy, the mass fraction of manganese, silicon, and carbon in the ferroalloy; the initial and final manganese, silicon, and carbon concentrations in the steel; the calculated initial and final oxygen concentration in the steel, and the initial and final concentrations of the slag components (MnO , SiO_2 , MgO , CaO , FeO). Intentionally, no fluxes were added to the slag during the experiment. As a result, the mass of lime (CaO) in the slag was kept constant. The refractory of the slag line was MgO-C (10% C). The calculated alloy losses are summarized in Table VI. The results for Heat 2 were generally similar, except that the gas flow rate was only $0.113 \text{ Nm}^3/\text{min}$, so flow velocities and mixing were slower.

Development of Computational Model

The model consists of two calculation steps. First, the three-dimensional multi-phase flow field in the vessel is calculated based on the flow caused by the jet of injected gas. Secondly, the ferroalloy addition, melting and dissolution are modeled.

A single set of Navier-Stokes equations is solved for the liquid phase and a discrete-phase model is used for the gas phase. The liquid phase equations are as follows.

Continuity equation:
$$\nabla \cdot \underline{u} = 0 \quad (1)$$

Momentum conservation:
$$\rho \left(\frac{\partial \underline{u}}{\partial t} + \underline{u} \cdot \nabla \underline{u} \right) = -\nabla p + \nabla (\mu + \mu_t) \nabla \underline{u} - \rho \underline{g} + \sum_{i=1}^{N_b} F_{D,i} (\underline{u} - \underline{u}_{b,i}) Q_b dt \quad (2)$$

where \underline{u} is the time-averaged fluid velocity, ρ is the density of liquid steel, p is the pressure, μ is the molecular viscosity of liquid steel, μ_t is the turbulent viscosity, \underline{g} is the gravitational acceleration, N_b is the total number of bubbles in the domain, $F_{D,i}$ is the drag force from each bubble as described later, $\underline{u}_{b,i}$ is the time-averaged velocity of each bubble, and Q_b is the gas flow rate. The last term of equation (2) represents a momentum source due to bubble flotation, found by summing the local contributions from each individual bubble in the domain. The subscript i refers to the number of each bubble. The standard k- ε model is used to model turbulence in the liquid phase.

Turbulent viscosity, μ_t :
$$\mu_t = C_\mu \rho \frac{k^2}{\varepsilon} \quad (3)$$

Transport equation of turbulent kinetic energy in the liquid phase, k :

$$\rho \left(\frac{\partial k}{\partial t} + \underline{u} \cdot \nabla k \right) = \nabla \left(\frac{\mu_t}{\sigma_k} \nabla k \right) + G_k - \rho \varepsilon \quad (4)$$

Transport equation of dissipation rate of turbulent kinetic energy in the liquid phase, ε :

$$\rho \left(\frac{\partial \varepsilon}{\partial t} + \underline{u} \cdot \nabla \varepsilon \right) = \nabla \left(\frac{\mu_t}{\sigma_\varepsilon} \nabla \varepsilon \right) + C_1 \frac{\varepsilon}{k} G_k - C_2 \rho \frac{\varepsilon^2}{k} \quad (5)$$

where the generation of turbulent kinetic energy, G_k :
$$G_k = \mu_t \left(\frac{\partial u_i}{\partial x_j} + \frac{\partial u_j}{\partial x_i} \right) \frac{\partial u_i}{\partial x_j} \quad (6)$$

and where C_1 , C_2 , C_μ , σ_k , σ_ε are the empirical constants whose values are 1.44, 1.92, 0.09, 1.0 and 1.3 respectively.

The Ar gas bubbles are treated as discrete second phase particles. The trajectory of each bubble is calculated in each time step according to the buoyancy force and the drag force between the bubble and the flow field. Thus, the flow and the bubble trajectory equations are fully coupled. Additionally, the chaotic effect of turbulence on the trajectories is considered using the random walk model as described later. The equations for the bubble trajectories and drag forces are as follows.

Bubble trajectories:
$$\underline{x}_{b,i} = \int (\underline{u}_{b,i} + \underline{u}'_{b,i}) dt \quad (7)$$

Force balance on each bubble:
$$\frac{d\underline{u}_{b,i}}{dt} = F_{D,i} (\underline{u} - \underline{u}_{b,i}) - \frac{(\rho - \rho_b)}{\rho_b} \underline{g} \quad (8)$$

Drag force on each bubble:
$$F_{D,i} = \frac{18\mu}{\rho_b d_{b,i}^2} \frac{C_{D,i} \text{Re}_i}{24} \quad (9)$$

Particle Reynolds number:
$$\text{Re}_i = \frac{\rho d_{b,i} |\underline{u} - \underline{u}_{b,i}|}{\mu} \quad (10)$$

Drag coefficient:

$$C_{D,i} = \frac{24}{\text{Re}_i} \left(1 + b_1 \text{Re}_i^{b_2} \right) + \frac{b_3 \text{Re}_i}{b_4 + \text{Re}_i} \quad (11)$$

where $\underline{x}_{b,i}$ is the position of each bubble, $\underline{u}'_{b,i}$ is the fluctuation velocity of each bubble due to turbulence, ρ_b is the density of the bubble, $d_{b,i}$ is the diameter of each bubble, and $C_{D,i}$ is its drag coefficient. In equation (11), $b_1 \sim b_4$ are parameters in the non-spherical particle drag model by Haider and Levenspiel.⁶²

$$\begin{aligned} b_1 &= \exp(2.3288 - 6.4581\phi + 2.4486\phi^2) \\ b_2 &= 0.0964 + 0.5565\phi \\ b_3 &= \exp(4.905 - 13.8944\phi + 18.4222\phi^2 - 10.2599\phi^3) \\ b_4 &= \exp(1.4681 + 12.2584\phi - 20.7322\phi^2 + 15.8855\phi^3) \end{aligned} \quad (12)$$

where ϕ is the shape factor, defined as
$$\phi = \frac{s}{S} \quad (13)$$

where s is the surface area of a sphere having the same volume as the particle, and S is the actual surface area of the particle.

The bubble size and shape are estimated using the following equations. The shape of the bubble is assumed to be spheroidal with uniform size. This simplification allows a single set of discrete particle equations to model the gas phase.

Bubble size is characterized by its equivalent diameter, using the empirical correlation with flow rate by Johansen and Boysan.⁶³

$$d_{b,i} = 0.35 \left(\frac{Q_b^2}{g} \right)^{0.2} \quad (14)$$

Bubble shape is given by its eccentricity e , the ratio of the length between the shorter axis and the longer axis, as estimated from measurements in various media by Wellek et al..⁶⁴

$$e = 1 + 0.163 \text{Eo}^{0.757} \quad (15)$$

$$\text{Eo} = \frac{d_{b,i}^2 g (\rho - \rho_b)}{\sigma} \quad (16)$$

where Eo is the Eotvos number which corresponds to the ratio between the buoyancy force and the surface tension force, and σ is the surface tension of the fluid. The fluctuating component of the particle velocity is found according to the local level of turbulent kinetic energy using the turbulent random walk model as follows:

$$\underline{u}'_{b,i} = \varsigma \sqrt{\frac{2k}{3}} \underline{e}_R \quad (17)$$

where ς is a random number uniformly distributed between 0 and 1, and \underline{e}_R is a unit vector in a random direction. The fluctuation velocity is kept the same during the following random eddy lifetime τ_e .

$$\tau_e = -C_L \frac{k}{\varepsilon} \log_{10} r \quad (18)$$

where r is a random number uniformly distributed between 0 and 1, and C_L is an empirical constant (=0.15).

Development of Ferroalloy Model

Next, the ferroalloy addition, transport, melting and mixing are modeled. In the experimental study, SiMn ferroalloy is added from above the surface of the stirring ladle. Thus, the ferroalloy addition is first treated as discrete second-phase particles with a common initial velocity added into the flow field computed based on stirring alone. Then, after some melting time and distance traveled through the flow field, each ferroalloy particle disappears and turns into a mass source of liquid solute that diffuses through the molten steel. In this study, manganese is the only solute considered. Ferroalloy particle transport is calculated using the same equations as those for Ar bubbles (7)~(11), except that the ferroalloy particle is assumed to be spherical and the following equation for the drag coefficient is used.

$$C_D = a_1 + \frac{a_2}{\text{Re}} + \frac{a_3}{\text{Re}^2} \quad (19)$$

where the constants a_1 , a_2 , and a_3 are given by Morsi and Alexander.⁵ For these calculations, the liquid steel flow field is fixed. Thus, the coupling due to momentum exchange from the ferroalloy particles to the flow field (the last term of equation (2)) is ignored.

A solidified steel shell is formed around the surface of the ferroalloy particle when it first enters into the molten steel. This initially prevents any alloy mixing. Then, as the ferroalloy particle is heated by the surrounding liquid, the steel shell melts and finally disappears. Because the melting point of SiMn (1215°C) is much lower than that of steel, the ferroalloy particle should be fully liquid when the steel shell disappears. Thus, the molten ferroalloy is suddenly introduced into the liquid where it starts to diffuse. The time when this occurs matches the duration of the solidified steel shell, which is modeled by Zhang and Oeters.⁶⁶

$$t_l = \frac{C_{pA} \rho_A d_A}{\pi h} \frac{T_s - T_0}{T_M - T_s} \quad (20)$$

where t_l is the shell existence time, C_{pA} is the specific heat of ferroalloy, ρ_A is the density of ferroalloy, d_A is the diameter of ferroalloy particle, h is the heat transfer coefficient at the surface of the ferroalloy particle, T_s , T_M and T_0 are the solidification temperature of the melt, the temperature of the melt and the initial temperature of the ferroalloy particle respectively.

The heat transfer coefficient h is estimated from the Nusselt number Nu , derived from the Reynolds number Re and the Prandtl number Pr of the flowing steel using the following correlation by Whitaker.⁶⁷

$$\text{Nu} = \frac{d_A h}{k_M} \quad (21)$$

$$\text{Nu} = 2 + (0.4 \text{Re}^{1/2} + 0.06 \text{Re}^{2/3}) \text{Pr}^{0.4} \quad (22)$$

$$\text{Re} = \frac{\rho d_A |\underline{u} - \underline{u}_A|}{\mu}, \quad \text{Pr} = \frac{C_{pM} \mu}{k_M} \quad (23)$$

where \underline{u}_A is the velocity of the ferroalloy particle, C_{pM} is the heat capacity of the molten steel, and k_M is the thermal conductivity of the molten steel. As the ferroalloy particles melt, the species transport model applies. The turbulent diffusion of the ferroalloy element (Mn in this case) is calculated by solving the following equation.

$$\frac{\partial}{\partial t}(\rho C_M) + \nabla \cdot (\rho \underline{u} C_M) = \nabla \cdot \left(\rho D_M + \frac{\mu_t}{\text{Sc}_t} \right) \nabla C_M \quad (24)$$

where C_M is the mass fraction of the solute, D_M is the diffusion coefficient of the solute, and Sc_t is the turbulent Schmidt number which is set to 0.7.

The ladle shown in Figure 9 is modeled as a complete three dimensional computational domain of 130 tonnes, based on filling to a depth of 3.277m, leaving a freeboard of 0.3m. Argon gas is injected through a porous plug set at the bottom of the ladle. Five active sites generating Ar bubbles are assumed at the

surface of the porous plug. Substituting the operational Ar flow rate $Q_b=5.055 \times 10^{-3} \text{ kg/s}$ ($0.17 \text{ m}^3/\text{min}$) into equation (14), the mean bubble diameter is estimated to be 28.2mm. From equations (15) and (16), e is estimated as 3.61 and the shape factor ϕ in the equation (13) is obtained as $\phi=0.736$.

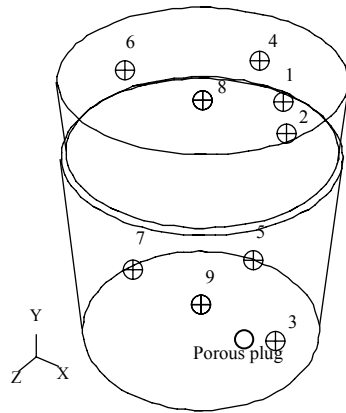
SiMn containing 71.8 wt% manganese is used as the ferroalloy. For simplicity, the diameter of each ferroalloy particle is assumed to be 30mm. The ferroalloy is added at a constant rate of 59.85 kg/s for 37 seconds. Ferroalloy transport, melting and mixing calculations are continued until 300 seconds after the starting time. As mentioned in the experimental section, the ferroalloy is added in a 400mm diameter circle region centered in the eye above the porous plug. The initial velocity of each ferroalloy particle at the steel surface is set to 6.26

m/s vertically downward, corresponding to a two-meter free fall velocity. In order to evaluate the mixing time in various locations in the ladle, nine monitoring points are chosen in the domain including the sampling location as shown in Figure 11.

The top surface boundary condition depends on the region, as shown in Figure 12. One region is covered with slag, and the other is the slag-free eye above the plume region. The 1,000mm diameter circle region directly above the porous plug is assumed as the plume region. The boundary conditions are as follows.

Plume region (no slag): Free shear condition $\tau_{xy} = \tau_{yz} = 0, u_y = 0$ (25)

Covered region (with slag): No slip condition $\underline{u} = 0$ (26)



No.	Position (x, y, z)
1	(651.6, 2977, -
2	464.2)
3	(1000, 2977, 0)
4	(1000, 300, 0)
5	(0, 2977, -1000)
6	(0, 300, -1000)
7	(-1000, 2977, 0)
8	(-1000, 300, 0)
9	(0, 2977, 0)
	(0, 300, 0)

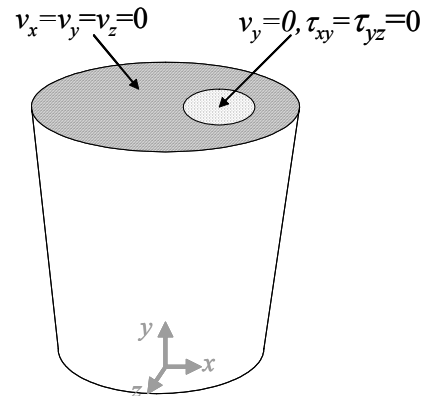


Figure 11 Monitoring locations inside ladle

Figure 12 Boundary condition at the top surface showing eye caused by plume moving away slag cover

The boundary conditions on the side and the bottom walls are set to the no slip condition, $\underline{u}=0$. The list of constants is shown in Table VII.

Table VII. List of constants

Property	Symbol	Value	Unit
Specific heat of liquid steel	C_{pM}	820	J/kg·K
Specific heat of SiMn	C_{pA}	845.7	J/kg·K
Diffusion coefficient manganese in liquid steel	D_M	5.5×10^{-5}	m ² /s
Gravitational acceleration	G	9.8	m/s ²
Thermal conductivity of liquid steel	k_M	40.3	J/m·s·K
Initial temperature of SiMn	T_0	293	K
Liquidus temperature of steel	T_s	1803	K
Viscosity of liquid steel	μ	0.0067	Pa·s
Density of liquid steel	ρ	7,000	kg/m ³
Density of SiMn	ρ_A	6,120	kg/m ³
Density of argon	ρ_b	1.6228	kg/m ³
Surface tension of liquid steel	σ	1.4	N/m

Discussion of Ladle Metallurgy Experimental and Modeling Results

The equations and boundary conditions described above were solved using FLUENT ver. 6.1.22.⁶⁸ The computational domain is divided into about 40,000 hexahedral cells. The second-order implicit time discretization scheme is used for the unsteady discrete-phase calculation, with a chosen time step of 0.01 second. The convergence criteria are set to 10^{-5} for the residuals of the continuity equation, the momentum equations, the transport equations of k and ε , and the transport equation of Mn.

For the multi-phase flow field calculation, an efficient algorithm was developed by combining a steady flow field calculation with an unsteady discrete phase calculation, instead of using a fully-coupled unsteady flow field and discrete-phase algorithm. In this method, the unsteady discrete phase calculation is first solved in a fixed flow field for ten seconds of argon injection. After each bubble location is updated, the steady flow field is then calculated for the fixed bubble locations, including their effect on the flow field as momentum sources. These two steps are carried out alternatively until the flow field reaches steady state, which means that the flow field has little change in two successive calculation sets. Six sets of calculations were needed to achieve this. This algorithm improved the computational time for the flow field calculation from 120 hours for the fully unsteady algorithm to only 0.9 hour, using Windows XP PC with Pentium® 4 3.20GHz CPU and 2Gbyte of RAM.

For the ferroalloy calculation, a user-defined function (UDF) was developed to install the ferroalloy melting model into FLUENT. In the user-defined function, the melting time is defined as a constant. Thus, after the melting time passed from the time when each particle is introduced into the computational domain, the ferroalloy particle turns into a mass source of manganese at the particle location. It takes 8 hours to finish the 300 seconds of ferroalloy melting and mixing calculation using the same PC described above.

Figure 13 shows the calculated time-averaged flow field in the steady state. The upstream jet due to bubble injection from the porous plug forms a plume that expands as it rises. The plume splits into two main streams that swirl diagonally across the top surface, flow down the far side, and converge towards the bottom corner on the opposite side of the porous plug. The returning flow pushes the plume toward the wall. The upward velocity in the plume region is given experimentally by Xie and Oeters.⁶⁹

$$u_y^{\max} = 8.64 Q_{b,V}^{0.25} \quad (27)$$

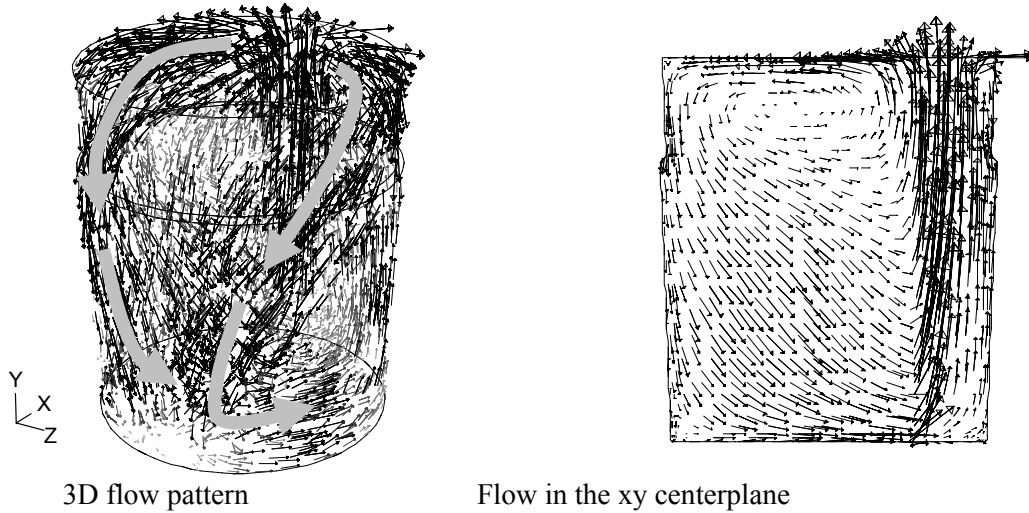


Figure 13 Calculated time-averaged flow field (FLUENT output)

where u_y^{max} is the maximum velocity in the vertical direction in cm/s, and $Q_{b,v}$ is the volumetric gas flow rate in cm^3/s . The plume velocities from FLUENT and from equation (27) are compared in Figure 14. The computed plume velocity in this study matches well with the experimental equation (27).

Figure 15 shows the gas bubble distribution in the ladle. As it forms part of the plume, the bubble column is also pushed outward by the returning stream. There are about 1,700 bubbles (28.2mm diameter each) in the ladle under pseudo-steady state conditions, and the average bubble dwell time is 3.4 seconds.

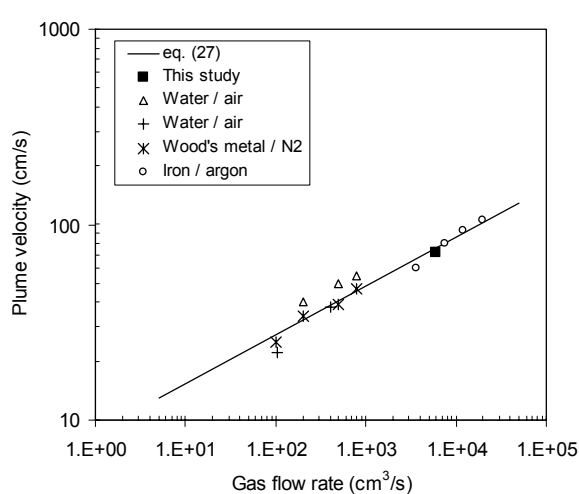


Figure 14 Comparison of the plume velocity

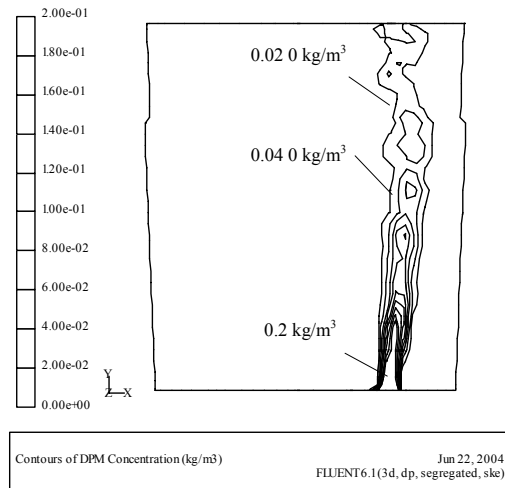


Figure 15 Bubble distribution in the xy centerplane (FLUENT output)

Ferroalloy Melting and Mixing

Because the ferroalloys are not exactly spherical, $d_A=15\text{mm}$ was set in equation (20) to represent the average minimum thickness of the ferroalloy particles. The relative velocity $|u-u_A|=0.4\text{m/s}$ is given from the surface velocity of the computed flow field. From the constants in Table V, equations (21) ~ (23)

give $Re=6269$, $Pr=0.1363$, $Nu=25.46$ and $h=6.84 \times 10^4 \text{ W/m}^2\text{K}$. Substituting h and other constants into equation (20), the ferroalloy melting time is obtained as follows.

$$t_1 = \frac{271}{\Delta T} \quad (28)$$

where $\Delta T = T_M - T_s$ is the superheat of the melt. The ΔT in the plant at the beginning of the operation is $20^\circ\text{C} \sim 60^\circ\text{C}$. Thus, the ferroalloy melting time t_1 is estimated to range from 4.5 second ($\Delta T = 60^\circ\text{C}$) to 13.6 second ($\Delta T = 20^\circ\text{C}$).

Figure 16 shows the particle distribution during the ferroalloy addition. Because the density of SiMn is less than that of the molten steel, the ferroalloy particles float up immediately after addition, and drift along the surface just beneath the slag. They accumulate around the perimeter of the top surface opposite from the plume. Furthermore, since the ferroalloy particles reach the perimeter only 6 seconds after addition, all of the ferroalloy melting takes place in this region of the top surface perimeter. These results confirm the operational experience that ferroalloy recoveries depend on the oxygen potential of the slag, which is most likely at equilibrium with the steel at the well-mixed slag steel interface. As expected, recovery rates were strongly correlated with initial oxygen concentration during all experiments ($R^2 = 0.97$). The measured recovery of manganese ranged from 91% to 97%.

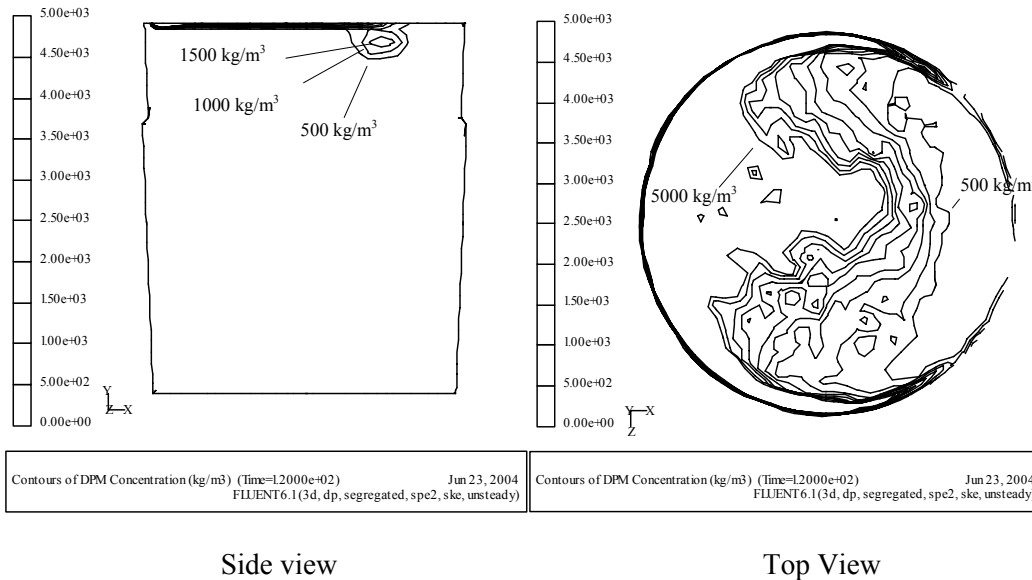


Figure 16 Ferroalloy particle distribution during addition (20 seconds after start - FLUENT output)

Figure 17 shows the mixing behavior in the xy centerplane sections. The superheat for this case is 20°C and the corresponding ferroalloy melting time is 13.6 seconds. Note that solute is generated at the dense region at the top left corner where the ferroalloy particles melt. It then circulates in the ladle, and mixes by turbulent diffusion. The solute concentration finally approaches the well-mixed value of 1.26% for Heat 1.

Figure 18 compares the mixing behavior measured in the plant with the computed concentration histories at the sampling location. The normalized concentration is $(C - C_0)/(C_\infty - C_0)$, where C is the concentration at a given time, C_0 is the initial concentration, and C_∞ is the fully homogenized concentration. The two computed curves are calculated using the operational condition of Heat 1 (i.e. $Q_b=0.17\text{Nm}^3/\text{s}$) for two superheats, 20°C and 60°C to study the effect of superheat on ferroalloy melting and corresponding mixing. The measured data from Heat 2 are also shown in comparison. However, the lower argon flow rate ($Q_b=0.113\text{Nm}^3/\text{s}$) likely causes the longer mixing time. The computed lines reproduce the qualitative

behavior of the plant data, including its oscillating nature. However, there is some difference in the peak positions, which suggests that the model may predict faster mixing than measured in the actual ladle.

The variations between the measurements are likely caused also by the significant turbulent fluctuations in the molten steel, which lead to different mixing behavior depending on the local flow conditions at the instant of ferroalloy addition. This phenomenon has also been found in studies of particle motion in the continuous casting mold.⁷⁰ In addition, the sampling location may vary slightly for each data point. A comparison of Figure 10 and 18 reveals that there is a large concentration gradient at and near the sampling location during and immediately after the ferroalloy addition. As a result, slight deviation of the sampling location could have contributed to the difference between trial and modeling data.

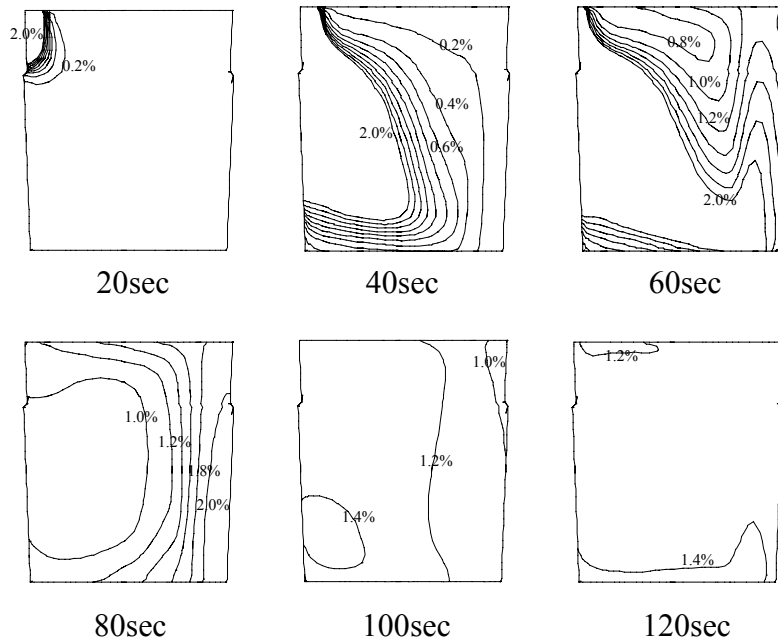


Figure 17 Mixing behavior in the xy centerplane
(indicated time is the time after ferroalloy addition starts)

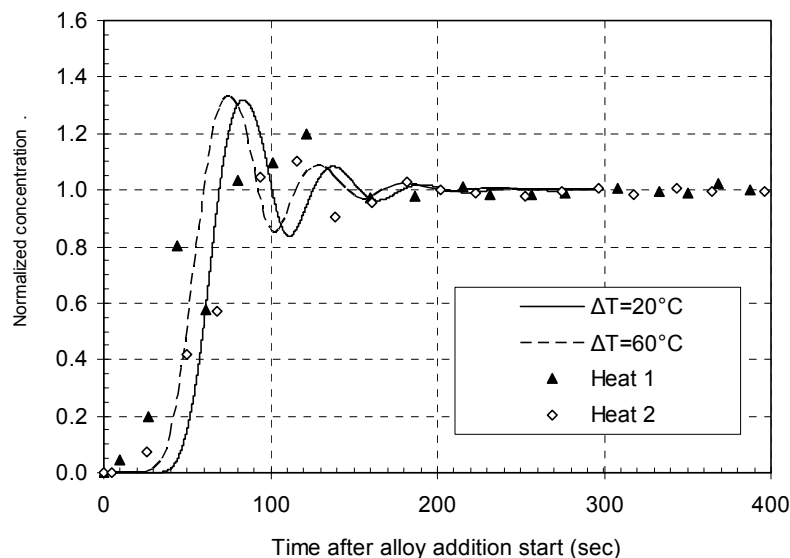


Figure 18 Computed concentration profiles at the sampling point compared with plant measurements

The results in Figure 18 also show that quantifying the mixing behavior with a mixing time to reach a given percentage (e.g. 95%) is not appropriate. This is because both the measurements and computations show that the circulating region of solute-rich fluid causes an initial concentration peak that exceeds 100% well before mixing is complete. Thus, mixing time is better defined as the time when the normalized concentration reaches $100\% \pm$ variation limits and subsequently never goes outside of this range.

Using this definition, the mixing times at various sampling points are shown in Figure 19. The mixing time was calculated for two variation limits, 1% and 5%. The location with the maximum mixing time is monitoring point 5 for $\pm 1\%$ and monitoring point 7 for $\pm 5\%$. Thus, the region near the bottom corner of the ladle determines the mixing time needed for homogeneity of the entire molten steel heat. The mixing times range from 88 to 187s, depending on the definition and location of mixing. Thus, it is important to carefully choose the sampling point and then to examine the entire mixing curve.

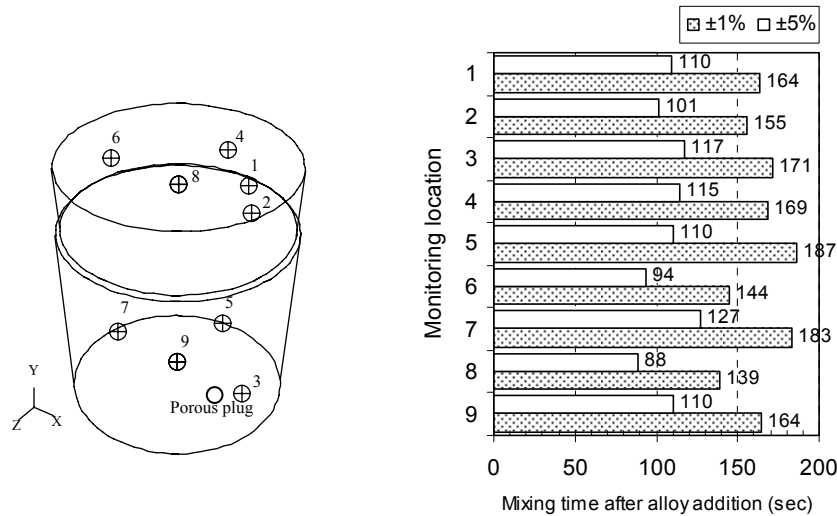


Figure 19 Mixing time at various monitoring locations

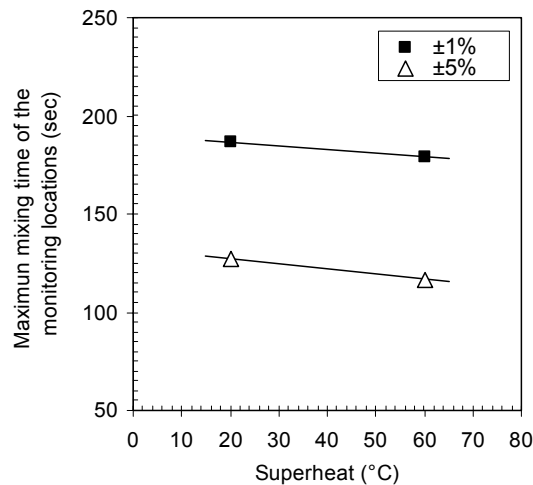


Figure 20 The relationship between superheat and mixing time

Finally, the relationship between the superheat of the molten steel and the mixing time is shown in Figure 20. The maximum value of the mixing time at the nine monitoring locations is taken as the maximum mixing time. The superheat only affects the mixing times by about 10 seconds, which is the difference in the ferroalloy melting times. Thus, the mixing time mainly depends on the flow field.

Summary of Findings from Gas-Stirred Reactor Mixing Studies

The three-dimensional multi-phase turbulent flow field and ferroalloy mixing in an off-centered gas-stirred ladle of 130 tonne nominal capacity was investigated using plant measurements and computational models. The computed plume velocity agrees well with a previous empirical equation. A complex three-dimensional swirling flow pattern due to off-centered Ar bubbling is predicted, with about 1,700 Ar bubbles distributed in the pseudo-steady flow field. Flow from the plume traverses the top surface, down the far walls of the ladle, and circulates back across the bottom, where it bends the plume slightly.

Alloy mixing was measured after a SiMn addition with alloy recoveries well over 90%. The SiMn melting time was from 4.5 to 13.6 seconds, according to the superheat. Computations show that the low density ferroalloy particles floated quickly back to the surface of the molten steel, were transported across the ladle surface by the steel flow, and melted at the far perimeter of the ladle surface. Ferroalloy mixing behavior is simulated by coupling the melting model with a turbulent species diffusion computation in the flowing liquid. The predicted mixing behavior matches the plant measurements qualitatively, but is slightly faster. Both exhibit significant variations, with normalized concentrations that exceed 100% before mixing is complete.

Finally, mixing times depend greatly on the definition of mixing (eg. $\pm 1\%$ or $\pm 5\%$) and on the sampling location used to infer the state of mixing. In this ladle system, mixing took 1½ to 3 minutes. This time depends mainly on the flow field and little on the ferroalloy melting time.

Use of Computation Fluid Dynamics to Simulate Continuous Steelmaking Vessels

Owing to the tremendous cost of pilot-plant-scale industrial trials, previous attempts to develop new metallurgical processes have generally relied on scaling up small bench-scale experiments. Due to the lack of true understanding of the rate constants, mixing phenomena, and geometric effects which control the success of the real process, many previous pilot-plant operations have been unsuccessful. With the tremendous increases in the power of computer hardware and modeling software, computational modeling offers a better design tool for creating new processes. Numerical simulation has the potential to quantify the phenomena taking place in a commercial-scale process before it is constructed. In order to achieve success, the model must accurately predict the phenomena of true interest, which for steelmaking processes include:

- Multiphase and turbulent fluid flow and within each vessel in the process, incorporating the effects of gas stirring (oxygen gas or argon gas), and including transient variations, which are the main source of variability in the product
- Mixing phenomena in each vessel, including solidification, heating, and remelting of a steel layer around alloy particle additions, which directly controls the success of alloying, and is important to other reactions as well
- Inclusion nucleation, growth, motion and removal in the molten steel;
- Heat transfer phenomena, including temperature drops between each vessel;
- Evolution of composition during each vessel, including the thermodynamics and kinetics of the reactions between the molten steel and interfaces with the top slag and bubble surfaces, coupled with fluid flow and mixing phenomena;
- Effects of the true three-dimensional features of the vessel shape (including location of inlet and outlet launder), gas injection location and flow rates, and other operating conditions on the above phenomena.

These phenomena are equally important to conventional steelmaking processes. Thus, initial development of the computational models has focused on model validation by matching with industrial measurements of fluid flow and alloy dispersion in the molten steel during LMF steel refining. Although much work remains to be done regarding model development, the current paper is to show how the modeling tools have already been applied to help design the new process. Specifically, this paper presents numerical simulations to compare two different designs of the oxidizer vessel, based on the fluid flow, mixing phenomena and inclusion motion. The second design was chosen to improve on perceived faults in the first design, including impingement of the inlet jet on the bottom of the inlet launder, and short circuiting of the fluid flow pattern. Further examples of vessel designs based on numerical simulations are planned for future publications.

Experimental Technique – Mathematical Formulations and Computational Conditions

The equations for transient three-dimensional fluid flow are solved in this work. The k- ϵ two-equation model is used to simulate turbulence, which solves two equations for the transport of turbulent kinetic energy and its dissipation rate to obtain the effective viscosity field, μ_{eff} . The trajectory of each particle (bubble and inclusion) is calculated by integrating its local velocity, defined by considering the different forces which act on it, as given in Eq.(29) for direction i .

$$\frac{du_{pi}}{dt} = F_D(u_i - u_{pi}) + \frac{\rho_p - \rho}{\rho} g_i + \frac{1}{2} \frac{\rho}{\rho_p} \frac{d}{dt}(u_i - u_{pi}) + \frac{\rho}{\rho_p} u_i \frac{\partial u_i}{\partial x_i}, \quad (29)$$

$$F_D = \frac{18\mu}{\rho_p d_p^2} \frac{C_D \text{Re}_p}{24} \quad (30)$$

$$\text{Re}_p = \frac{\rho d_p |u - u_p|}{\mu} \quad (31)$$

$$C_D = \frac{24}{\text{Re}_p} \left(1 + 0.186 \text{Re}_p^{0.6529} \right) \quad (32)$$

where ρ_p and ρ are the particle and liquid densities (kg/m^3), u_i and u_{pi} are fluid velocity and particle velocity at direction i (m/s), t is time (s), C_D is the drag coefficient as a function of particle Reynolds number (Re_p), g is gravity acceleration, μ viscosity of the fluid (kg/m-s), and d_p is particle diameter (m).

The first term in Eq.(29) is the drag force per unit particle mass. The second term is the gravitational force, the third term is the “virtual mass” force accelerating the fluid surrounding the particle, and the fourth term is the force stemming from the pressure gradient in the fluid. The effect of turbulent fluctuation on particle motion can be modeled crudely by adding a random velocity fluctuation ($\xi\sqrt{2k/3}$) to the mean fluid phase velocity at each step, where ξ is a random number and k is the local turbulent kinetic energy, i.e.,

$$u = \bar{u} + \xi\sqrt{2k/3} \quad (33)$$

A Lagrangian multi-phase model is used to simulate the argon gas stirred multiphase fluid flow in this work. In this model, only one velocity field is solved (the Eulerian fluid phase), but the liquid volume fraction is included in every term. The liquid volume fraction is calculated from the gas volume fraction, which is solved from the particle trajectory calculations Eq. (29). As the trajectory of a bubble is computed, the momentum gained or lost by the bubble motion is incorporated in the subsequent continuous phase calculations. Two-way coupling is accomplished by alternately solving the discrete and continuous phase equations until the solutions in both phases have stopped changing. The momentum transfer from the continuous phase to the discrete phase is computed by examining the change in momentum of each bubble as it passes through each control volume. This momentum exchange is given by Eq.(34), which appears as a sink term in the continuous phase momentum balance equations.

$$F_i = \sum_{cell} \left\{ \left[F_D(u_i - u_{pi}) + \frac{\rho_p - \rho}{\rho} g_i + \frac{1}{2} \frac{\rho}{\rho_p} \frac{d}{dt} (u_i - u_{pi}) + \frac{\rho}{\rho_p} u_i \frac{\partial u_i}{\partial x} \right] \cdot m_p \cdot \Delta t \right\}, \quad (34)$$

where the sum is over all the bubbles in the cell, m_p is the mass flow rate of each bubble stream (kg/s), and Δt is the time step (s).

Alloy dispersion or tracer dispersion were simulated by solving the following solute transport equation,

$$\frac{\partial C}{\partial t} + u_{ip} \frac{\partial C}{\partial x_i} = \frac{\partial}{\partial x_i} \left(D_{eff} \frac{\partial C}{\partial x_i} \right) \quad (35)$$

where C is the solute concentration or volume fraction, D_{eff} is the effective diffusion coefficient (m^2/s), depending on turbulent viscosity, given by

$$D_{eff} = D_o + \frac{\mu_{eff}}{\rho \cdot \text{Sc}_t} \quad (36)$$

where D_o is the laminar diffusion coefficient (m^2/s), μ_{eff} is the effective turbulent viscosity (kg/m-s), and Sc_t is the turbulent Schmidt number, set here to equal 0.7.

For the simulation of fluid flow, a fixed velocity condition is imposed at the domain inlet, and a “pressure outlet condition” is used at the outlets. The top surface is assumed to be flat and no slag phase, with zero shear stress. No-slip boundary condition is used at wall, with standard “wall functions” in order to capture the steep gradients with reasonable accuracy on a coarse grid. The particles are assumed to escape at the top surface and the outlet, and be reflected at other walls. 5000-10000 inclusions each size are injected into the domain through the inlet in order to get a statistical average of inclusion removal to the top surface. For the solute transport, the zero flux boundary condition is used at walls and top surface, and zero concentration at outlet. All of the equations are solved using FLUENT⁶⁸.

The vessel is cylindrical, with an inlet launder and an outlet launder, as shown in Figure 21. In Design I, gas is injected from the two porous plugs at the bottom, and in Design II there are three porous plugs at the bottom. The parameters are shown in Table VIII. In Table VIII, the theoretical residence time of the molten steel is the ratio between the domain volume and the steel flow rate.

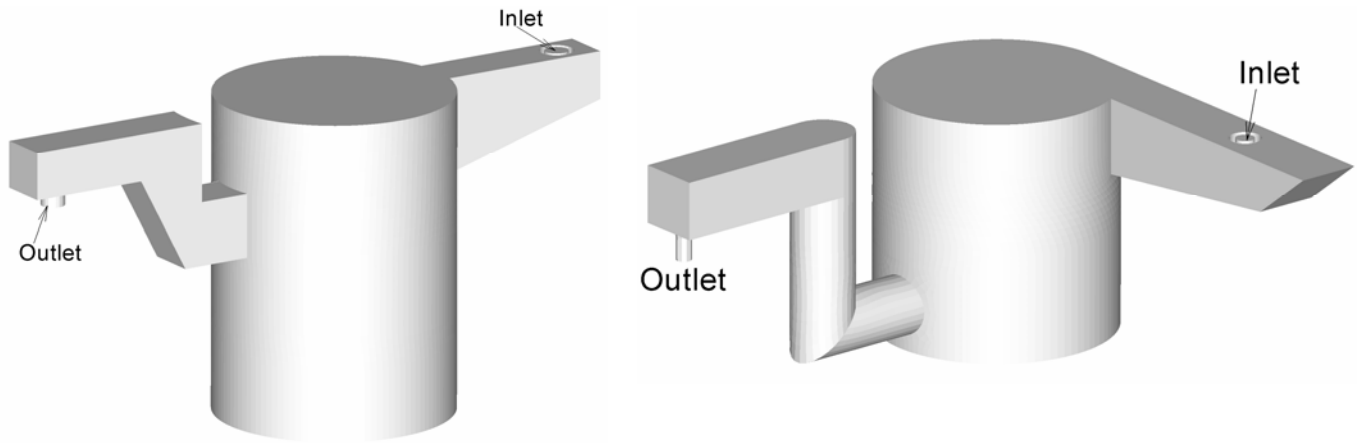


Figure 21 Schematic of Design I (left) and Design II (right) of the Oxidizer vessel in Figure 1

The cold gas flow rate (at 300K) $Q_{g,cold}$ can be converted to hot gas flow rate (at 1900K) $Q_{g,hot}$ by Eq.(37).

$$Q_{g,hot} = Q_{g,cold} \frac{T_o P_\infty}{T_\infty (P_\infty + \rho g H)} \quad (37)$$

where P_∞ is room pressure. $T_\infty=300K$. T_o is the temperature of the molten steel, 1900K. H is the depth of molten steel in the vessel (m). The bubble diameter d_B (m) depends on the gas flow rate according to:

$$d_B = 0.35 \left(\frac{Q_g^2}{g} \right)^{0.2} \quad (38)$$

Thus the number of bubbles injected into the system per unit time N_B (#bubbles/s) can be expressed by

$$N_{B,hot} = \frac{Q_{gas,hot}}{V_{B,hot}} \quad (39)$$

where V_B is the volume of a single bubble.

Table VIII Dimensions and parameters for the two designs of the Oxidizer vessel

	Design I	Design II
Dimension of the vessel	φ1.4m, H2.0m	φ1.5m, H1.65m
Inside volume of the whole domain (m ³)	3.393	3.636
Inner diameter of inlet (mm)	140	120
Submergence depth of the inlet shroud (mm)	220	150
Temperature of the molten steel (K)	1900	1900
Steel flow rate (tons/hour)	99.5	99.5
Steel flow rate (m ³ /s)	0.003572	0.003572
Theoretical residence time of the molten steel (s)	950	1018
Inlet velocity (m/s)	0.232	0.3158
Inlet turbulent energy (m ² /s ²)	3.1×10^{-4}	5.619×10^{-4}
Inlet turbulent energy dissipation rate (m ² /s ³)	4.0×10^{-4}	1.140×10^{-3}
Steel density (kg/m ³)	7020	7020
Argon density (kg/m ³)	1.6228	1.6228
Argon gas flow rate at 300K (m ³ /min)	0.49	0.49
Argon gas flow rate at 300K (m ³ /s)	0.01325	0.01325
Argon gas flow rate at 1900K (m ³ /s)	0.0219	0.0219
Bubble size at 1900K (mm)	36.4	31.0
Number of porous plug at the bottom	2	3
Total bubble injection at 1900K (#/s)	864	1406
Inclusion density (kg/m ³)	5000	5000

Results – Fluid Flow and Particle Motions – No Argon Injection

Steady-state flow without gas injection in the vessel is calculated first. In Design I, a simple open-bottom inlet nozzle is used. As shown in Figure 22, the inlet jet from this nozzle design impinges strongly against the shallow bottom of the inlet launder, so splashing and erosion of the refractory bricks might be a problem. To avoid this problem, Design II uses a side-opened inlet nozzle, (like a one-port continuous casting nozzle), so there is minimal jet impingement on the bottom of the inlet launder.) Without gas injection, in Design I, the molten steel enters the vessel from the inlet launder with a downward angle, quickly traverses across the vessel, then directly leaves through the outlet launder (Figure 23). This indicates strong short circuiting, which would be very detrimental for the process. Any time the gas injection failed, this situation would occur. To avoid this problem, Design II introduces a swirl into the flow by angling the inlet launder to avoid direct alignment with the outlet launder. As shown in Fig.22, a large, general swirl (rotating) flow pattern is generated in the whole domain. It should be noticed that without gas injection, in Design II, there is a strong backward flow toward the inlet launder along the top surface, which likely would push some slag along the surface towards the inlet nozzle (Fig23b). In Design I, this back flow is not so strong when there is no gas injection. Fig.23b also indicates that Design II has less surface turbulence in the small space to the right hand of the nozzle when there is no gas injection. The surface velocity in the inlet launder of Design I is ≤ 0.1 m/s, and ≤ 0.2 m/s in Design II.

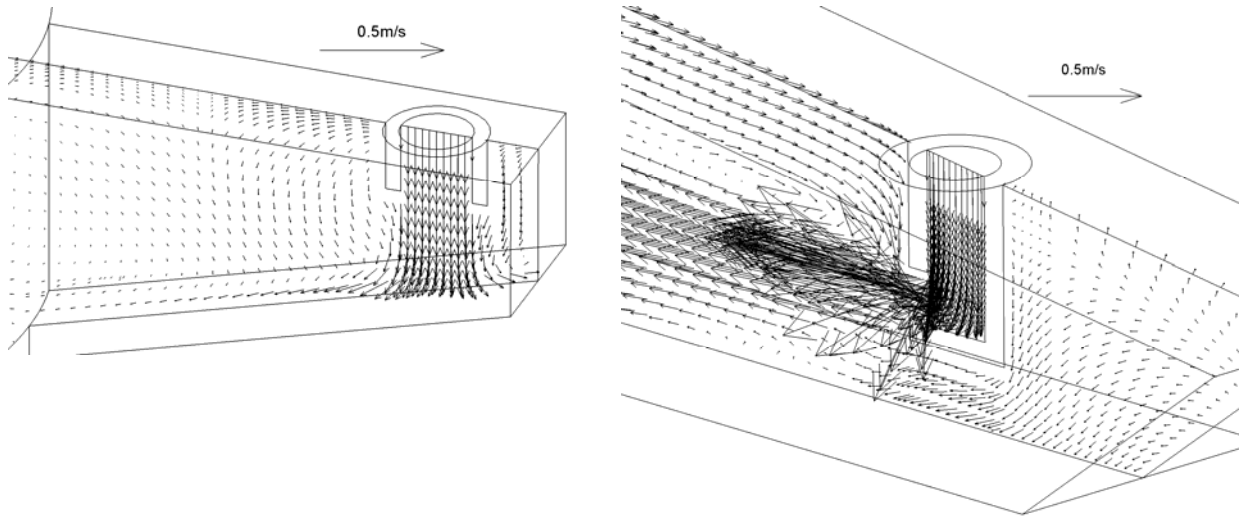
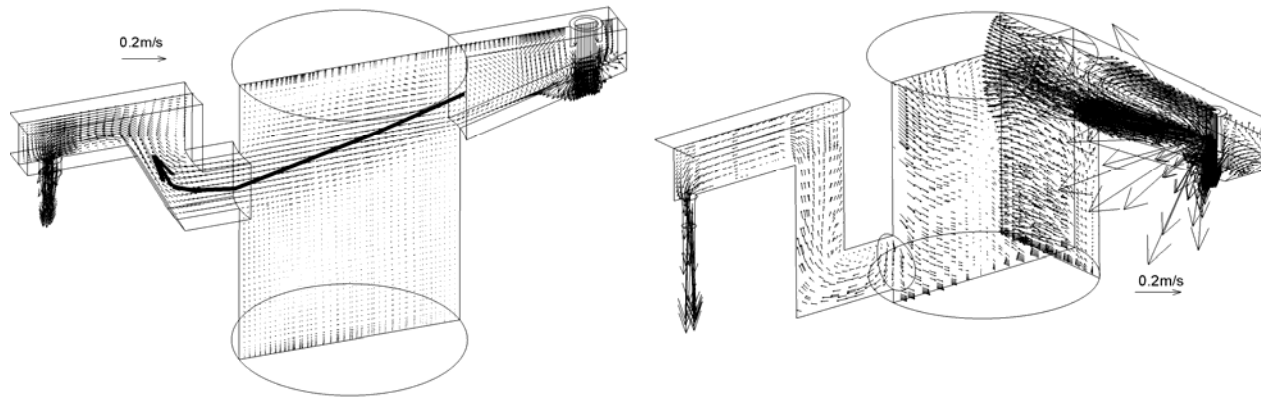


Figure 22 Velocities on centerline slices through the inlet launders in Design I (left) and II (right)

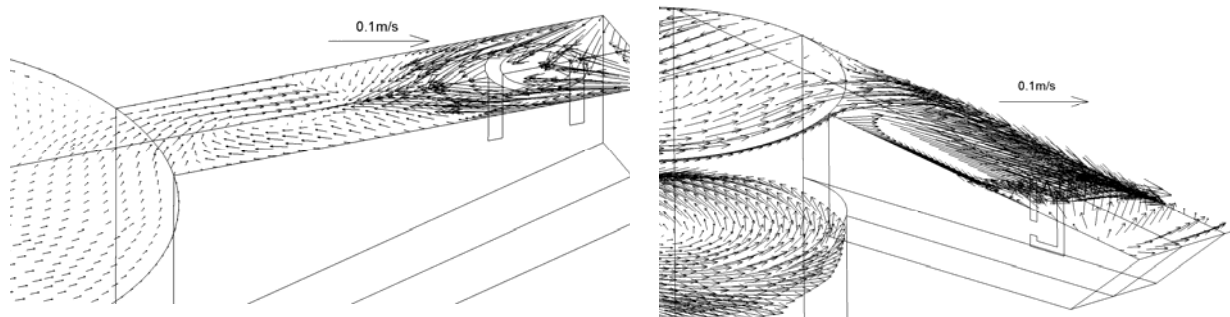
Results – Fluid Flow and Particle Motions – With Argon Injection

Argon gas is injected through the porous plugs at the bottom of each vessel. The argon gas flow rate is $0.49 \text{ m}^3/\text{min}$ (“cold” gas at 25°C and 1atm), and the bubble size is 36.4mm for Design I, and 31.0mm for Design II at 1900K . Figure 24 gives the iso-surface of 0.001 volume fraction of argon gas in the vessel. Design I seems to generate more dispersion of argon bubbles. The average residence time of bubbles in the vessel is 1.24s in Design I, with an average rising speed of 1.61m/s , while bubbles in Design II have an average residence time of 0.87s , and rising speed of 1.90m/s . The volume-averaged turbulent kinetic energy is $2.76 \times 10^{-2} \text{m}^2/\text{s}^2$ in Design I, and $1.31 \times 10^{-2} \text{m}^2/\text{s}^2$ in Design II. The volume-averaged turbulent energy dissipation rate is $5.46 \times 10^{-2} \text{m}^2/\text{s}^3$ in Design I, and $2.15 \times 10^{-2} \text{m}^2/\text{s}^3$ in Design II. At pseudo-steady state, there are 1075 bubbles in the entire liquid volume in Design I, and 1223 bubbles in Design II. The fluid flow velocities are shown in Figure 25, which indicates that Design II has a smaller average velocity than Design I. The volume-averaged velocity magnitude is 0.241m/s in Design I, and is 0.171m/s in Design II.

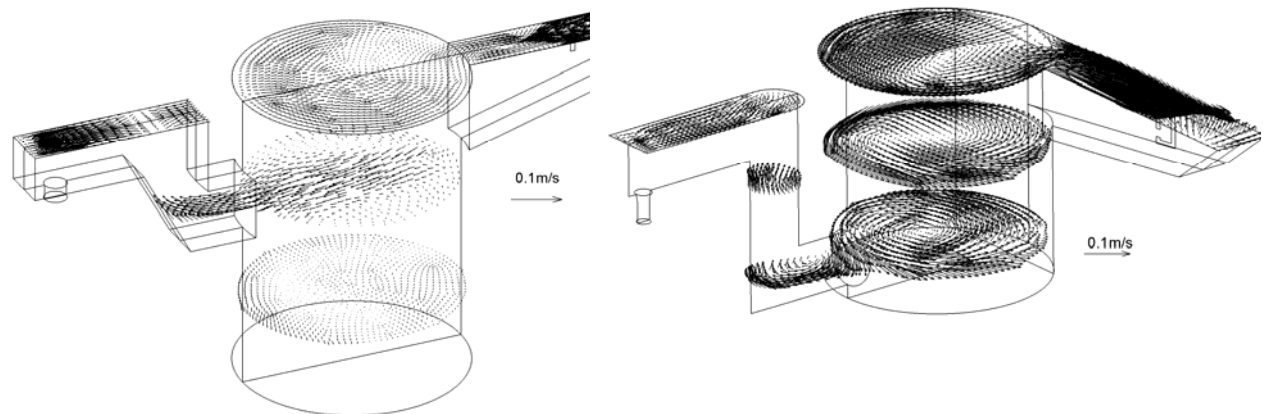
Velocity distributions within some horizontal sections in the vessel are shown in Figure 26. With gas injection, the top surface has large velocities. There is a strong backflow along the top surface into the inlet launder in Design I. There is an asymmetrical (swirl) backflow along the top of the inlet launder in Design II, that is weaker than in Design I. The molten steel directly flows into the outlet launder from the main vessel in Design I (Fig.26a). In Design II, there is a strong swirl between the vessel and the outlet launder, as the rotating flow pattern in the vessel persists even though it is diminished somewhat by the three gas plumes (Fig.26b). Design I has two independent fully-recirculating flow patterns induced by the two gas plumes.



(a) Velocity within the centerline slice in Design I (left), and through inlet and outlet launders in Design II (right)



(b) Fluid flow velocities on the top surface of the inlet launder



(c) Fluid flow velocities in different horizontal sections in Design I (left) and II (right)

Figure 23 Fluid flow without gas injection in Design I (left) and Design II (right)

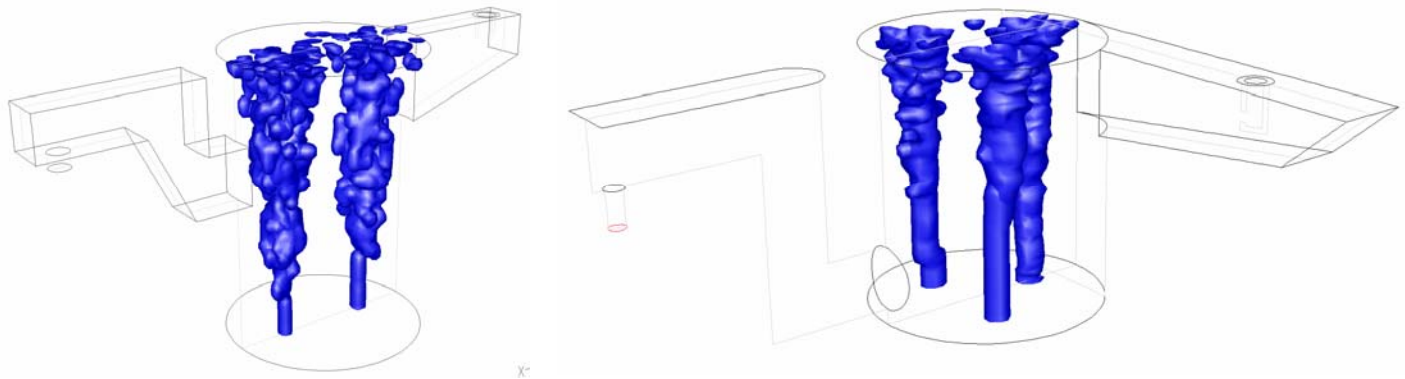


Figure 24 Bubble plumes in the vessel (Left: Design I, Right: Design II)

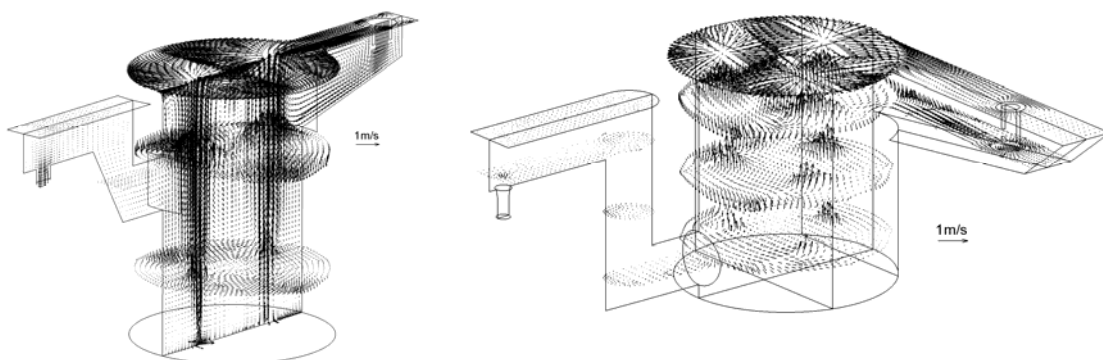
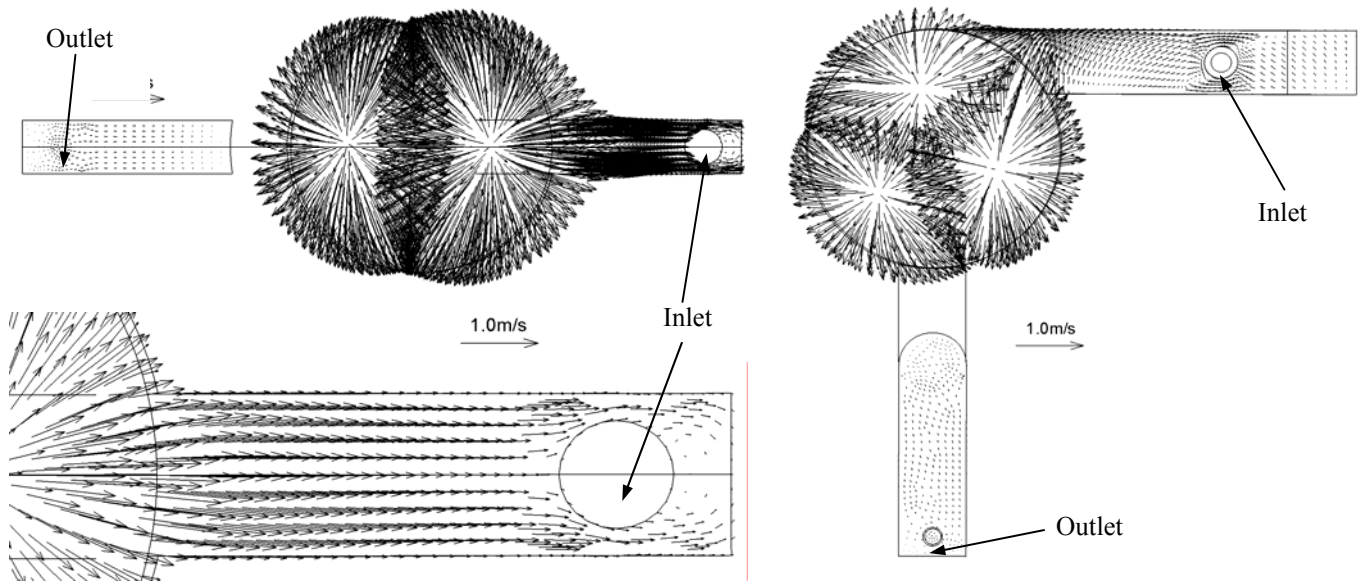
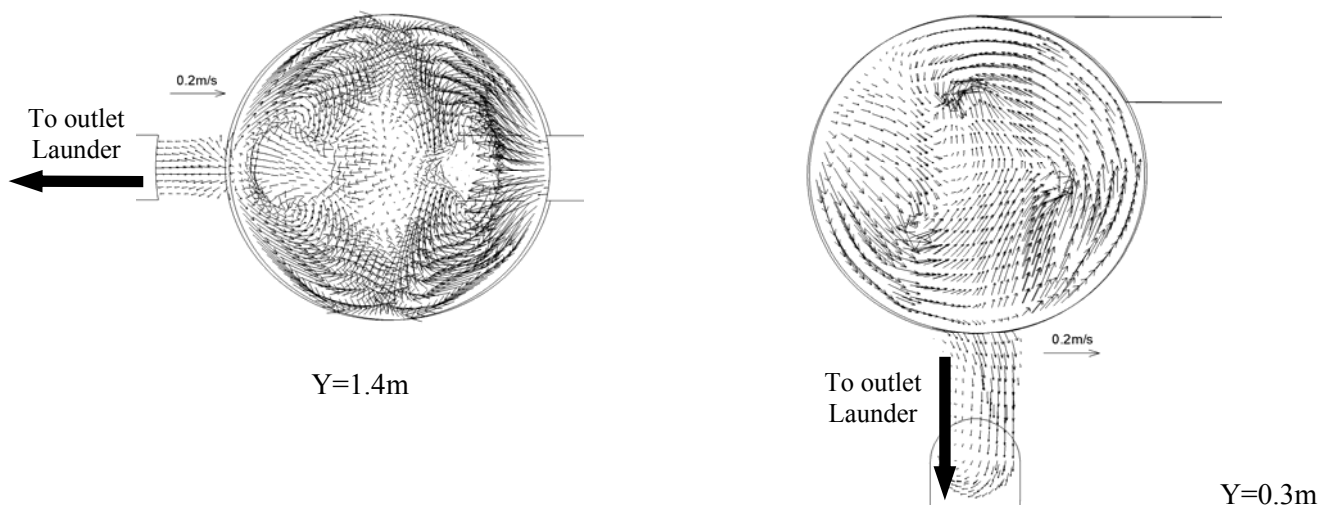


Figure 25 Fluid flow in the vessel (Left: Design I, Right: Design II)

Velocity distributions on some vertical slices through the vessels are shown in Figures 27 and 28. The molten steel flows upwards in the gas plume and downwards along walls, generating a strong recirculation within the entire height of the vessel. Therefore particles (or solute fluids) may recirculate a long time in the domain, as discussed later, which provides a good opportunity for chemical reactions. Fig.27 indicates again that fluid flow in Design I is stronger than in Design II. Figure 29 shows the turbulent energy dissipation rate in the vessel. In Design I, the top surface and the gas plume have energy dissipation rates $>1.0\text{m}^2/\text{s}^3$ (1000 W/ton), far larger than at other places. In Design II, this value is $0.37\text{m}^2/\text{s}^3$ (370W/ton). This big stirring power at the top surface is likely to be beneficial for the chemical reactions between the molten steel and the slag.



(a) At the top surface



(b) On the horizontal section passing through connection between the main vessel and the outlet launder
Figure 26 Velocity distribution details in two horizontal sections (Left: Design I, Right: Design II)

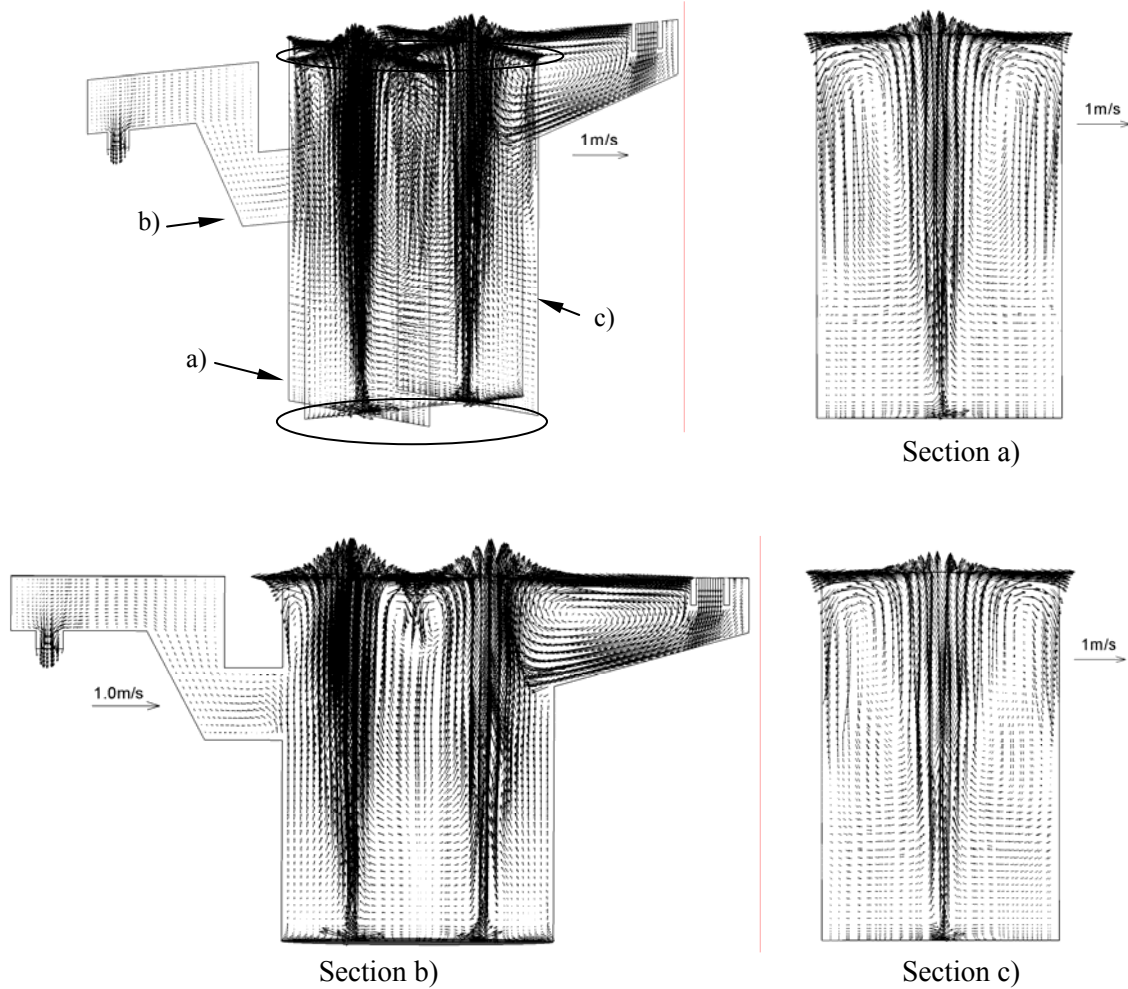


Figure 27 Velocity distributions on vertical slices in Design I

Solute transport is calculated in order to simulate the dissolution and dispersion of the alloy added into the molten steel. Unlike the continuous nature of the real process, the solute is added here as a tracer for better visualization, and convected outflow is ignored. The place of the tracer alloy addition and points to monitor its local volume fraction change with time are shown in Figure 30. The alloy is added into the domain at the center plane midway between the center axis and inlet launder exit, 0.1m below the surface. Figure 31 shows the changes of the volume fraction with time at the monitoring points. Points 8 and 9 in Design I and point 6 in Design II are close to the connection between the main vessel and the outlet launder. The earlier that alloy appears there, the more serious is the problem of short circuiting through the domain. Fig.31 and Figure 32 indicate that the alloy starts to reach these place at only 5-7s in Design I, but is 14s in Design II. From this point of view, Design II is better than Design I. Fig.31 also indicates that the alloy volume fraction at different monitoring points fluctuates with time until converging together, and eventually dropping down with increasing time. The average volume fractions of the solute are 2.95×10^{-4} for Design I, and 2.75×10^{-4} for Design II. The time when all of the points reach the same value is defined as the mixing time. This mixing time is observed in Fig. 12 to be 90s for Design I, and 110s for Design II. From this definition, Design I has a little faster mixing than Design II. After around 2000s, all the tracer alloy has left the Oxidizer vessel to the next vessel. The theoretical residence time of the molten steel in the domain is 950s for Design I, and 1018s for Design II, which is around 10 times larger than the mixing time. Thus the mixing conditions are judged to be good in both vessels. It should

be mentioned that a residence time exceeding the mixing time is sufficient for homogenization but not always enough for reactions. Of greater importance is the need to avoid short circuiting flow and to transport the inclusions to the top slag. Reactions also depend on interfacial area between the steel and gas, emulsification between steel and slag, and thermodynamics.

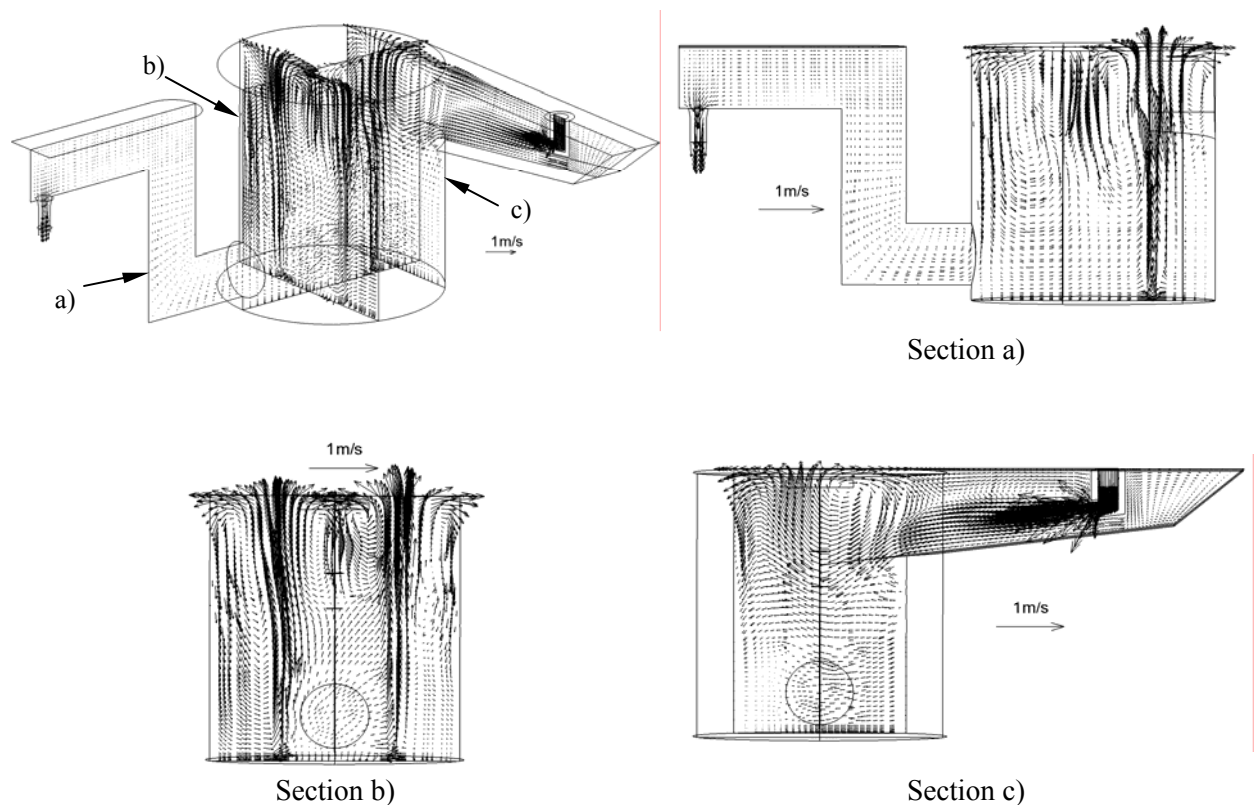


Figure 28 Velocity distributions on vertical slices in Design II

The relationship between the mixing time and the stirring power is shown in Figure 33, which is consistent with the correlation of other investigations. The iso-surfaces of the alloy volume concentration in the domain are shown in Figure 34. Design I has a flow condition similar to a pair of well-mixed vessels in series, as the two strong gas injection plumes partly separate the two flow recirculation regions in the vessel from each other. In Design II, the three gas injection jet and the swirl fluid flow avoids this behavior.

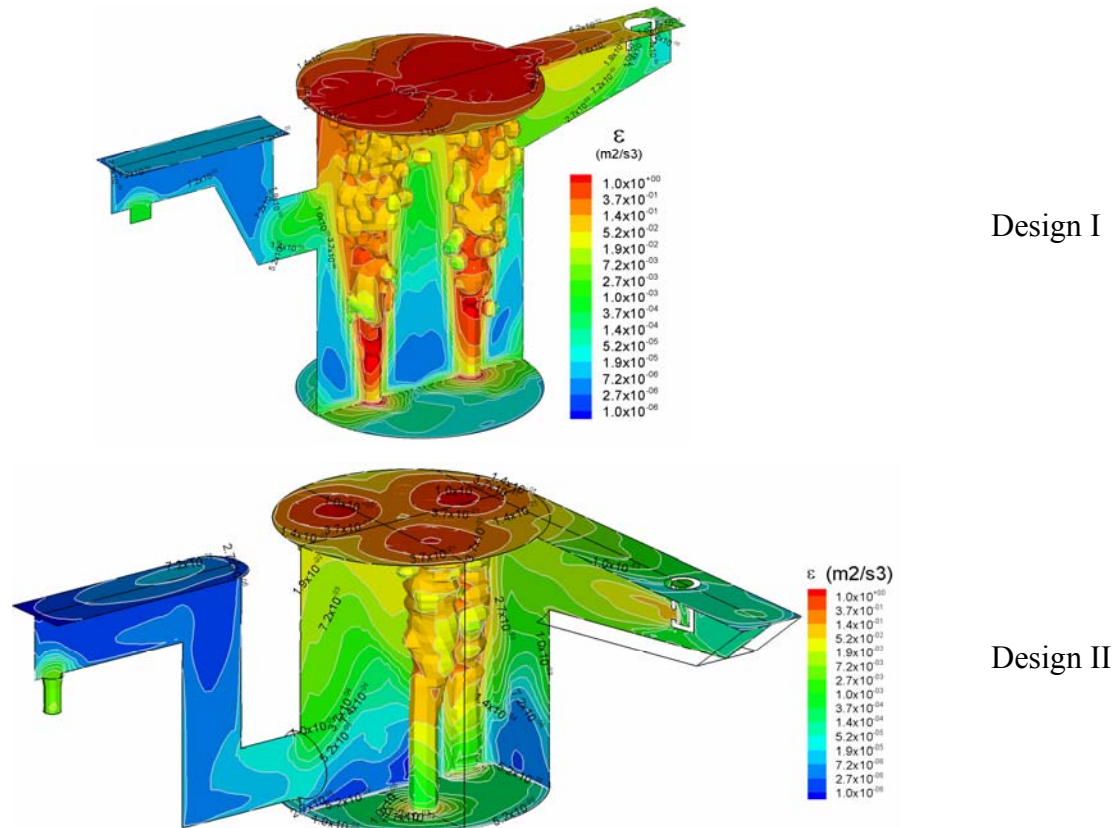


Figure 29 Turbulent energy dissipation rate in the vessel

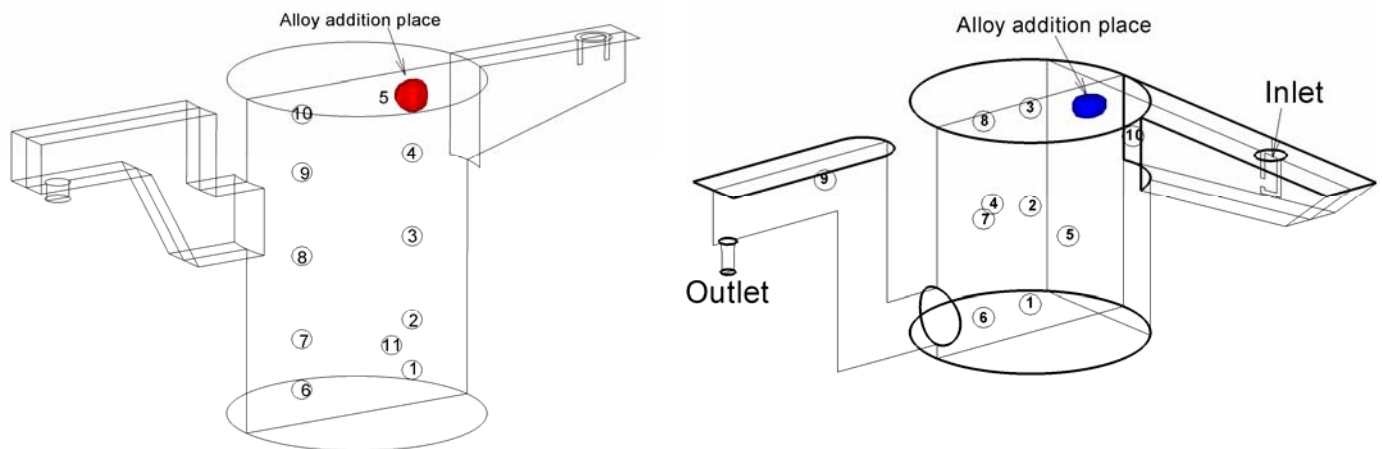


Figure 30 Addition point of alloy and points monitoring concentration (Left: Design I; Right: Design II)

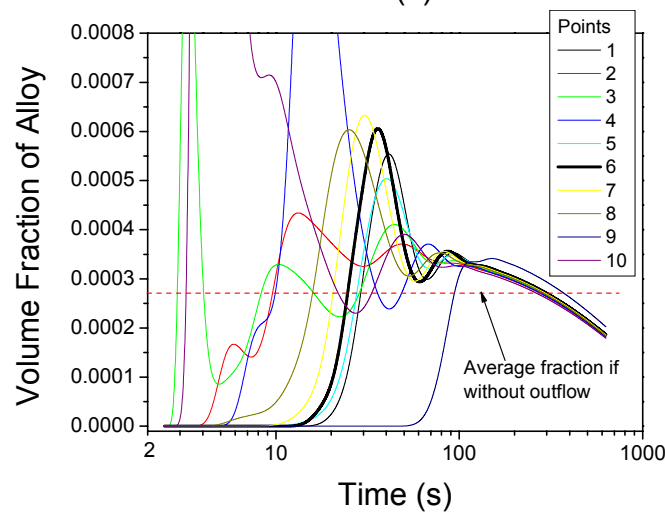
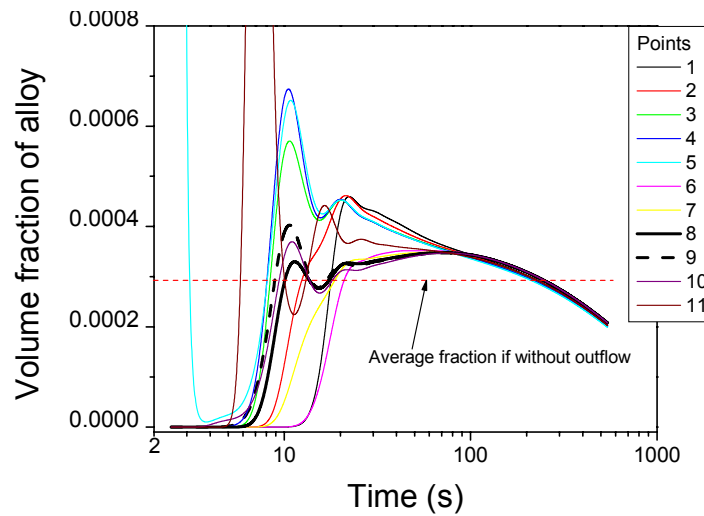


Figure 31 Dispersion of alloy in the vessel

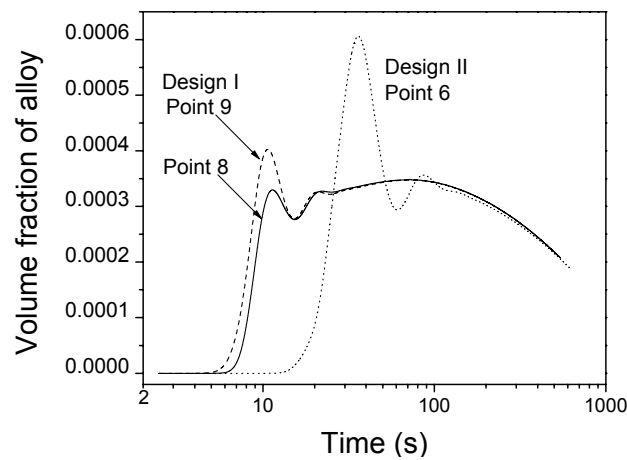


Figure 32 Alloy dispersion near the connection between the main vessel and the outlet launder

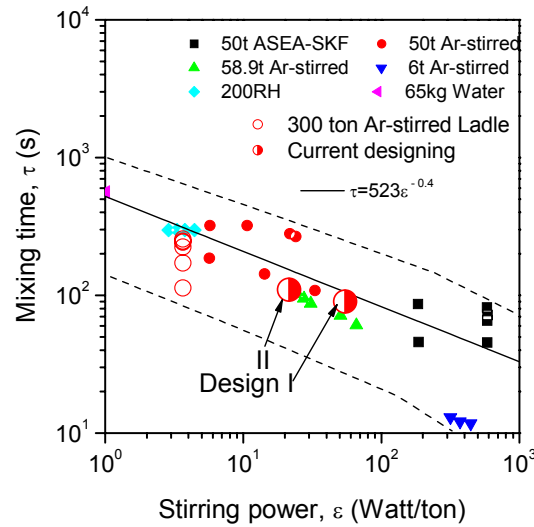


Figure 33 Mixing time as a function of stirring power of the two designs compared with literature data⁷¹

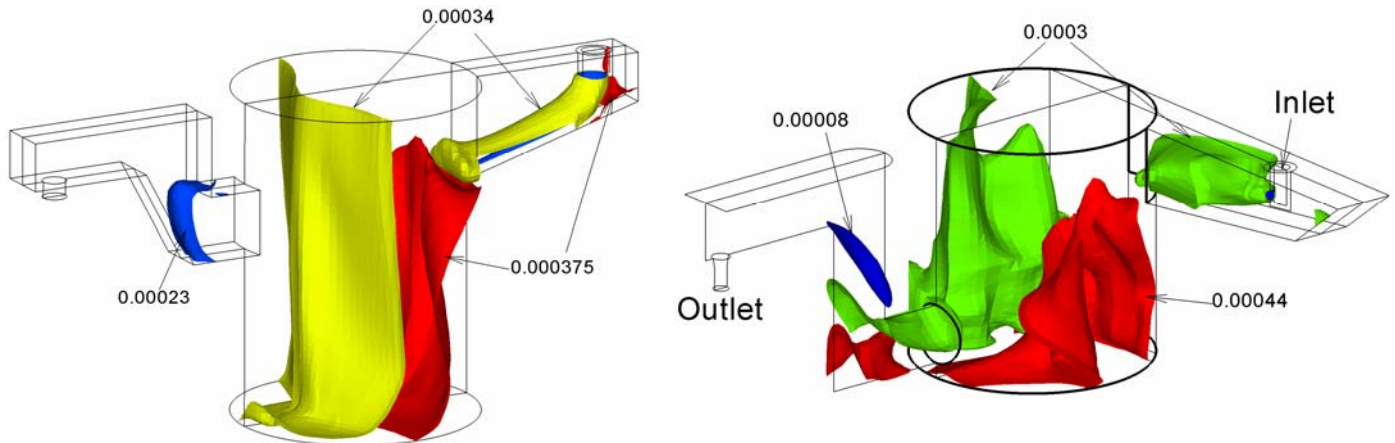


Figure 34 Alloy iso-surface at 50.5s (left: Design I; right: Design II)

Summary of Results from CFD Modeling of Continuous Steelmaking Vessels

Advanced computational fluid dynamics (CFD) models of turbulent, multiphase flow were applied to aid in the design of continuous steelmaking. The current work focuses on comparing transient fluid flow, alloy mixing, and inclusion particle transport in two different designs of the Oxidizer vessel. The design with a side opened inlet nozzle diminishes jet impingement on the bottom of the inlet launder. The design with inlet launder not in the same line as the outlet launder produces swirl, which stabilizes the flow pattern, avoids short circuiting, and likely lessens variability in the product. This swirl design has more inclusion removal and roughly the same mixing conditions as the design without swirl.

Experimental Study of Steel Treatment to Model Continuous Steelmaking Kinetics

Ladle Metallurgical Furnaces (LMF's) are used for steel temperature control, deoxidation of the steel, reduction of sulfur, alloy additions, inclusion flotation and modification, as well as holding units if delays occur during production. Reaction rates that lead to the desired steel composition within short times are desired in order to increase production or to avoid delays. The steel is stirred to achieve homogeneity and to transport it to the slag/steel interface where most reactions occur. Industrial trials were performed at two different LMF stations to gather information about the correlation of the argon flow rate, reaction rates, and thermodynamic factors that could influence the necessary treatment time of the steel at these LMF's. The results of this study were used to design and simulate the new continuous steelmaking process.

Experimental Procedure – Industrial Trials

The treatments of 20 heats at two different LMF's were observed at different argon flow rates. The monitored heats included 12 heats with Al-killed steel at LMF 1, using argon flow rates between 50 and 63 scfm and 8 heats with Si-deoxidized steel at LMF 2, using argon flow rates between 0 and 15 scfm. The experiments were a detailed time study of ladle additions, stirring conditions, and the resulting steel and slag compositions and steel temperatures. The recorded details of the ladle treatment included amount, time, and type of alloys and fluxes, temperature measurements, dissolved oxygen measurements, start and end of arcing, start and end of argon stirring with corresponding flow rates and pressures, estimated steel masses, estimated amount of solid and liquid slag, as well as miscellaneous information such as the falling of a scull from the roof into the steel. A video camera was used to record times of additions, samples, and temperature measurements with a precision of one second.

The change of the composition of the steel and slag was measured by taking 25 to 30 steel samples and 3 to 6 slag samples while the steel was treated at the LMF. The treatment durations ranged between 25 and 45 minutes. Steel samples were taken every 30 to 90 seconds and slag samples were taken every 5 to 10 minutes. A time was assigned to each sample based on video recording during treatment of each heat. Each steel sample was dropped into labeled steel cans after being taken and later placed into labeled envelopes. The chemistries of the steel samples were analyzed with a mass spectrometer. A LECO analyzer was used to determine the nitrogen and total oxygen of each steel sample.

The slag samples were taken with a pole at LMF 1 and with a spoon at LMF 2 and placed in labeled envelopes. The slag samples from LMF 1 were analyzed with an X-ray fluorescence (XRF) machine. The slag samples from LMF 2 were analyzed by ACME Analytical Laboratories using Induction Coupled Plasma Emission Spectrometer (ICP-ES) for determining the concentrations of all oxides except FeO, dichromate titration for determining the FeO, a LECO analyzer for determining the sulfur, and ion electrode analysis for determining the fluorine content of the slag. In addition to ACME's chemical analysis, 9 slag samples from LMF 2 that contained little CaF₂ were analyzed by XRF. The double analysis confirmed agreement for the two analysis techniques. A magnet was passed over the ground slag powders before the analysis to remove metallic iron.

Experimental Procedure – Metsim Thermodynamic and Kinetic Modeling

Metsim is a program capable of performing dynamic simulations of a multitude of processes. A model was designed to simulate the 20 heats. The model uses data from the industrial trials as inputs, including the initial compositions and estimated masses of the steel and slag, time, type, and amount of additions, and temperatures. The estimated initial slag mass was adjusted based on actual flux and reaction product additions and the measured concentration changes in the slag. The outputs of the Metsim program are the

calculated steel and slag concentrations at associated times. This output was graphed together with the concentration and time data from the industrial trials. The mass transfer rate constant was adjusted within the Metsim model until the calculated concentrations agreed with the measured data for all components of the steel and slag. In this way, the simulations were used to determine 26 different mass transfer rate constants for 26 different argon flow rates. These mass transfer rate constants not only reflect the concentration change of one steel component (e.g. S) but the concentration changes of all components of the steel and slag.

The value of the mass transfer rate constant (k) represents the fraction of the steel that reacts with the slag during one minute. It has the unit of inverse minute (min^{-1}). Equation 40 shows a first-order rate equation with the mass transfer rate constant. The solution of Equation 40 is Equation 41, which is an exponential function that describes the decrease of concentration (C) over time (t), starting with an initial concentration (C_o). The equilibrium concentration (C_{equ}) is assumed constant.

$$\frac{dC}{dt} = -k(C - C_{\text{equ}}) \quad (40)$$

$$C = C_{\text{equ}} + (C_o - C_{\text{equ}})e^{-kt} \quad (41)$$

Process models may be built with a multitude of modules and streams within Metsim. Free Energy Minimizer (FEM), mixer, and splitter modules as well as streams were used to create a model of a ladle as illustrated in Figure 35. Streams allow for material flow among the modules in metric tons per hour (mt/hr).

The slag/steel reactions were calculated with the Interface FEM and the reaction within the steel were calculated with the Bulk FEM. The temperature for the calculations in these FEM's was set to be the measured temperature from the trials. The pressure was set at 1.3 atm in the Bulk FEM and at 1 atm in the Interface FEM. Activity coefficients (γ) of elements and compounds were chosen based on FactSage calculations so that the Metsim FEM's produced similar results to the FactSage FEM for the range of the measured steel and slag chemistries. This procedure required numerous iterations of the Metsim simulations and the change of some activity coefficients during the calculations. For instance, the activity coefficient of liquid FeO had to be adjusted during and after deoxidation of the steel. The values of the FeO activity coefficients ranged between 0.9 and 3.2.

The wide, solid streams (1, 2) in Figure 35 represent the bulk flow of the steel that does not react with the slag during one calculation. The width of these streams indicates that the majority of the steel does not react with the slag during each calculation. The time step for each calculation was chosen to be ten seconds. The flow of stream 1 is the quotient of the total steel mass and the time step. The flow of the returning stream 2 is the difference between stream 1 and the flow of the Kinetic Stream 3. The flow of the Kinetic Stream 3 is the product of the total steel mass and the mass transfer rate constant (k). This flow was adjusted until the simulation results agreed with the data from the industrial trials. Stream 4 represents the steel flow from the slag/steel interface back into the bulk. Alloys with compositions as provided by the suppliers were added through stream 5 at times that were recorded during the industrial trials.

Streams that carried oxides or other non-metallic liquids are represented by double lines. Stream 6 transported inclusions from the Bulk FEM to the Interface FEM. Stream 7 and 8 carried slag between the Interface FEM and the Slag mixer, representing a well mixed slag. Fluxes with compositions as provided by the suppliers were added with stream 9 at times that were recorded during the industrial trials. Dashed lines in Figure 35 illustrate gas streams. Argon entered the Bulk FEM at the recorded flow rates. The

product gases from the Bulk FEM mixed with air and then reacted with the steel and slag in the Interface FEM. The air intake was adjusted so that the model predicted the measured nitrogen increase. Off-gases left the system from the interface FEM.

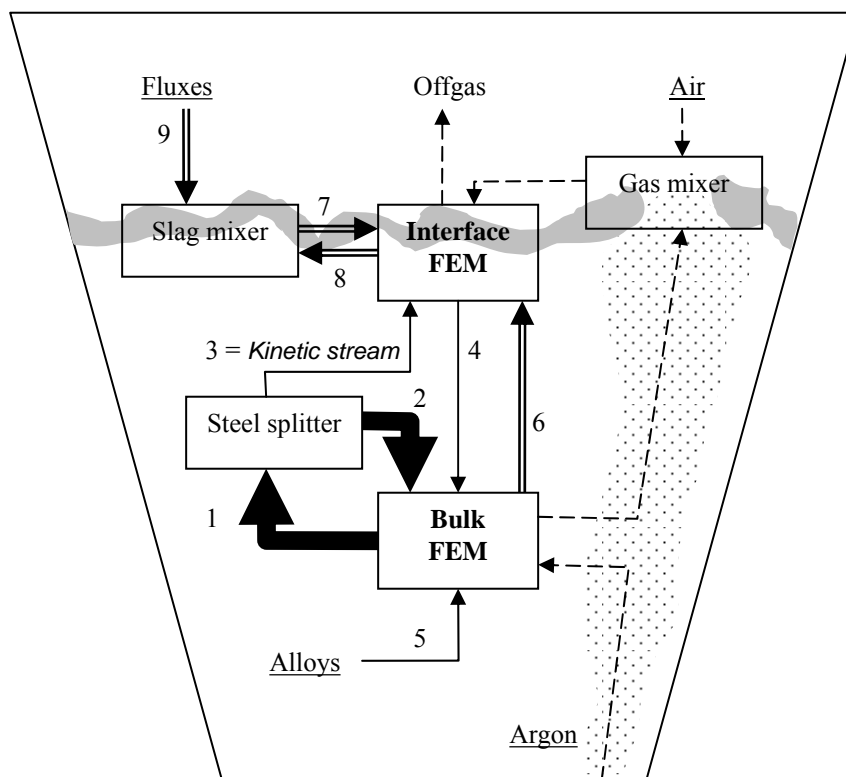


Figure 35: Illustration of Metsim model used for simulation of steel treatment in the ladle

The rate of the reactions on the slag/steel interface depends on the mass transport of all reactants to the interface and the mass transport of all products away from the interface. Reactions rates are increased if species are frequently transported to and away from the interface and if the interface is large.

Argon stirring is usually chosen as the preferred stirring method for refining (over induction stirring) because it not only transports the species to and away from the slag/steel interface but it also creates a large slag/steel interface or emulsion in the upper part of the ladle. Lachmund et al.⁷² recorded in detail the number, sizes, and size distribution of slag droplets within the steel in the upper part of an industrial ladle, documenting a significant formation slag/steel emulsion during argon stirring. Grip and Jonnson⁷³ measured slag compositions at different locations and could not find a significant difference between their measurements, drawing the conclusion that the slag is well mixed. In addition, Grip and Jonnson⁷³ recorded that the steel splashes on top of the slag, creating slag/steel emulsions. Vigorous mixing of the slag with the steel was also observed during the treatment of all 20 heats that are evaluated in this report. For instance, numerous slag particles were observed in the steel samples even at argon flow rates as low as 2 scfm. These observations and results agree with the findings of El-Kaddah and Szekely⁷⁴ who concluded that the limiting factors for reaction kinetics within argon-stirred ladles are the bulk transport of the steel to slag/steel interface and the thermodynamic equilibrium at the slag/steel interface but not the emulsion or interfacial area.

An early version of the Metsim ladle model included a slag splitter, allowing for the calculation of the mass transfer rate constant on the slag side of the slag/steel interface. The results of this more complex model were compared to the results of the simpler model that is shown in Figure 35, finding no significant differences between the two models. This result can not only be explained with a well-mixed, low-volume slag, and with the ease of creating slag/metal emulsions but also with the relationship among the different mass transfer rate constants. Equation 42 describes the relationship between the overall mass transfer rate constant (k), the mass transfer rate constant for the slag (k_S), and the mass transfer rate constant for the steel (k_M).

$$\frac{1}{k_S L} + \frac{1}{k_M} = \frac{1}{k} \quad (42)$$

The distribution ratio (L) of a species (e.g. S) is the ratio of the concentration of this species on the slag/steel interface in the slag and the concentration of the species on the slag/steel interface in the steel. The distribution ratios range between 100 and 700 for sulfur, making the first term of Equation 42 significant smaller than the second term for slags that are at least as well stirred as the steel. As a result, the overall mass transfer rate constant is determined by the mass transfer rate within the steel ($k \approx k_M$).

Discussion of Experimental Data and Simulation Results

The chemical analysis of the 600 steel and 100 slag samples were compared with the Metsim simulations, requiring the use of 80 graphs. Because it is not feasible to report all of the data and simulation results in this paper, only one representative heat from each LMF was chosen for illustration of data and simulation results.

The estimated steel and slag masses, recorded lime additions, and average temperatures together with ladle dimensions (fill height, average and top inner diameters) and numbers of porous plugs for each LMF are summarized in Table IX. Flux additions during or after the deoxidation of the steel included lime for all heats as well as 250 lbs to 750 lbs of bauxite during the treatment of heats 1 to 6 (LMF 1) and 375 lbs of spar and 40 lbs to 80 lbs of MgO during the treatment of all heats from LMF 2 (heats 13 to 20). The slag masses in Table IX are based on adjustments to the initial estimates made during the simulations. The initial slag is the slag that was taken after the Al-kill for LMF 1 and before the Si-deoxidation for LMF 2.

Table IX: General information from each LMF (averages)

	Steel	Initial slag	Final slag	Lime	Temp.	Fill height	Ladle D_{avg}	Ladle D_{top}	plugs
	tons	tons	tons	tons	°F	inches	inches	inches	number
LMF 1	151	2.0	3.3	1.2	2932	119	115	118	2
LMF 2	123	1.6	3.0	1.0	2837	121	103	108	1

The change of steel and slag composition during the treatment of two heats over 30 minutes is shown in Figure 36. The data and simulation results from heat 8 (LMF 1) are shown in the left column (Figure 36a) and the data and simulation results from heat 16 (LMF 2) are shown in the right column (Figure 36b). The measured data are presented as discrete data points whereas the results from the simulations are presented as continuous lines. The simulations reproduced the measured steel and slag concentrations in these two examples as well as the other 18 heats.

The concentrations of C, P, S, Si, and Al in the steel are reported in the first row of Figure 36 followed by the concentrations of Mn, V, N, and total O in the second row. The concentration of nitrogen was multiplied by 100 in order to present several elements in one graph. The graphs in the last rows show the

composition of the slags, reporting CaO, SiO₂, Al₂O₃, P. Heat 8 was stirred with 50 scfm with a corresponding mass transfer rate constant of 0.18 min⁻¹; and heat 16 was stirred with 7 scfm with a corresponding mass transfer rate constant of 0.06 min⁻¹.

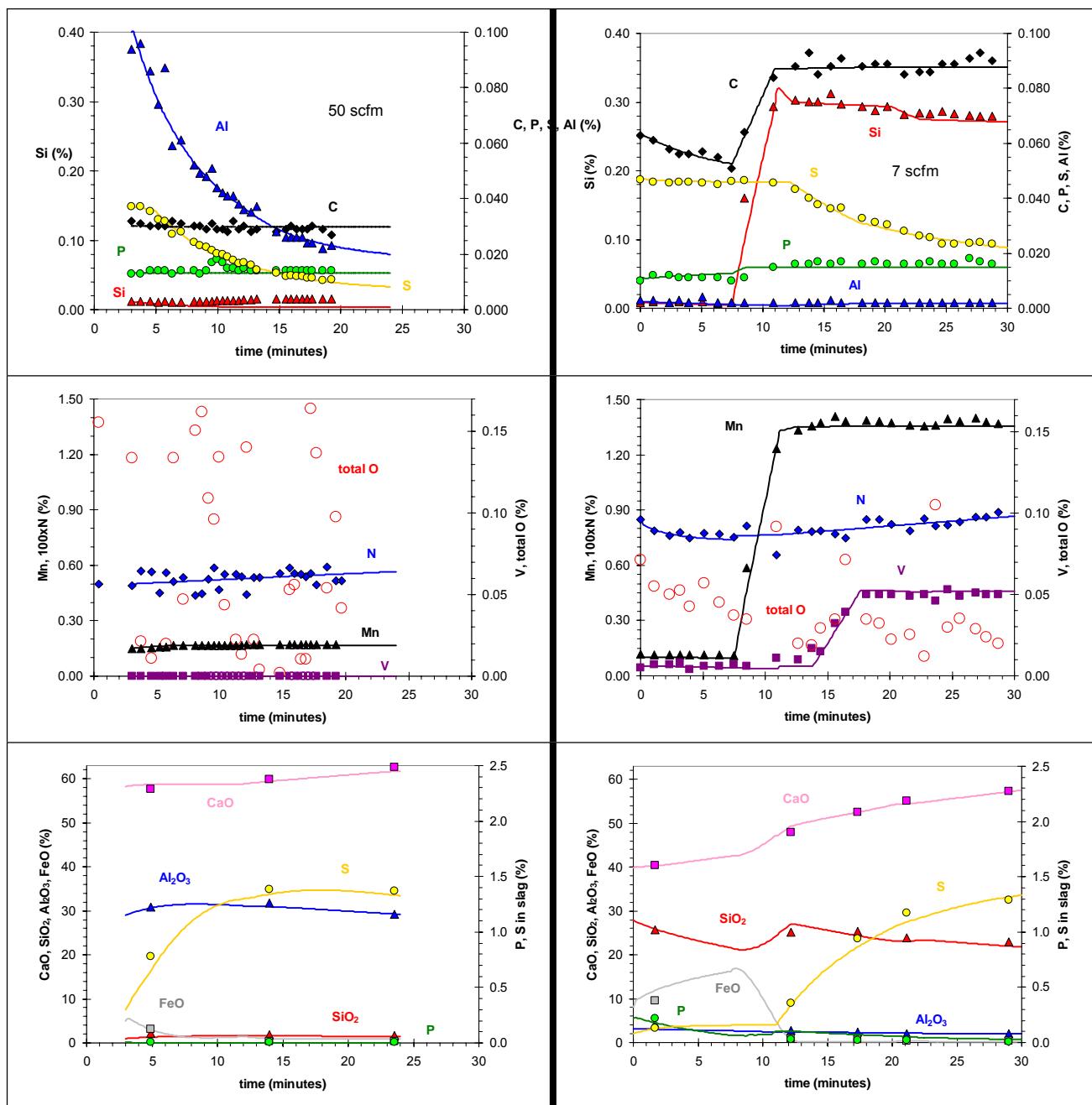


Figure 36a: Data and simulation results from heat 8

Figure 36b: Data and simulation results from heat 16

Al-killed steel was produced with heat 8. Aluminum was added during the first 3 minutes of the treatment. Lime was added after the first minute (1000 lbs), the eight minute (785 lbs), and the 15th minute (800 lbs), increasing the basicity of the slag and aiding desulfurization (de-S). 500 ft of Al-wire was added after the last steel sample was taken shortly before the ladle left the LMF. Al decreased from

0.094% to 0.023% and S decreased from 0.037% to 0.011% while steel samples were taken. The Al_2O_3 content in the slag slightly decreased during the treatment because lime was added. This decrease reduced the activity of Al_2O_3 , resulting in rapid de-S. The rate of de-S was also enhanced by the decrease of the FeO content from 5% to 1% during the first 5 minutes after the kill. The activity coefficient of FeO was decreased from 1.9 to 1.0 at the 5th minute during the simulation. A total of 350 lbs of iron oxide (Fe_2O_3) had to be artificially added during the simulation in order to reproduce the decrease of the aluminum concentration. The sulfur content of the slag increased from 0.3% to 1.4%.

The concentration of carbon and phosphorus did not change while samples were taken. Their concentrations were 0.030% and 0.014% respectively. Alloys were not added to the steel during the treatment of this heat. The manganese increased slightly due to the reduction of MnO during and after the kill. The Si concentration increased from 0.012% to 0.015% during the treatment, indicating the reduction of SiO_2 from the slag. However, the simulation could not predict the Si-reversion.

The nitrogen increased from 50 ppm to 55 ppm over a period of 20 minutes due to the open stirring eye where the steel is exposed to the air. The steel was not heated with the electrodes during the entire treatment since the temperature of the steel was 3010°F at the end of the kill and 2936°F after 19 minutes. The total oxygen varied between 22 ppm and 1700 ppm during the entire treatment time, while the dissolved oxygen was measured to be 4.2 ppm. The “shot-gun” pattern of the total oxygen indicates that significant slag is entrapped in the steel as an emulsion, qualitatively reproducing the results from Lachmund et al⁷².

The total oxygen varied between 120 ppm and 1050 ppm during the treatment of heat 16 while Si-deoxidized steel was produced. These results agree with previous measurements reported at LMF 2. The lower maximum total oxygen (as compared to heat 8) could be an indication that the slag/steel emulsion is less at lower argon flow rates. However, the nitrogen increase during steel treatment does not seem to be a function of argon flow rate, the size of the open eye, nor the duration of arcing. The nitrogen increased at the same average rate (0.25 ppm / min) during heat 16 as during heat 8. The nitrogen increased from 80 ppm before the 7th minute to 86 ppm after 30th minute. Heat 16 was periodically arced, maintaining an average steel temperature of 2850°F.

The nitrogen slightly decreased from 84 ppm to 80 ppm during the first seven minutes of the treatment of heat 16 due to a carbon boil. The carbon decreased from 0.063% to 0.051% during the boil. The only steel treatment during this time was argon stirring and the addition of 120 lbs of lime. The simulation predicted that the FeO content of the slag increased from 8% to 16% during these seven minutes. A FeO concentration of 9.5% was measured after the second minute. Prolonged argon stirring before the addition of deoxidants and alloys is usually not practiced. It was done during the trials to test the amount of carbon that could be removed with such a practice within a reasonable time.

The FeO concentration of the slag decreased within four minutes to a value of 0.9% while 4682 lbs of SiMn, 264 lbs of FeSi, 375 lbs of spar, and 500 lbs of lime were added. The low FeO concentration was necessary for de-S to start around the 12th minute. The FeO activity coefficient was decreased from 2.6 to 1.4 at the 11th minute during the simulation. The phosphorus increase (0.002%) during alloy additions originated to 80% from the SiMn, which contained 0.45% P while the rest of the phosphorus increase was due to reversion from the slag. The carbon content of the steel increased from 0.051% to 0.088% during the alloy addition because the SiMn contained 1.9% C. The SiO_2 content of the slag increased during deoxidation of the steel while the MnO concentration decreased. The SiO_2 concentration decreased after

deoxidation due to continuous lime additions, decreasing the activity of SiO_2 and supporting rapid de-S. The CaF_2 content of the slag increased to 9.3% during the alloy additions and decreased afterwards to a final value of 6.0% due to continuous lime additions and evaporations. The CaF_2 concentration of 0.7% before the addition of spar indicates that approximately one-half of a ton of slag from the previous heat was left in the ladle.

Vanadium (100 lbs) and MgO (40 lbs) were added after the 14th minute, increasing the vanadium concentration to its final value of 0.051%. Part of the scull from the LMF roof fell into steel around the 20th minute, supplying iron oxide to the system. It was estimated that 230 lbs of Fe_2O_3 entered the ladle at this time as this amount was added to the model to reproduce the measured concentrations. The supply of iron oxide caused a decrease of the silicon concentration in the steel and a slowing of the de-S rate, in spite of the 78 ft of CaSi wire that was added two minutes after the oxidized scull fell into the steel.

Correlation Between the Mass Transfer Rate Constant and the Specific Stirring Power

The mass transfer rate constants of all 20 heats together with the corresponding argon flow rates and specific stirring powers are listed in Table X. Previous researchers^{72,75-75} compared the mass transfer rate constant to the specific stirring power (ϵ). The specific stirring power is a function of the argon flow rate at standard temperature and pressure (Q), the steel mass (m), the injection depth of the argon (h), the ambient pressure above the bath (P_o), and the absolute steel temperature (T). Metric units are required when the stirring power formula is used as it is written in Equation 43. The specific stirring power has the unit watts per metric ton (W/mt). Lehner⁷ published a derivation of the stirring power formula, accounting for the buoyancy work and pressure-volume work that is transferred to the steel during the rise of gas bubbles. The stirring power formula assumes that each steel particle receives the same, average amount of kinetic energy during the time of argon stirring.

$$\epsilon = 14.23 \frac{QT}{m} \log_{10} \left(1 + \frac{h}{1.5P_o} \right) \quad (43)$$

Table X: Measured argon flow rates, calculated specific stirring powers and mass transfer rate constants

LMF 1															
Heat number		1	2	3	4	5	6	7	8	9	10	11	12		
Ar	scfm	60	61	63	63	63	52	61	50	56	61	55	62		
ε	W/mt	159	160	165	165	171	136	159	135	148	162	146	164		
K	min ⁻¹	0.19	0.18	0.18	0.20	0.20	0.17	0.17	0.18	0.20	0.20	0.16	0.21		
LMF 2															
Heat number		13			14	15	16	17			18			19	20
Ar	scfm	2	4	6	15	4.5	7	10	0	4	13	0	4	13	8
ε	W/mt	6	13	19	47	14	23	32	0	13	42	0	13	42	26
K	min ⁻¹	0.05	0.05	0.11	0.12	0.08	0.06	0.10	0	0.06	0.12	0	0.07	0.10	0.08

In the two LMF's studied, the specific stirring power is mainly a function of the argon flow rate and steel mass because the other factors are essentially fixed: the ambient pressure was always one atmosphere, the

absolute temperature varied little, and the argon was injected through the bottom of both ladles filled with approximately 10 feet of steel. The relationship of the mass transfer rate constant to the specific stirring power is shown in Figure 37 for the 26 different argon flow rates used during the treatment of 20 heats.

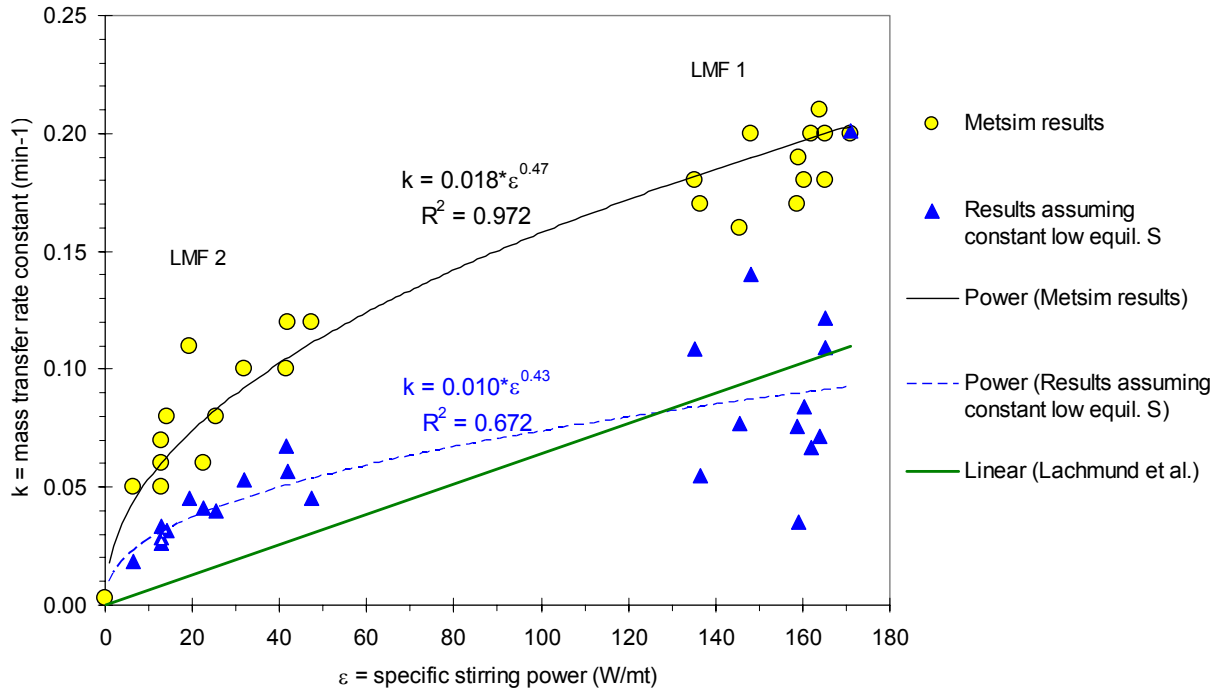


Figure 37: Relationship between mass transfer rate constant and the specific stirring power

$$k = 0.018\epsilon^{0.47} \quad (44)$$

$$k = 0.010\epsilon^{0.43} \quad (45)$$

The circles in Figure 37 represent the values of the mass transfer rate constants that were calculated with Metsim. Equation 44 ($R^2 = 0.97$) describes the relationship between the specific stirring power and the Metsim values as a power function with an exponent of 0.47. This relationship was expressed with similar power functions by previous researchers. Ghosh⁷⁵ and Qu⁷⁶ published summaries of the results from previous work. The reported exponents for industrial reactors range between 0.27 and 1.0 with an average of 0.54.

The triangles in Figure 37 represent the exponent of Equation 42 calculated by fitting an exponential function to the recorded times and the differences between the measured sulfur concentrations and the final equilibrium sulfur concentration. The final equilibrium sulfur concentrations were calculated with FactSage and ranged between 3 ppm and 41 ppm for both types of steels. Equation 42 assumes that the equilibrium sulfur concentration at the slag/steel interface is constant and at its final value during the entire refining time. This assumption is incorrect because simulation results show that the equilibrium sulfur concentration at the steel/slag interface at the start of de-S is up to 50% of the initial bulk sulfur concentration, depending on the activity of the FeO in the slag at this time and the choice of deoxidant

(Al or Si). If the assumption of a constant, low value of the equilibrium sulfur concentration was correct, there would be a weak correlation between the mass transfer rate constant and the specific stirring power, especially for data from LMF 1 (Al-killed steel).

Equation 45 ($R^2 = 0.67$) describes the relationship between the specific stirring power and the values that were calculated with the assumption of a constant, low equilibrium sulfur concentration as a power function with an exponent of 0.43. The values of the mass transfer rate constants that are predicted by Equation 4b are lower than those values calculated by Equation 44 but similar to results from Lachmund et al⁷² (straight line in Figure 37).

The current work could approximately reproduce the average of the published exponents (~ 0.5) for the power function (Equation 44) that describes the relationship between the mass transfer rate constant and stirring power. These results point to a square-root relationship between the mass transfer rate constant and the stirring power.

$$\tau = \frac{1}{m} \sqrt{14.23 \frac{QTA_{top}}{N^{1/4}} \log_{10} \left(1 + \frac{h}{1.5P_o} \right)} \quad (46)$$

Equation 46 defines the “specific steel transport rate” (τ). This name was chosen because it includes the argon flow rate as well as the change of momentum that the argon flow rate can transfer to the steel to make it flow (transport). The force that is transferred to the steel by a specific argon flow rate increases if the steel mass is minimized and if the top area and injection depth are maximized. The unit of the specific steel transport rate includes the change of momentum of the steel in Newtons (N), the argon flow rate in cubic meters per second (m^3/s), and the steel mass in metric tons (mt). Equation 46 predicts a square-root relationship between the mass transfer rate constant and the argon flow rate and it implies that the shape of an ideal refining vessel is a cone.

A cone-shaped reactor would minimize the amount of steel that needs to be transported by the argon flow while maintaining a sufficient top area to maximize slag/metal reactions and a sufficient fill height to maximize the power input from the argon flow. It maximizes the fraction of the steel that is highly stirred because the largest velocities, turbulences, and energy dissipation rates occur within the plume and in the vicinity of the slag/metal interface, which make up a larger fractional volume of a cone as compared to a cylinder.

Specific Steel Transport Rate

The specific steel transport rates of the 20 heats and 26 argon flow rates are plotted against the Metsim-calculated mass transfer rate constants in Figure 38. The relationship between these two variables is Equation 47 ($R^2 = 0.96$), which requires metric units and the argon flow rate at STP. The y-intercept of Equation 47 is zero, indicating that the parameters that influence emulsification do not affect the mass transfer rate constant for the production conditions of these two LMF's. This conclusion agrees with the calculations from El-Kaddah and Szekely⁷⁴.

$$k = \frac{0.08}{m} \sqrt{14.23 \frac{QTA_{top}}{N^{1/4}} \log_{10} \left(1 + \frac{h}{1.5P_o} \right)} \quad (47)$$

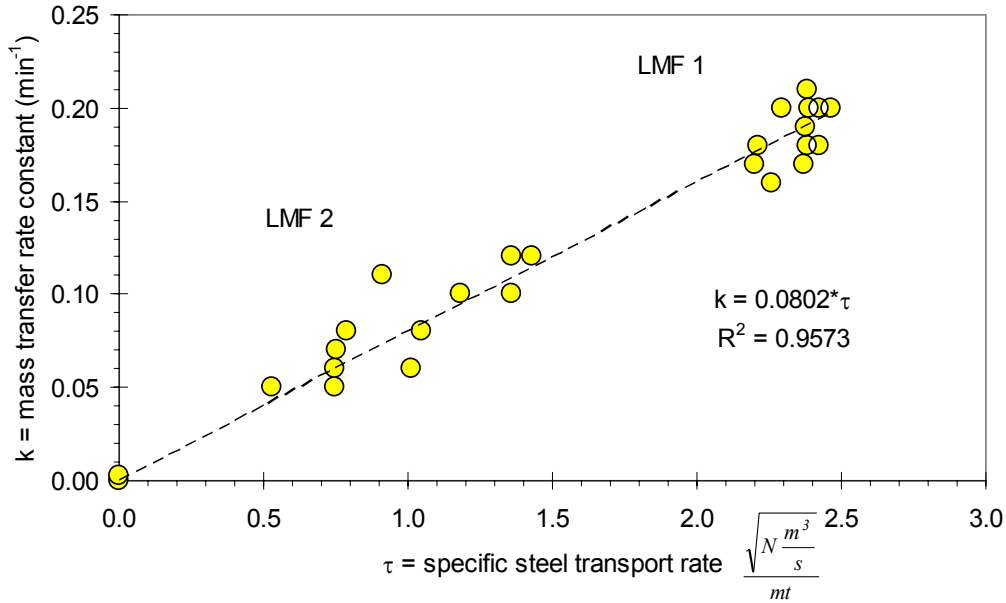


Figure 38: Relationship between mass transfer rate constant (Metsim) and the specific steel transport rate

Thermodynamic Factors that Affect Reaction Rates

Large reaction rates not only require frequent transport of steel to the slag/steel interface (e.g. large τ) but also thermodynamical conditions at the slag/steel interface that favor desired reactions (e.g. de-S). The thermodynamic equilibrium on the slag/steel interface was different for each heat, causing different de-S rates for similarly stirred heats.

The rate of de-S and the change of Al, Al_2O_3 , and FeO concentrations during the treatment of heats 1 and 5 are shown in Figure 39 from the start of de-S until the end of the ladle treatment at LMF 1. The mass transfer rate constant was 0.19 min^{-1} during the treatment of heat 1 and 0.20 min^{-1} during the treatment of heat 5. The bulk sulfur and aluminum concentrations decreased linearly at a rate of 0.001 \%S per minute and 0.002 \%Al per minute during steel refining of heat 1; whereas these concentrations decreased exponentially at an average rate of 0.003 \%S per minute and 0.005 \%Al per minute during the treatment of heat 5. The FeO content before de-S was 12.4% in the slag of heat 1 and 3.2% in the slag of heat 5. The Al_2O_3 content of the slag from heat 1 increased from 19% to 34% during the first twelve minutes of de-S and the Al_2O_3 content of the slag from heat 5 was approximately 35% during the entire time of de-S. The basicity (B) of the liquid slag before de-S was 3.3 for heat 1 and 2.4 for heat 5. The basicity (B) was calculated according to Equation 48, using the weight percent of liquid slag components based on measured slag concentrations and FactSage calculations.

$$B = \frac{\text{CaO} + 1.4\text{MgO}}{\text{SiO}_2 + 0.6\text{Al}_2\text{O}_3} \quad (48)$$

Sulfur decreased at a slow constant rate during the treatment of heat 1 while it decreased at a fast exponential rate during the treatment of heat 5. The high FeO concentration during de-S and the high slag basicity before the de-S caused the low de-S rate during the refining of heat 1 although it was stirred as strongly as heat 5. A high basicity of the slag decreases the activity coefficient of the FeO, slowing the reduction of the FeO by the aluminum. The aluminum decreased slower during heat 1 as compared to

heat 5 although the initial FeO concentration was four times larger. The aluminum decreased at a fast, exponential rate during refining of heat 5, reducing the FeO that was produced on the slag/steel interface due to sulfur reduction. The addition of 750 lbs of bauxite to the slag of heat 1 during the first four minutes of de-S as compared to 250 lbs of bauxite addition before the Al-kill of heat 1 also hindered the de-S reactions at the slag/steel interface. The late bauxite addition raised the Al_2O_3 concentration of the slag, increasing the activity of Al_2O_3 , which is a reaction product of de-S. In addition, the bauxite contained 26% hematite, adding to the FeO of the slag.

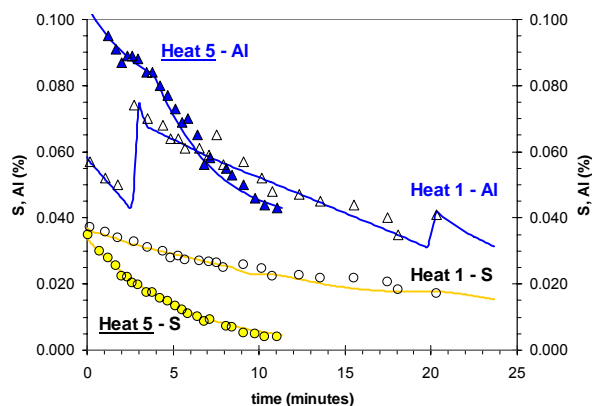


Figure 39a: S and Al conc. of heats 1 and 5

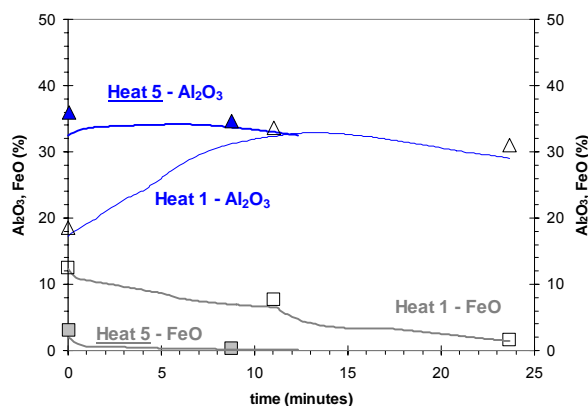


Figure 39b: Al_2O_3 and FeO conc. of heats 1 and 5

The FeO content of the slag during de-S influences the rate of de-S. Figure 40 illustrates the de-S reactions at the slag/steel interface together with the reactions that include the FeO from the slag. Iron oxides are supplied to the slag/steel interface by the reduction of sulfur, by the liquid FeO, by the air, and by sources that include bauxite, solid oxidized slags, refractory corrosion, and an oxidized scull on the equipment such as the LMF roof. The existing liquid FeO may originate from EAF carry-over slag, slag from the previous heat (estimated to be $\frac{1}{2}$ ton), oxidized steel heel from the previous heat, and iron oxides produced during the cleaning of the porous plug and/or tap hole. These iron oxides need to be reduced by the deoxidant (in this case Al) for de-S to proceed.

The reduction of sulfur also needs free oxygen anions or a basic slag, requiring the addition of lime after de-O. Lime additions not only increase the basicity of the slag but they also sustain de-S by maintaining or decreasing the concentration of Al_2O_3 or SiO_2 . However, the increase of basicity causes a decrease of the activity coefficient of FeO. The decrease of the activity coefficient of FeO during lime additions makes it increasingly more difficult to reduce the FeO after the de-S started. In addition, the ratio of Fe^{3+} and Fe^{2+} cations in the liquid slag increases with increasing basicity, sustaining the supply of oxygen from the air, through the slag, to the slag/steel interface. Consequently, de-S rates are increased if the FeO is reduced before the basicity of the slag is raised with lime. This procedure was practiced during the treatment of heat 5 but not during the treatment of heat 1.

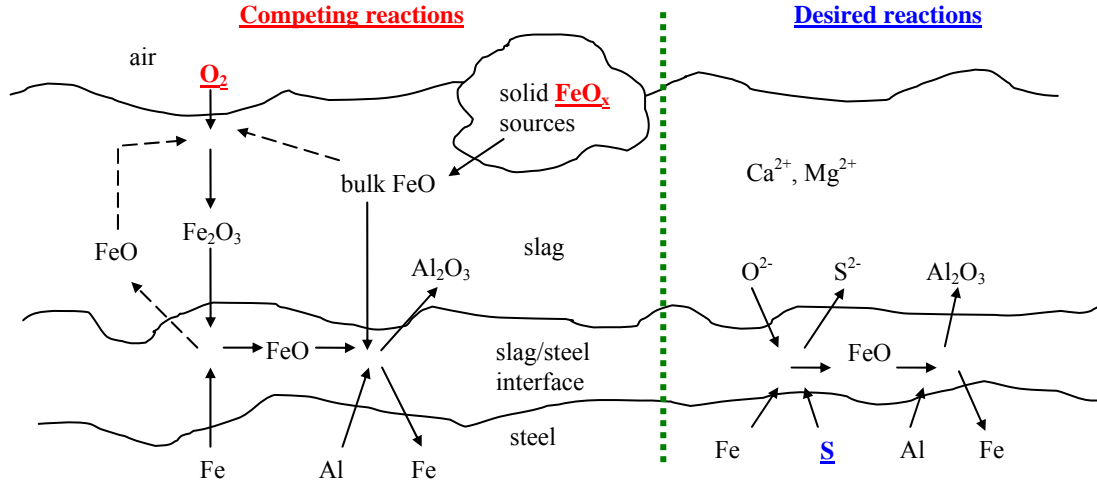


Figure 40: Desired de-S reactions and competing reactions within slag and slag/steel interface

Apparent Reaction Order

High FeO concentration and basicity before de-S decreased the driving force ($C-C_{eq}$) more during the beginning of de-S than during the end of refining. This decrease resulted in a linear, slow reduction of the bulk sulfur concentration because the driving force remained effectively constant during de-S, implying a zero-order de-S reaction with respect to the driving force. However, Equation 41 assumes that de-S is a first-order reaction with respect to the driving force. The exponents that were calculated with Equation 41 were lower than the MetSim calculated mass transfer rate constants. The “apparent reaction order” (r) was defined as the quotient of the exponent from the line fit and the mass transfer rate constant (Equation 49). It ranged between 0.18 (heat 1) and 1.00 (heat 5).

$$r = \frac{\text{exponent from line fit}}{k} \quad (49)$$

The bulk sulfur concentration decreased at a fast and exponential rate when the apparent reaction order was high or when the basicity and the FeO concentration were low before de-S started, indicating a relationship between the apparent reaction order and the basicity and FeO concentration. Equation 50 is the result of a line fit between the apparent reaction order of heats 1 to 12 (LMF 1), producing Al-killed steel, and ratio of the inverse exponential of the B-ratio (e^{-B}) and the %FeO as measured before de-S. Equation 51 shows the result of a similar line fit for heats 13 to 20 (LMF 2), producing Si-deoxidized steel and using spar. The inverse exponential of the B-ratio (e^{-B}) was used because it is approximately proportional to the activity coefficient of FeO. The relationships of Equations 50 and 51 and the corresponding data are shown in Figure 41. The B-ratio, the concentration of FeO as measured before the start of de-S are listed with the apparent reaction order and mass transfer rate constants in Table XI for all 20 heats.

$$r_{Al} = 0.2 + \frac{28e^{-B}}{\%FeO} \quad (50)$$

$$r_{\text{Si}/\text{CaF}_2} = 0.31 + \frac{2.6e^{-B}}{\% \text{FeO}} \quad (51)$$

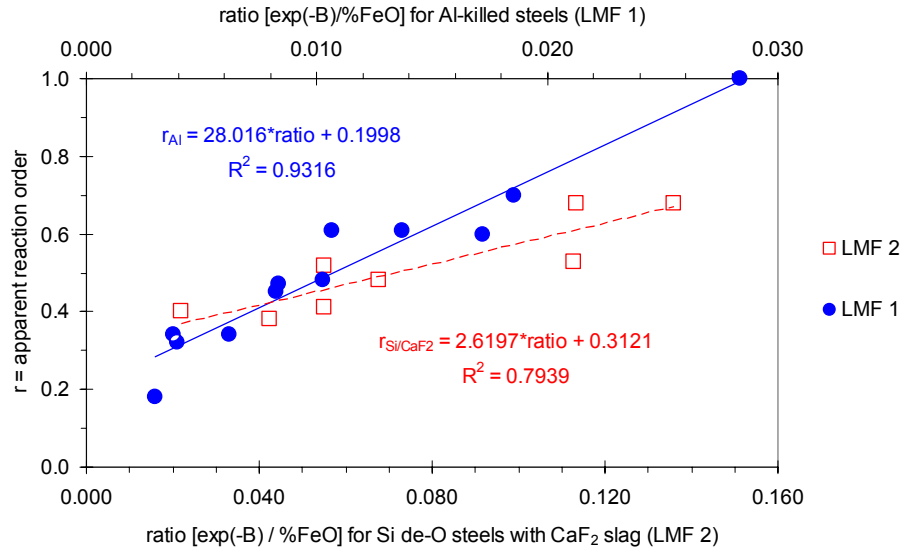


Figure 41: Relationships of Equations 50 (LMF 1) and 51 (LMF 2) with data from Table XI

The basicity and the concentration of the FeO before de-S are lower for Si-deoxidized steel as compared to Al-killed steels for the same value of the apparent reaction order. The average B-ratio is 1.9 for Si-deoxidized steels (LMF 2) and 2.6 for Al-killed steels (LMF 1) because the slag of the heats from LMF 2 contained up to 10% spar. Spar (CaF_2) is a strong base but it is not a part of the B-ratio. The average FeO concentration before de-S is 3.1% in Si-deoxidized steels (LMF 2) and 9.0% for Al-killed steels (LMF 1) because the silicon is a weaker deoxidizer than the aluminum, requiring a lower FeO concentration before de-S can start. The lower affinity of silicon to oxygen causes the formation of SO_2 until the partial pressure of oxygen at the slag/steel interface and the FeO concentration of the slag are decreased. A peak of SO_2 in the off-gas is reported to be observed at the beginning of the ladle treatment at LMF 2.

The wide range of the exponents that were obtained from a line fit of the de-S data from Al-killed steels (LMF 1) in Figure 37 could be explained with the deoxidation strength of aluminum. The use of aluminum makes it possible to start the de-S at higher FeO concentrations as in Si-deoxidized steel when lime is added early. However, lime additions (beyond tap additions) before the FeO is reduced prolong the necessary time to achieve the final bulk sulfur concentration. The exponents from the line fit of de-S data from Si-deoxidized steels (LMF 2) in Figure 37 approximately follow the trend line, indicating that a similar low FeO concentration at the beginning of de-S is necessary for Si-deoxidized heats. A low basicity of the slag until the FeO is reduced improves de-S rates as well. The addition of lime and spar approximately five minutes after the addition of SiMn and FeSi would support rapid FeO reduction.

Decarburization of the Steel During Argon Purging

Heats 13 through 20 were argon purged during the first five to nine minutes of the treatment at LMF 2, causing a decrease of the carbon concentration that ranged between 0.005 %C (heat 18) and 0.012 %C (heat 13). The treatment of the steel during this time was argon stirring and arcing during a maximum of

64% of the purging time. The lime addition during de-C was 120 lbs during heats 14 and 16 and no lime for the other six heats. FeSi, SiMn and additional fluxes were added after de-C.

Table XI: B-ratios and %FeO after de-O (before de-S), apparent reaction order (r) and mass transfer rate constant (k)

Constant (a)

LMF 1															
Heat number		1	2	3	4	5	6	7	8	9	10	11	12		
B ratio		3.3	2.3	2.5	2.5	2.4	2.9	2.5	2.9	2.3	3.1	2.5	2.4		
% FeO		12.4	12.0	6.0	7.7	3.2	14.0	10.0	3.2	5.4	12.0	8.0	14.6		
r		0.18	0.47	0.61	0.61	1.00	0.32	0.45	0.60	0.70	0.34	0.48	0.34		
k	min ⁻¹	0.19	0.18	0.18	0.20	0.20	0.17	0.17	0.18	0.20	0.20	0.16	0.21		
LMF 2															
Heat number		13			14	15	16	17			18			19	20
B ratio		1.8			1.8	1.5	2.1	2.0			2.0			2.4	n/a
% FeO		3.0			3.9	10.2	0.9	1.2			2.0			0.8	
R		0.52	0.52	0.41	0.38	0.40	0.68	0.53	-	0.53	0.48	-	0.48	0.68	0.65
k	min ⁻¹	0.05	0.05	0.11	0.12	0.08	0.06	0.10	0	0.06	0.12	0	0.07	0.10	0.08

Figure 43 shows that the de-C rate was highest (0.0025 %C /min) when the FeO concentration increased by 5.0% during the argon purge (heat 13) and lowest (0.0006 %C /min) when the FeO concentration decreased by 2.0% (heat 18). The change of the FeO concentration was controlled by the duration of arcing so that the rate of de-C was actually a function ($R^2 = 0.85$) of the percentage of time that the heat was arced during purging. Long times of arcing reduced the de-C rate, independently of the argon flow rate.

The increase of the FeO concentration of the slag and the decrease of carbon concentration of the steel were caused by the transfer of oxygen from the air, through the slag, into the steel. The mechanism was illustrated in Figure 40. The arcing with carbon electrodes reduced the FeO in the slag and hindered the transfer of oxygen from the air into the slag, inhibiting a carbon boil below the slag. The carbon boil was sustained when arcing was stopped, indicating that solid sources of iron oxides (e.g. oxidized solid slag) were not the source of the FeO increase because solids would have preferable been melted during arcing.

The measured concentration changes of deoxidants (Al or Si), sulfur, vanadium, manganese, MnO, and FeO indicated oxidation and required the artificial addition of 53 lbs (heat 5) to 540 lbs (heat 12) of Fe₂O₃ to the slag as an oxygen source during each Metsim simulation. On the average, 90 lbs or two gallons of Fe₂O₃ were added during simulation of each heat, independently of the FeO concentration in the slag. This artificial addition represents the iron oxide from sources including solid slags, refractory corrosion, or miscellaneous sources such as an oxidized scull from the LMF roof. In addition, an average of 1.4 lbs of Fe₂O₃ was artificially added per minute of refining time for each percent of FeO in the slag, indicating the increase of the oxygen transfer from the atmosphere through the slag to the slag/steel interface with increasing FeO concentration.

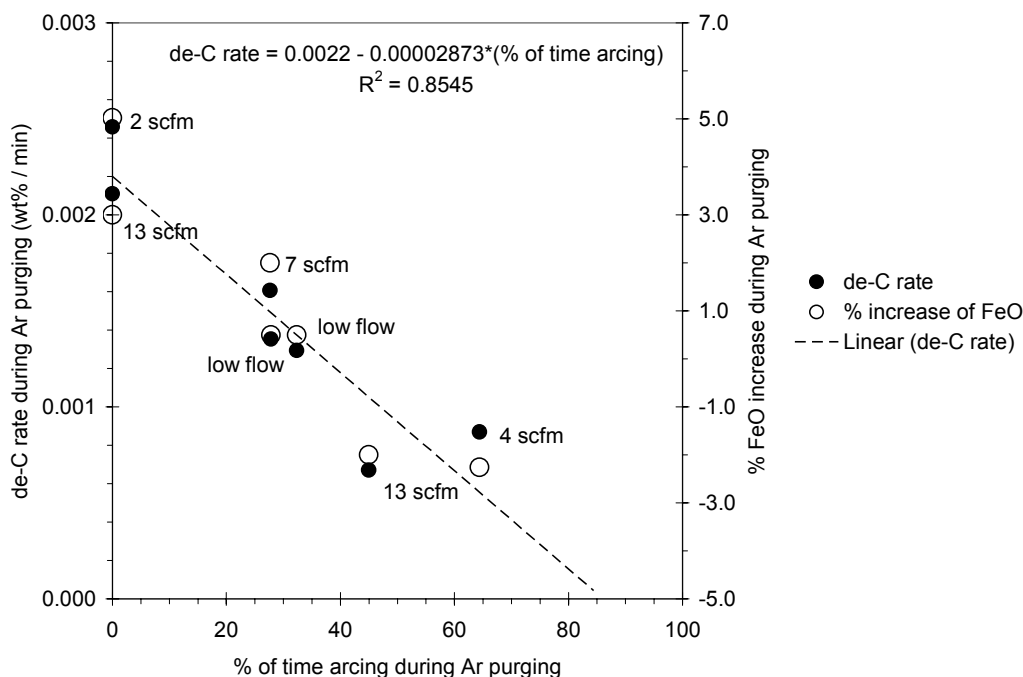


Figure 43: De-C rate as a function of FeO change and duration of arcing during argon purge

Summary of Findings - Experimental Study of Reaction Kinetics in Industrial Reactors

The process simulation program Metsim and the thermodynamical program FactSage were used to model and simulate ladle refining at two different LMF's, refining Al-killed and Si-deoxidized steels. The simulations accurately reproduce measured steel and slag concentrations during the treatment of twenty heats, determining 26 mass transfer rate constants. The relationship between the mass transfer rate constant (k) and the argon flow rate, ladle geometry, ambient pressure, as well as steel temperature is best described with the specific steel transport rate (Equation 47).

The reaction kinetics during ladle refining depend on the bulk transport of the steel to the slag/steel interface (k) and the thermodynamical equilibrium at the slag/steel the interface. Desulfurization reactions are slow and nearly zero-order reactions with respect to the driving force ($C-C_{eq}$) if the FeO concentration of the slag is not reduced before the start of de-S and when the activity coefficient of FeO is low during the deoxidation reactions. Lime additions (beyond tap additions) before the FeO is reduced prolong the necessary time to achieve the final sulfur concentration because lime additions raise the basicity of the slag and therefore lower the activity coefficient of the FeO. Lime needs to be added to start and to sustain de-S. Lime additions raise the basicity of the slag and decrease or maintain the Al_2O_3 or SiO_2 concentrations.

The iron oxide content in the ladle before and during refining should be minimized because iron oxides need to be reduced before de-S can proceed. More oxygen enters the steel from the air through the slag than through the open eye if the slag contains more than 2 wt% FeO. The transfer of oxygen from the air through slag to the slag/steel interface is large enough to sustain a carbon decrease of 0.0025 %C per minute. The average nitrogen increase during argon stirring is 0.25 ppm N per minute.

Design of Novel, Scrap-Based, Fully Continuous Steelmaking Process

The proposed continuous steelmaking process, as shown in Figure 44, is designed to replace a steelmaking shop that currently uses an Electric Arc Furnace (EAF), a Ladle Metallurgy Furnace (LMF), and a Continuous Caster (CC). The process is designed to allow for variation of the production rate as required between 70 t/hr and 170 t/hr, making the process flexible to changing demands. It is estimated that the process could operate for one week or longer without interrupting the steel production with an expected weekly maintenance downshift of 8-12 hours.

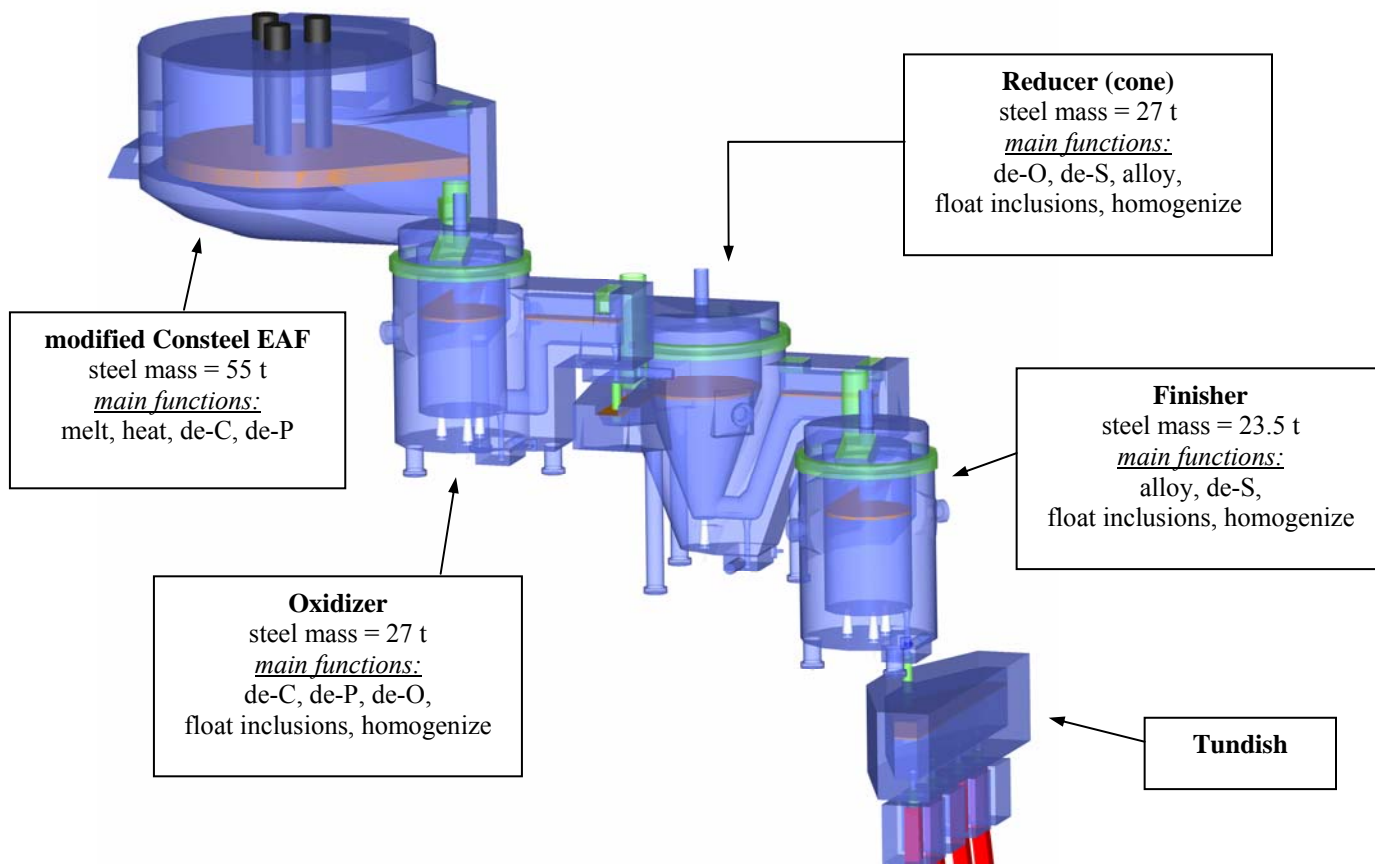


Figure 44: Transparent side view of the fully continuous steelmaking process (right side)

Steel will continuously flow through five interconnected vessels during the operation of the continuous steelmaking process. Preheated scrap will be continuously charged and melted in the first vessel (modified AC Consteel EAF). Melting will be accomplished with electrical and chemical energy while maintaining a foamy slag and performing preliminary de-C and de-P. Final de-C and de-P will be achieved in the second vessel (Oxidizer). Near-equilibrium conditions allow for a partial de-O of the steel

in the Oxidizer, depending on the required final carbon concentration. In the third vessel (Reducer), steel will be continuously de-O, de-S, and alloyed. The cone-shaped Reducer is designed to increase the kinetics and decrease the final sulfur concentration while maintaining a high production rate. Steel that has a composition that is close to the final chemistry will enter the fourth vessel (Finisher). The operations in the Finisher will include final trimming, additional de-S, inclusion floatation, and homogenization before the steel will flow into the fifth vessel (Tundish).

The vessels are designed for fast, near-equilibrium reactions to ensure a large degree of control, productivity, flexibility, and to reduce maintenance with oxidizing conditions in the first two vessels (EAF, Oxidizer) and reducing conditions in the Reducer and Finisher. A series of two vessels with similar near-equilibrium conditions allows for optimum refining and for the minimization of variations in fluid flow (residence time distributions) and composition (chemistry, inclusion), contributing to the reliability and flexibility of the process. The sequential refining and the near-equilibrium, steady-state operation of the continuous process allow for increased refining and reduced alloy and flux consumptions as compared to the current EAF-LMF steelmaking route.

The continuous steelmaking meltshop, as sketched in Figure 45, is projected to require less than one third of the footprint of a conventional meltshop, decreasing capital and operational costs, man-hours per ton of cast steel, and processing times. A typical scrap-based meltshop that uses a Consteel EAF is sketched next to the projected continuous steelmaking meltshop in Figure 45, illustrating the size difference between these two types of meltshops. The continuous steelmaking meltshop will be smaller than current meltshops because the transport and maintenance of ladles will be eliminated and because the size and amount of equipment will be reduced.

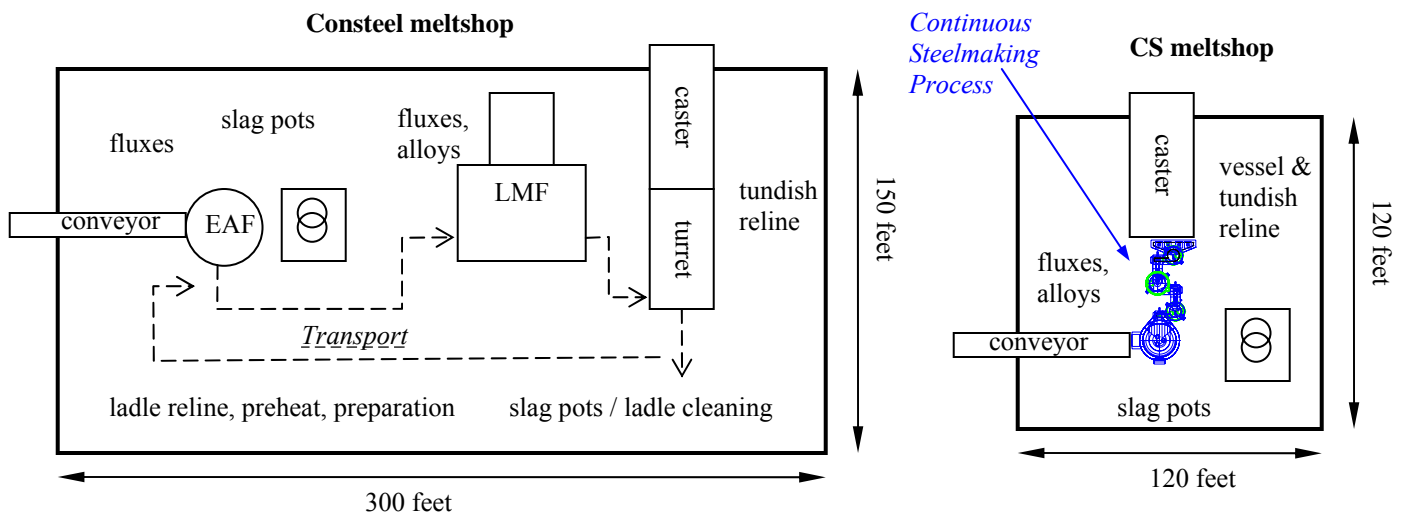


Figure 45: Comparison of current Consteel meltshop and new Continuous Steelmaking (CS) meltshop

The capacity of the EAF (55 tons) will be less than one-half of the size of a typical EAF that produces steel at a rate of 170 t/hr. The LMF and all the auxiliary equipment would be replaced by three small refining vessels, reducing the number of alloy and flux hoppers and eliminating one transformer and the associated energy. The elimination of ladles, including their transport and maintenance, results in the reduction of size and number of over-head cranes and their energy usage as well as the elimination of the

space and energy for cleaning, storing, transporting, relining, and reheating ladles. These changes not only reduce costs and auxiliary energy consumption but also increase safety because less heavy equipment will be moved during steel production and overhead transport of hot, liquid steel will be eliminated.

The continuous steelmaking process is compact, using approximately the same amount of space as a typical turret system at a continuous caster. The size of the continuous steelmaking design as compared to two 150-ton ladles, sitting in the casting and holding position of a turret, is illustrated in Figure 46 and 47. Figure 46 shows that the new design would occupy approximately one thousand square feet in front of the caster. It is shown in Figure 47 that the top of the EAF would be approximately 30 feet above the tundish or 15 feet above the top of a ladle, sitting in the casting position.

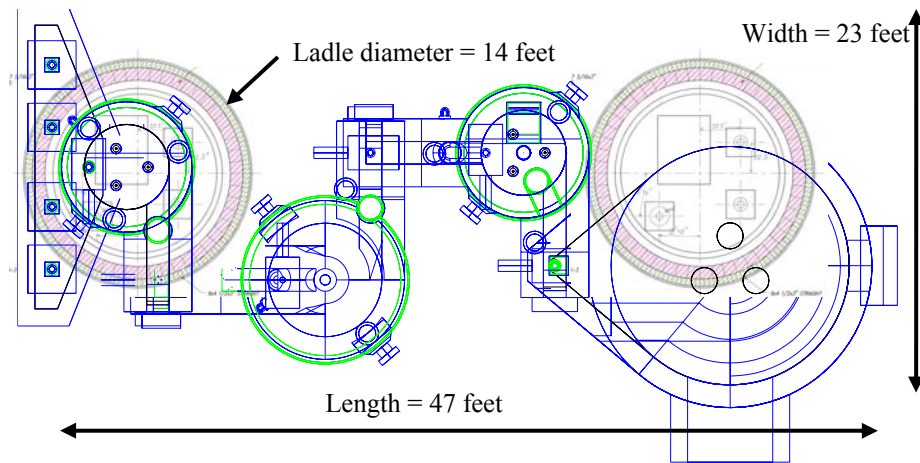


Figure 46: Top view of continuous steelmaking superimposed on two ladles sitting on a typical turret

Description of Modified Consteel EAF (vessel 1)

Preheated scrap and fluxes will be charged continuously into a modified AC Consteel EAF as illustrated in Figure 48. Preheating the scrap reduces the size of the vessel by minimizing the amount of required electrical energy. By charging and tapping continuously, the furnace will run with 100% power-on and a constant 55-ton liquid heel (full furnace). An AC power supply was chosen to avoid the maintenance of a bottom electrode, increasing the duration of continuous campaigns.

The inner diameter of the furnace is 13.8 feet and the fill height is 2.3 feet. The tap hole is 4 inches in diameter, similar to the tap holes in vessels 2 through 4. The EBT bottom is lowered so that it is level with the lowest point of the furnace. This modification together with the constant high fill height eliminates the carry-over slag during steady-state operation and it allows for the complete draining of the EAF into the Oxidizer without tilting the furnace. The flow from the EAF into the inlet launder of the Oxidizer will be regulated by a slide gate.

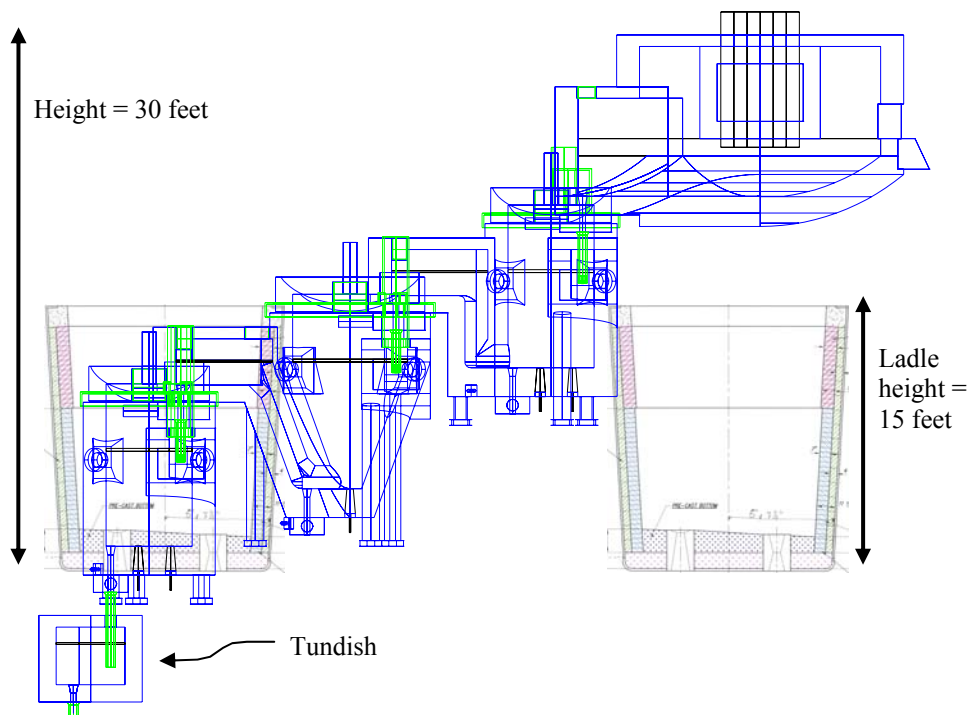


Figure 47: Left-side view of continuous steelmaking superimposed on two ladles sitting on a typical turret

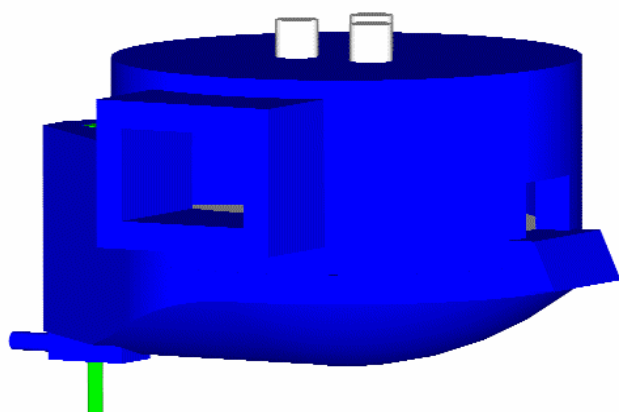


Figure 48a: Left-side view of modified Consteel EAF

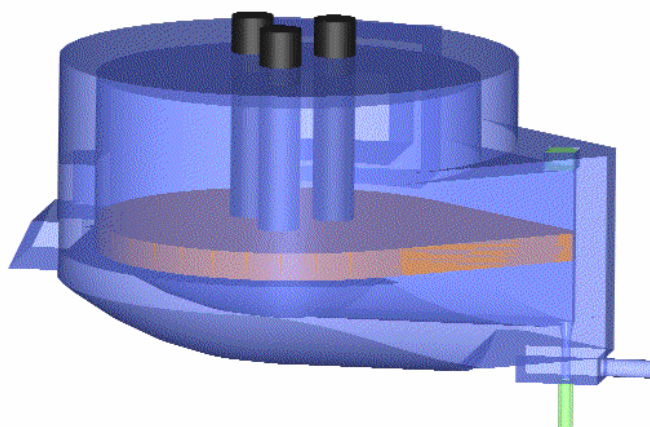


Figure 48b: Transparent right-side view of vessel 1

Description of Oxidizer (vessel 2)

Additional de-C and de-P will be accomplished in the 27-ton Oxidizer shown in Figure 49, allowing for high carbon content and iron yield in the EAF and low final carbon and phosphorus concentration. The steel enters the cylindrical vessels through a 1.3-ft wide by 4.0-ft long inlet launder that is located off-center to the main vessel, producing a swirl in the steel bath and minimizing the chance of short circuiting. The Oxidizer has an inside diameter of 4.9 ft and is designed to operate at a bath depth of 5.4 ft, providing 3.7 ft in freeboard above the bath. The bath will be stirred by injecting argon through three

bottom porous plugs, ensuring constant and homogeneous stirring even if one porous plug fails. Three porous plugs produce small bubbles, increasing the gas/steel interface to promote degassing reactions and the floatation of inclusions.

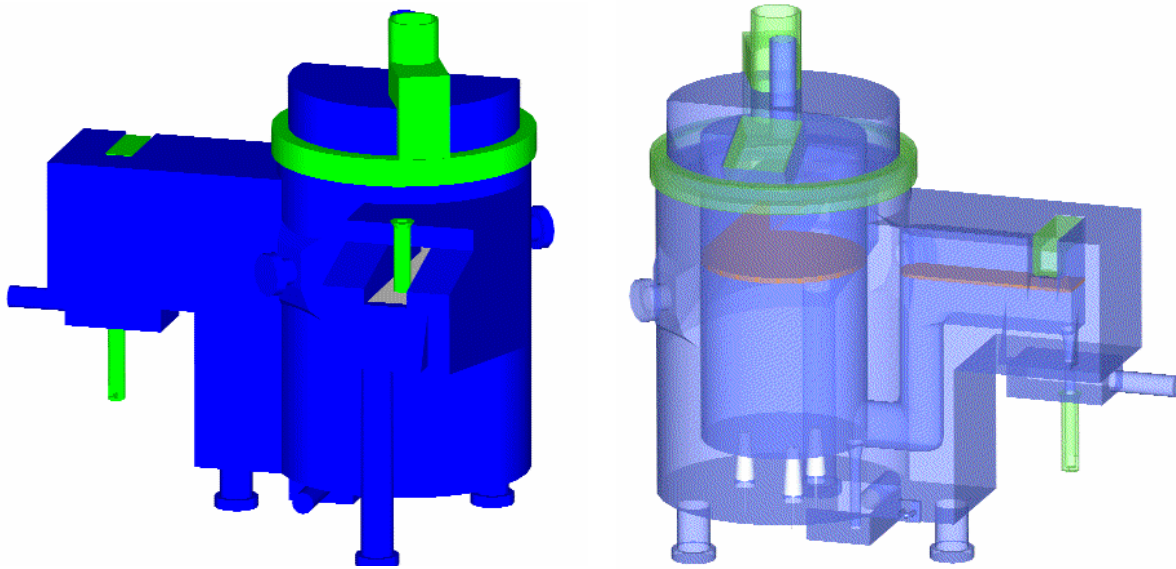


Figure 49a: Left-side view of Oxidizer (vessel 2) Figure 49b: Transparent right view of vessel 2

The metal exits the Oxidizer through a 1.3-ft wide by 5.5-ft exit channel, which is designed to remove steel from the vessel near the bottom to reduce short circuiting and slag carryover without requiring the height that would be needed with a bottom tap design. If required, the steel can be removed through a bottom tap hole or by pouring the steel through the inlet channel after the vessel is removed from its location and tilted by a crane. A door in the outlet channel allows for periodic renewing of the slag cover in this channel and for access to the tap hole that is equipped with a slide gate.

Spent slag will be continuously removed through the inlet launder. The inward stream of steel within the inlet launder creates an outward flow on the upper surface, continuously transporting the slag to an overflow and eventually into the slag pot placed below the inlet launder. Off-gases will be evacuated through a duct in the removable roof that rests on the main vessel. A door located in the angled part of the roof provides access and a mean of observation during operation. Fluxes (and alloys if required) are periodically added through the center of the roof.

The wall of the vessel is 16 inches thick, allowing for the placement of 9-inch refractories and 5-inch insulating bricks as well as the structural support of a steel shell. Magnesia-graphite refractory will be used for the slag line and the rest of the vessel will be lined with resin-bounded magnesia. These materials resist penetration because they have little porosity. Refractory losses associated with thermal cycling, erosion, and corrosion will be reduced as compared to ladle treatment because consistent temperature and chemical conditions exist in each refining vessel and because frequent forceful tapping streams and the cleaning of ladles with oxygen will be eliminated.

Description of Reducer (vessel 3)

The steel is deoxidized, desulfurized, and alloyed in the 27-ton Reducer illustrated in Figure 50. The steel enters the vessel in an inlet launder similar to the inlet launder used in the Oxidizer, which is designed to enhance homogenization of the bath. The conical-shaped vessel is designed with an upper inner diameter of 6.6 ft, a lower inner diameter of 1.3 ft, and an operating depth of 7.2 ft of steel, providing 3.7 ft of freeboard similar to the Oxidizer. Steel will be stirred with argon through one porous plug located in the bottom of the vessel. The top area of the steel bath is 34 ft², nearly twice the top area of the Oxidizer, which has similar tonnage capacity. The conical shape increases the fraction of the steel that is highly stirred and the slag/metal interface. These improvements maximize the energy input to the steel bath, the reaction rates, the sulfur removal, the homogenization of temperature and chemistry, as well as possible production rates.

In addition, the conical shape allows for concentration differences between subsequent grades because lowering the fill height during grade change to the level of the outlet tap hole results in the removal of half of the steel from the Reducer. The exit channels of the Oxidizer and Reducer are similar except that the emergency bottom tap hole of the Reducer is moved. Other similarities between the two vessels are the continuous deslagging through the inlet launder, the location of the alloy and flux chute, the wall design, and the ability to empty the vessel by tilting. The off-gas system is designed to provide improved control of the atmosphere within the Reducer by minimizing air infiltration.

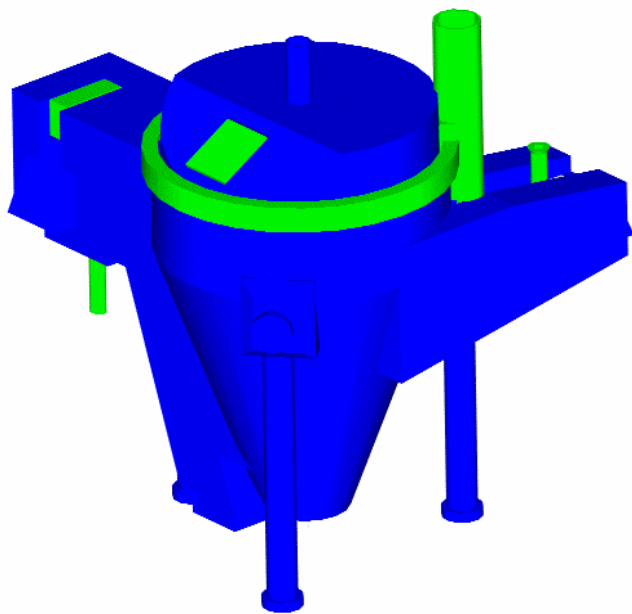


Figure 50a: Left-side view of Reducer (vessel 3)

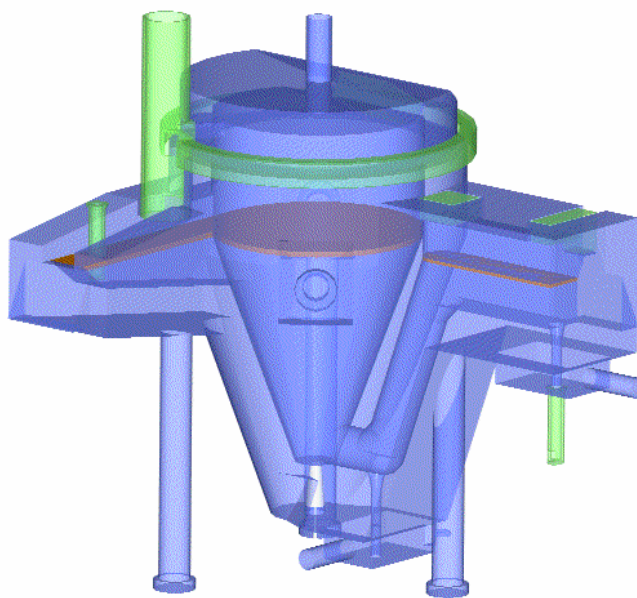


Figure 50b: Transparent right-side view of vessel 3

Description of Finisher (vessel 4)

Final alloying or trimming as well as additional de-S is performed in the 23.5-ton Finisher illustrated in Figure 51. The Finisher is similar to the Oxidizer except that the off-gas system is designed to minimize air entrapment and the steel is tapped through the bottom tap hole. Bottom-tapping allows for complete

emptying of the Finisher during grade changes similar to ladles in current casting operations. However, during normal operations, the steel level remains constant with continuous argon bubbling at low flow rates, maximizing chemistry and temperature homogeneity and the cleanliness of the steel. Auxiliary heating of the steel during refining is not required during normal operation of the continuous steelmaking process. If unexpected delays require additional heating, it could be done with a non-contact twin plasma torch³ in the Finisher by inserting the heater through the roof door.

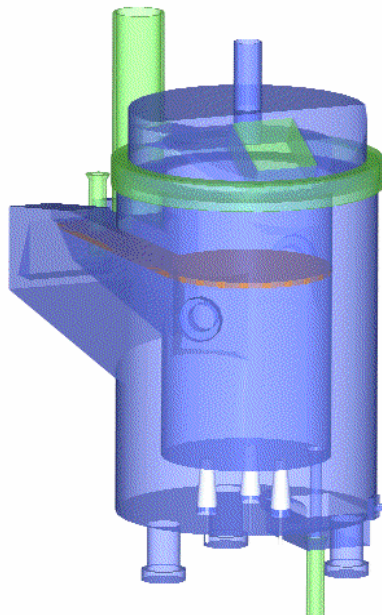
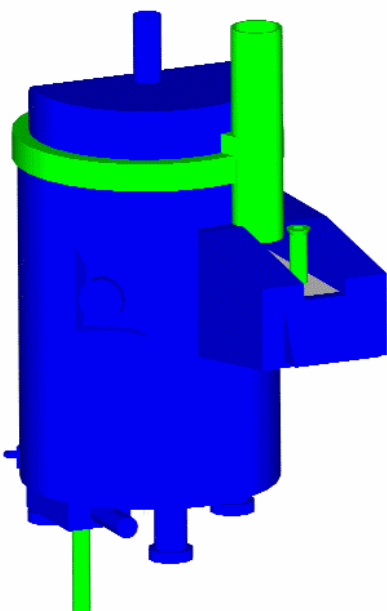


Figure 51a: Left-side view of Finisher vessel 4 Figure 51b: Transparent right view of vessel 4

Steady State Operation of the Continuous Steelmaking Process

The new process would make it possible to convert solid scrap to finished continuous cast product in less than two hours at a production rate of 110 t/hr. The average residence time is 30 minutes in the EAF and approximately 15 minutes in each of the three refining vessels and the tundish.

The vessels of the continuous steelmaking process are shown with the placement of slag pots and partly-drawn working platforms in Figure 52. Each of the three slag pots are placed to allow for collection of the slag from one entry launder and from the exit door of the previous vessel in the same slag pot. The working platforms are designed to provide access to all doors and the entry launders so that each vessel can be maintained and operated.

The operation of the EAF requires continuous loading of fluxes and scrap on the conveyor and the continuous injection of carbon and oxygen to maintain a constant foamy slag with deslagging out the door. This procedure is not much different from many modern Consteel furnace operations. However, a major difference in the continuous steelmaking design is continuous tapping of liquid metal into the Oxidizer instead of periodical tapping into ladles. The operation of the Consteel EAF in a continuous mode (tapping while melting and refining) was successfully tested at the Gerdau-Ameristeel plant of Charlotte in North Carolina.

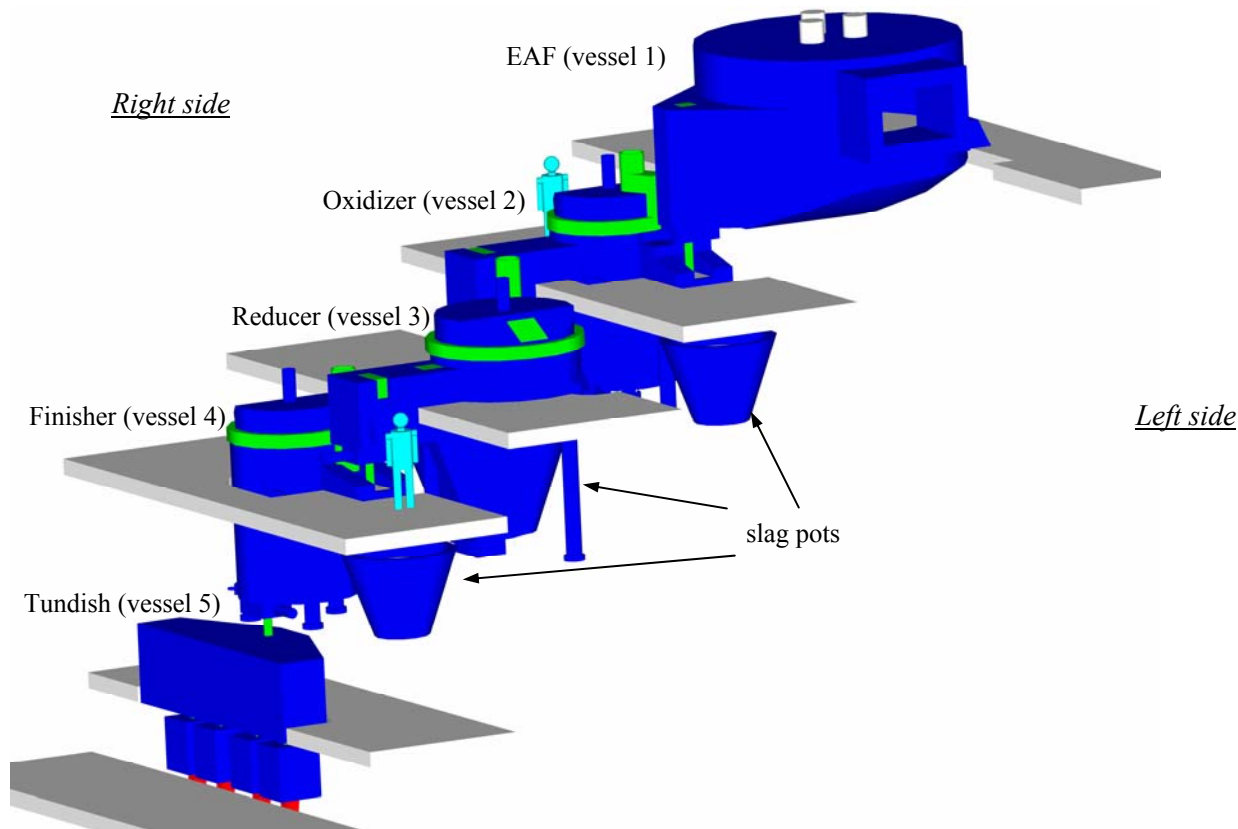


Figure 52: Left-side view of process, showing slag pots and partly-drawn working platforms

Steel leaves the EAF and cascades through the three refining vessels before entering the tundish. The treatment of the steel in each refining vessel will include the periodical addition of fluxes and alloys (every two to three minutes) as well as the continuous removal of the slag through the entry launders into slag pots. The slag pots are designed to hold approximately six tons, requiring replacement every eight hours. The operation of the tundish would be similar to current casting operations except that there would be no ladle changes and therefore no temperature and level fluctuations within the tundish, decreasing turbulence, reoxidation, and improving the cleanliness of the cast steel. Periodic temperature and chemistry measurements will be made to allow sufficient time for corrective action. Continuous temperature and chemistry measurement technologies that are in the process of commercialization would optimize control of the process. In addition, each of the five vessels works as a thermodynamical buffer due to constant near-equilibrium reactions and the series of reactors provides an opportunity to offset variations through differentiated refining and alloying in each vessel.

Procedures for Grade Changes

In preparation for a grade change, alloying will be decreased in the Reducer and increased in the Finisher, diluting the alloy concentration in the Reducer. At the same time the superheat will be increased in the EAF to offset heat losses associated with flow interruptions. After the steel temperature in the EAF and Oxidizer is increased, the flow through these two vessels will be temporarily stopped, providing a break between grades. Since there will be no steel flowing into the Reducer, alloying in the Reducer will be completely discontinued as the bath level drops. Steel will be continued to be alloyed in the Finisher until

the level in the Reducer has dropped to approximately 13 tons. At this point, the Reducer will be closed and the steel in the Finisher represents the end of the old grade and will be drained similar to the last ladle at a grade change in traditional casting operations. As the Finisher drains, flow will be reopened from the first two vessels to the Reducer and a combination of dilution and increased alloying prepares the steel in the Reducer for the new grade. Once the Finisher is drained, the reopening of the Reducer along with alloy and flux additions at the rate required for the new grade will refill the Finisher with the new grade. The Finisher will be reopened after the steel in the tundish is lowered to minimize the amount of intermix material similar to traditional casting operations. Flow will resume at the normal steady-state rate after the Finisher is completely filled. If the steel temperature would decrease below the necessary superheat before steady-state conditions are reestablished, the steel can be heated in vessels 3 through 5 with a non-contact twin plasma torch.

In addition, it is possible to make a gradual change between grades. For many downstream applications, head-to-tail variations in a single slab are an issue, and these variations could be controlled by spreading out the grade change over several slabs, gradually increasing or decreasing the alloy additions. This practice could decrease the yield losses over current practices. Nevertheless, it will remain important to control and schedule grade changes to minimize the amount of downgraded intermix material.

Continuous steelmaking has a distinct advantage for companies that cast a variety of grades. Currently, steelmakers are limited in the product by heat size. For example, a steelmaker producing 175 ton heats is limited to casting in multiples of 175 tons. If a customer would like 100 tons of a special chemistry, the steelmaker would need to produce 175 tons due to the batch limitation. A customer ordering 200 tons would require 350 tons of production. There is no limitation to order size with continuous steelmaking, meaning that 100 tons of steel could be produced for a 100-ton order, resulting in efficiency, flexibility, and cost savings that are currently unrealized by batch limitations.

Procedure for Start up

Prior to start-up, vessels 2 through 5 will be preheated with natural gas burners. To start-up, a bucket of scrap will be charged to supply the EAF with a liquid heel before scrap is transported by conveyor into the EAF. When the steel level in the EAF has reached its nominal height, the scrap supply is temporarily stopped to superheat the steel so that the other vessels can be filled without freezing of the steel.

The EAF slide gate will be opened after the steel is superheated in the EAF, filling the Oxidizer. After the Oxidizer is filled, the steel flow will be stopped until the required steel and slag chemistry is achieved in the Oxidizer. The Reducer will be filled after the Oxidizer is opened and started to operate in a continuous mode. The steel flow will be halted again after the Reducer is filled, repeating the procedure that was practiced during the start-up of the Oxidizer. The same procedure will be applied to the Finisher. After the Finisher is filled, the filling of the tundish will start the fully continuous operation of the whole system. If required, the steel temperature could be adjusted in the tundish, Finisher or Reducer with a non-contact twin plasma torch³ during the start-up procedure.

Procedure for Shut down

The shut down of the process will start with the halting of the scrap conveyor, causing the steel level in the EAF to decrease while the steel continues to flow through the other vessels. After the EAF is completely drained, the steel level in the Oxidizer will decrease until its exit channel is empty. An overhead crane will lift and tilt the Oxidizer to completely drain the steel through its entry launder into the

Reducer. The same procedure will be repeated for the Reducer. The Finisher will be bottom-tapped into the tundish and the tundish into the caster.

Sufficient time to repair most typical furnace delays (conveyor repair, electrode additions, apron cleaning, gunning, etc.) will be available during the operation of the continuous process because the EAF is designed to always operate with a 55-ton liquid heel and because the EAF can be completely drained without tilting the furnace. Therefore steel could still be continuously transferred to the Oxidizer, processed in the refining vessels, and cast without charging any scrap for up to 30 minutes. During the furnace delay, the steel flow in the downstream vessels could be decreased to provide more buffer time (up to one hour) for completing the repair. The allowable variability in the casting speeds depends on the continuous caster. Plugging of strands in a multiple strand continuous caster provides more flexibility on production rates.

If a problem occurs with one of the refining vessels, the flow rate will be decreased in the other vessels and the steel flow in the problem vessel can be stopped for up to 15 minutes while the maintenance is accomplished. For instance, the slag line could be gunned in one of the refining vessels while the steel level is lowered. If a longer delay is encountered, the problem vessel could be exchanged with a preheated spare. Each of the refining vessels 2 through 4 and their slag pots sit on a car that resembles a small ladle car. These units can be moved to the side, making it possible to change each refining vessel on the fly as it is currently practiced during tundish changes. The Oxidizer and the Finisher can be moved to the right side and the Reducer to the left side to be exchanged with their preheated spares. The flow through the upstream vessels would have to be temporarily stopped during the change of the problem vessel. The replacement of refining vessels with their spares can also be used to increase campaign durations by performing maintenance of only one vessel at the time.

Simulation of Steady-state Operation

The simulation results and steady-state operation conditions during fully continuous production of Si-deoxidized steel are summarized in Table XII. The simulations were calculated with the process model program Metsim. The Free Energy Minimizer (FEM) of Metsim was adjusted based on thermodynamical calculations, using FactSage. The process models are currently being verified with industrial data⁷. Additional results, dynamic simulations, and model details will be discussed in subsequent publications. For instance, dynamic simulations will provide predictions about effects of Cu contaminations.

The simulation was based on a 110-t/hr production rate. The steel and slag masses and compositions of each vessel, as listed in Table XII, are the result of reactions of the incoming steel stream with alloys, fluxes, and air. The extent of these reactions and the composition of the steel and the slag depend on the mass transfer and thermodynamic conditions within each vessel. The mass transfer rate constant (k) was calculated by using the specific steel transport rate, which is a function of argon flow rate, vessel geometry, steel temperature, and pressure. The thermodynamic conditions in each vessel support fast reactions and the removal of impurities. For instance, the de-S rate is increased when less iron oxide is supplied to the bath. Iron oxide sources that include oxidized carry-over slags, oxidized skulls in ladles, slag from previous heats, and iron oxides from ladle cleaning would be minimized due to less emptying, cleaning, and refilling of vessels and because no EAF carry-over slag will enter the Reducer.

Table XII: Example of steady-state operation conditions, flux and alloy additions, and steel and slag chemistries for producing 110 t/hr

EAF (vessel 1)			steel	additions lbs / t	slag	liquid	solid
			wt%			wt%	wt%
electricity	320	kWh/t	C	0.08	high Ca lime	74	
oxygen	2000	scfm	Mn	0.20	dolomitic lime	42	CaO 52 1
scrap	120	t / hr	P	0.010	Ca-Aluminate	-	SiO ₂ 20 -
capacity	55	t	S	0.050	bauxite	-	Al ₂ O ₃ 4 -
temperature	2940	°F	Si	0	hematite	-	MgO 5 83
					SiMn	-	MnO 1 3
total slag	200	lbs/t	Al	0	FeSi	-	FeO _x 14 13
solid slag	4	wt%	V	0	FeV	-	other 4 -

Oxidizer (vessel 2)			steel	additions lbs / t	slag	liquid	solid
			wt%			wt%	wt%
capacity	27	t	C	0.04	high Ca lime	3.6	
flow rate	109	t / hr	Mn	0.18	dolomitic lime	1.0	CaO 52 33
temperature	2885	°F	P	0.003	Ca-Aluminate	-	SiO ₂ 11 -
argon	5	scfm	S	0.050	bauxite	3.0	Al ₂ O ₃ 16 -
k	0.15	min ⁻¹	Si	0	hematite	4.0	MgO 6 45
total slag	13.4	lbs/t	Al	0	SiMn	-	MnO 3 1
solid slag	2	wt%	V	0	FeSi	-	FeO _x 8 21
					FeV	-	other 4 -

Reducer (vessel 3)			steel	additions lbs / t	slag	liquid	solid
			wt%			wt%	wt%
capacity	27	t	C	0.06	high Ca lime	6.0	
flow rate	110	t / hr	Mn	0.90	dolomitic lime	2.0	CaO 50 29
temperature	2830	°F	P	0.007	Ca-Aluminate	5.0	SiO ₂ 18 -
argon	5	scfm	S	0.015	bauxite	-	Al ₂ O ₃ 15 -
k	0.25	min ⁻¹	Si	0.26	hematite	-	MgO 7 71
total slag	15.2	lbs/t	Al	0.002	SiMn	20.4	MnO - -
solid slag	2	wt%	V	0	FeSi	3.2	FeO _x - -
					FeV	-	other 10 -

Finisher (vessel 4)			steel	additions lbs / t	slag	liquid	solid
			wt%			wt%	wt%
capacity	23.5	t	C	0.06	high Ca lime	1.4	
flow rate	110	t / hr	Mn	0.90	dolomitic lime	-	CaO 49 12
temperature	2800	°F	P	0.007	Ca-Aluminate	2.4	SiO ₂ 11 -
argon	1	scfm	S	0.009	bauxite	-	Al ₂ O ₃ 24 -
k	0.06	min ⁻¹	Si	0.25	hematite	-	MgO 8 88
total slag	4.0	lbs/t	Al	0.005	SiMn	-	MnO - -
solid slag	2	wt%	V	0.040	FeSi	-	FeO _x - -
					FeV	1.0	other 8 -

The steel temperatures were calculated during the simulation based on the effects of additions, chemical reactions, and heat losses to the environment. The heat losses correlate to a cooling rate of 1.5°F per minute in ladles. This value was based on estimations of survey data from ladle treatment operations in eight meltshops. The data of recent temperature measurements during ladle refining will be evaluated to estimate the energy losses to the environment more accurately. The current simulation results indicate that

the steel only needs to be heated in the EAF during steady-state operations. The steel temperature in the EAF was set to be 2940°F. Steel of this temperature entered the Oxidizer where it cooled to 2885°F before entering the Reducer, where it cooled an additional 55°F. The steel that flowed from the Finisher into the tundish had a temperature of 2800°F. In general, the heating in the EAF is sufficient because of short processing times, efficient use of fluxes and alloys due to near-equilibrium conditions, and elimination of tapping into ladles that are below the steady-state temperatures.

Based on modern Consteel operations¹, it is estimated that the melting and heating of 120 tons of scrap per hour in the EAF requires 320 kWh/t electricity and the injection of oxygen at a rate of 2000 scfm. The steel flow from the EAF into the Oxidizer is estimated to be 109 t/hr, assuming a 91% metallic yield in the EAF. The liquid EAF slag has a FeO concentration of 14% and is in close equilibrium with the carbon content of the steel (0.08%) due to steady-state furnace operations. The carbon concentration of the steel in the EAF can be increased as compared to the current EAF-LMF steelmaking route because additional de-C is possible in the Oxidizer.

The carbon and phosphorus concentrations are decreased in the Oxidizer from 0.08% C to 0.04% C and from 0.010% P to 0.003% P due to the addition of 4 lbs of hematite per ton of steel. The concentrations of both elements are increased in the Reducer to 0.06% C and 0.007% P because the ferroalloys contain carbon and phosphorus. The refining conditions change from oxidizing to reducing when the steel flows from vessel 2 into vessel 3. The stirring of the steel and the addition of alloys and fluxes causes the de-S of the steel from 0.050% S to 0.015% S in the Reducer. Additional de-S from 0.015% S to 0.009% S is achieved in the Finisher. Some aluminum reversion was calculated during the refining in the Reducer and Finisher.

Steady-state Simulations of Upset Conditions

The simulation of continuous steelmaking operations was modified during five additional runs of the Metsim model. The final carbon, phosphorus, and sulfur concentrations after these runs are summarized in Table XIII. The values of simulation 1 in Table XIII represent the results that were discussed in the previous section and they are used as a baseline for the other simulations.

Table XIII: Final carbon, phosphorus, and sulfur concentrations as calculated during six different steady-state simulations

Simulation	1	2	3	4	5	6
Difference to Simulation 1	Baseline	Double production rate	Triple P Double S	Failure of porous plug in the Reducer		
				No actions	de-S in Oxidizer	↑ Ar in Finisher
wt% C	0.06	0.07	0.06	0.06	0.10	0.06
wt% P	0.007	0.014	0.016	0.007	0.019	0.007
wt% S	0.009	0.019	0.018	0.018	0.007	0.011

In simulation 2, the production rate (scrap and alloy addition rate) was changed from 110 t/hr to 220 t/hr without changing the amounts of flux additions or the values of the mass transfer rate constants. The concentrations of carbon, phosphorus, and sulfur increased during simulation 2 as compared to simulation 1; however, they were within common values after ladle refining of Si-deoxidized steel. It is expected that additional simulations will show that a proportional increase of flux additions and the increase of the argon stirring would make it possible to decrease these concentrations to values similar to simulation 1.

The result of simulation 2 indicates that it is possible to continuously vary the production rate during the operation of the continuous steelmaking process.

The effect of an initial impurity concentration increase in the scrap without detection was calculated during simulation 3. The phosphorus and sulfur concentrations of the steel that entered the Oxidizer were increased from 0.010% P to 0.030% P and from 0.050% S to 0.100% S without changing other operational conditions of simulation 1. The final sulfur and phosphorus concentration increased; however, they were again within common values after ladle refining of Si-deoxidized steel. This result indicates that final steel chemistry is still within typical steel specifications after undetected P and S increases in the scrap. Once the impurity increase is detected, corrective actions such as an increase in argon flow rate and flux additions could decrease the final P and S to values similar to simulation 1.

A failure of the porous plug in the Reducer was investigated during simulation 4. It was assumed that the swirl that is created in the vessel due to the off-center inlet stream² would still result in a mass transfer rate constant of 0.05 min^{-1} (down from 0.25 min^{-1} during argon stirring). The simulation was calculated without changing other operational conditions of simulation 1. The final sulfur concentration increased to 0.018%, which is a common value after ladle refining of Si-deoxidized steel. This result indicates that a failure of a porous plug would not necessarily lead to a final steel chemistry that is outside the grade specifications.

Two corrective actions of a porous plug failure in the Reducer were investigated during simulations 5 and 6. In simulation 5, the operation of the Oxidizer was modified by replacing the oxidizing slag with a reducing slag and making SiMn and FeSi alloys additions in the Oxidizer. All other operating conditions were the same as during simulation 4. The final sulfur concentration of simulation 5 was lower than the final sulfur concentration of simulation 1 because some sulfur was removed from the steel in all three refining vessels. The final carbon and phosphorus concentrations increased because these elements were not removed in the Oxidizer. Remarkably, the steel chemistry in the Oxidizer during simulation 5 (0.10% C, 0.019% P, 0.018% S) was similar to the final steel composition after ladle refining of Si-deoxidized steel. This result indicates that the steel treatment in only one of the three refining vessels can achieve similar refining to current ladle treatment.

Simulation 6 was similar to simulation 4 with the exception that the gas flow rate and the flux additions were increased in the Finisher, raising the mass transfer rate constant in this vessel to 0.15 min^{-1} . This change decreased the final sulfur concentration from 0.018% S (simulation 4) to 0.011% S while the final carbon and phosphorus concentrations were as low as after simulation 1. The increase of the argon flow rate in the Finisher has the potential to increase the inclusions in the final product due to increased turbulence and slag entrapment. Other corrective actions would also be possible. For instance, the meltshop crew could have chosen to exchange the Reducer on the fly after the porous plug failed.

Summary of Continuous Steelmaking Process Design and Simulation Results

A novel, scrap-based, fully continuous steelmaking process has the potential of increasing safety, productivity, quality, and capital utilization while lowering the energy consumption and production cost as compared to traditional EAF-LMF-CC steelmaking. The new process requires significant less space, decreasing the size of the meltshop building to approximately one third of a conventional EAF meltshop.

The new process will make it possible to continuously convert scrap to cast product in less than two hours. The vessels are designed for fast, near-equilibrium reactions to ensure a large degree of control,

productivity, flexibility, and to reduce maintenance. The new process has the potential to increase refining and decrease alloy and flux consumptions as compared to current operations and to minimize of variations in fluid flow and composition, ensuring a reliable operation. The production rate can be widely varied (between 70 t/hr and 170 t/hr for this particular design) during continuous operation, giving steelmakers a flexible tool that is able to respond to market demands, maintenance requirements, and unscheduled delays.

Simulations predict that the process can produce quality steel even during unexpected upset conditions in the production. The sudden increase of impurities during melting or a failure of part of the equipment does not necessary lead to a final steel chemistry outside of the grade specifications. The design of the process makes it possible to change grades without increasing the amount of down-graded transition steel when compared to current practices. In addition, continuous steelmaking has the advantage of only producing exactly the order amount of steel, decreasing yield losses associated with current full heat lots.

Accomplishments

The following is a listing of the milestones for the project and the accomplishments. All of the tasks were completed within the timeline for the project. The end result was a new design along with validated simulations of a continuous steelmaking melt shop capable of producing 1,000,000 tons per year at a significantly lower cost and energy consumption than current technology. Energy savings are calculated to be 10% lower than current EAF operations because no electrical power will be required for the LMF (saving 30 kWhr/t) and yield will increase by 4% (saving 10 kWhr/t) in addition to 20 kWhr/t saving in auxiliary energy. The new continuous steelmaking melt shop can be built for an estimated 30% less capital than traditional melt shops and will save 15% in operational costs due to increased yield and lower energy costs. The University of Missouri - Rolla has patented the technology and is presently working on partners to market the new process.

Milestone accomplishments:

ID Number	Task / Milestone Description	Planned Completion	Actual Completion	Comments
1	Process Design			
1.1	Collect necessary operating data from partners and literature			
1.1.1	Collect literature	8/31/03	8/31/03	100% Complete
1.1.2	Visit and survey industrial partners	8/31/03	8/31/03	100% Complete. 10 partner locations visited
1.1.3	Complete literature and industrial partner survey report	12/31/03	3/31/04	100% Complete
1.2	Process simulation			
1.2.1	Thermodynamic model of vessels	12/31/03	6/30/04	100% complete
1.2.2	Coupled model of vessels	6/30/04	9/30/04	100% complete
1.2.3	Fluid flow modeling of process	8/31/04	4/1/06	100% complete
1.2.4	Simulation of refractory performance	8/31/04	9/30/05	100% complete
1.3	Vessel connector design	12/31/04	12/31/04	100% Complete
1.4	Industrial Trials/Laboratory Experiments to Validate Design	3/31/05	5/31/05	100% Complete
1.5	Final Report	4/30/06*		

A total of 13 publications and 13 presentations at International Conferences plus one patent resulted from this research:

1. Webber, D.S., Peaslee, K.D., and Richards, V.L., "Alloy Dissolution in Argon Stirred Steel," *AISTech 2006 Proceedings - Vol. I*, 2006, pp. 741-752. (Presented May 2006, Cleveland, OH)
2. Peter, J., Peaslee, K.D., and Robertson, D.G.C., "Simulations of a New Continuous Steelmaking Process," *AISTech 2006 Proceedings - Vol. II*, 2006, pp. 445-469. (Presented May 2006, Cleveland, OH).
3. Peter, J., Peaslee, K.D., Robertson, D.G.C., Zhang, L., Thomas, B.G. "Introduction of novel, scrap-based, fully continuous steelmaking process," *AISTech 2005 Proceedings-Vol. II*, 2005, pp.623-634. (Presented May 2005, Charlotte, NC).
4. Peter, J., Peaslee, K.D., Robertson, D.G.C., Thomas, B.G. "Experimental Study of Kinetic Processes During the Steel Treatment at two LMF's," *AISTech 2005 Proceedings-Vol. I*, 2005, pp. 959-973. (Presented May 2005, Charlotte, NC).
5. Zhang, L., Aoki, J., Thomas, B.G., Peter, J., Peaslee, K.D. "Design of New Scrap-based Continuous Steelmaking Process using CFD Simulation," *ICS Proceedings - 3rd International Congress on Science and Tech. of Steelmaking*, 2005, pp. 577-590. (Presented May 2005, Charlotte, NC).
6. Webber, D.S., Peaslee, K.D., and Richards, V.L., "Nickel Dissolution in Argon-stirred Steel," *ICS Proceedings - 3rd International Congress on Science and Tech. of Steelmaking*, 2005, pp. 811-819. (Presented May 2005, Charlotte, NC)
7. Aoki, J., Zhang, L, and Thomas, B.G., "Modeling of Inclusion Removal in Ladle Refining," *ICS Proceedings - 3rd International Congress on Science and Tech. of Steelmaking*, 2005, pp. 219-331. (Presented May 2005, Charlotte, NC).
8. Webber, D.S., Richards, V., and Peaslee, K.D., "Foundry Size Ladle Metallurgy Vessel: Ferromanganese Dissolution," *AFS Transactions*, Paper 05-080, 2005. (Presented a Cast Expo, April 2005, St. Louis, MO)
9. Peter, J., Peaslee, K.D. and Robertson, D.G.C., "Review of Progress in Developing Continuous Steelmaking," *Iron & Steel Technology*, Vol. 2, No. 2, February 2005, pp. 53-60.
10. Peter, J., Peaslee, K.D., and Robertson, D.G.C., "Review of Progress in Developing Continuous Steelmaking," *AISTech 2004 Proceedings, Vol. I*, 2004, pp. 869-880 (Presented September 2004, Nashville, TN)
11. Peter, J., Peaslee, K.D., and Robertson, D.G.C., "Study of Current Steelmaking Practices to Evaluate the Viability of Continuous Steelmaking," *AISTech 2004 Proceedings, Vol. I*, 2004, pp. 1071-1084. (Presented Sept 2004, Nashville, TN)

12. Aoki, J., Thomas, B.G., Peter, J., Peaslee, K.D., "Experimental and Theoretical Investigation of Mixing in a Bottom Gas-Stirred Ladle" *AISTech 2004 Proceedings, Vol. I*, 2004, pp. 1045-1056 (Presented September 2004, Nashville, TN)
13. Zhang, L., Aoki, J., and Thomas, B.G., "Inclusion Removal by Bubble Flotation in Continuous Casting Mold," *MS&T 2004 Proceedings*, 2004, pp. 161-177. (Presented September 2004, New Orleans, LA)
14. Provisional patent application filed May 6, 2005, "Process to Continuously Melt, Refine, and Cast High-Quality Steel." Provisional patent number was 60/678,833. The final patent application was filed on May 5, 2006.

In addition, this grant provided funding for the education of several metallurgical engineering students at both UMR and UIUC:

The following students were supported by the project at University of Missouri – Rolla:

Jorg Peter – graduated with Ph.D in Metallurgical Engineering, May 2006 – now at Cascade Steel

Darryl Webber – expected Ph.D in December 2006 – Assistant Professor at Tri-State University

Emily Welch (graduated with BS in May 2005 – now at Nucor Yamato Steel)

Cole Ely (graduated BS in December 2005 – now at Olin Corp.)

Neal Ross (cooped at Nucor-Yamato Steel and now graduate student at UMR)

Ryan Spoering (summer intern at Nucor – expected graduation 2007)

Zane Voss (cooped at Nucor, expected graduation 2007)

The following students were supported by the project at University of Illinois – Champaign-Urbana:

J. Akoi – (MS 2005 – working in steel industry at Nippon Steel)

Conclusions

This research project was successful in that a new process was designed to continuously melt, refine, alloy and cast steel by continuously transporting liquid metal through four vessels. The four vessels are the melter (ConSteel Furnace) which is continuously fed with preheated scrap and continuously tapped into the second vessel. The melting is primarily accomplished through electrical energy but is supplemented with chemical energy which also accomplishes preliminary dephosphorization. The second vessel (oxidizer) continuously decarburizes and dephosphorizes the steel before continuously discharging low carbon and low phosphorus steel to the third vessel. In the third vessel (reducer), steel is continuously deoxidized, desulfurized and bulk alloyed to produce a generic semi-finished high quality liquid steel which continuously flows into the final vessel. In the final vessel (finisher) the final alloying is completed and inclusions are floated resulting in high quality steel continuously being discharged into the tundish of a continuous caster.

A total of 10% energy savings will occur by reducing the energy needed for auxiliary operations, increasing the yield, and reducing the tap temperature. No electrical power will be required for the LMF since it is eliminated (saving 30 kWhr/t) and yield will increase by 4% (saving 10 kWhr/t) in addition to 20 kWhr/t saving in auxiliary energy. The required capital for a new continuous steelmaking is 30% less than a traditional melt shop (\$35 million versus \$50 million for a 1,000,000 tpy facility) and will save 15% in operational costs (\$20 per ton) due to increased yield, 10% lower energy requirements and other associated cost savings.

The process has been patented (patent is pending) by the University of Missouri – Rolla and the first steps of commercialization have started. UMR's Director of Technology Commercialization and Economic Development has been contacting potential licensee's to begin applying the technology to the steel industry. We have also been contacted by companies that are interested in building a plant. Therefore, it is anticipated that commercialization would occur within 5 to 10 years.

References

1. Wathen, S. "Production processes and Organizational Policies" *International Journal of Operational & Production Management*, Vol. 13, No. 1, 1993, pp. 56- 70
2. Goršek, A., Glavič, P. "Design of batch versus continuous processes Part I: Single-Purpose Equipment" *Chemical Engineering Research and Design: Transactions of the Institute of Chemical Engineers*, Vol. 75, part A, No. 7, October 1997, pp. 709 – 717
3. Goršek, A., Glavič, P. "Design of batch versus continuous processes Part II: Multi-Purpose Equipment" *Chemical Engineering Research and Design: Transactions of the Institute of Chemical Engineers*, Vol. 75, part A, No. 7, October 1997, pp. 718 – 723
4. Goršek, A., Glavič, P. "Design of batch versus continuous processes Part III: Extended Analysis of Cost Parameters" *Chemical Engineering Research and Design: Transactions of the Institute of Chemical Engineers*, Vol. 78, part A, No. 2, March 2000, pp. 213 – 244
5. Crookes, William & Röhrig, Ernst "A practical treatise on Metallurgy" Vol. 3, *Steel, Fuel, Supplement*, John Wiley and Son, New York, 1870, pp. 795 – 803
6. Wheeler, F.M. "Gordon, Y.M. "CRISP – The Novel Hatch Compact Reduced Iron Steelmaking Process" *ISSTech 2003 Conference Proceedings*, pp. 1033 – 1041
7. Harbord, F.W., Hall, J.W. "The Metallurgy of Steel" Charles Griffin & Company, Limited, London, 1923, Volume I – Metallurgy, pp. 200 – 203
8. Fritz, E., Auer, W., Berger, H. "Developments in steelmaking" *Berg- und hüttenmännische Montashefte*, July 1996, Vol. 141, No. 7, pp. 288 – 301
9. Thring, M.W., Marsden, C., Jenkins, T.W. "Experiments on continuous steelmaking – A survey of postulated and operational systems" *IRON and STEEL*, May 1966, Vol. 39, No. 5, pp. 166 – 172
10. Royzman, S.E. "Method and plant for fully continuous production of steel strip from ore" *US patent No. 4664701*, 12. May 1987
11. Levenspiel, Octave "Chemical Reaction Engineering" John Wiley & Sons, 1999, Figure 10.2, p. 242
12. Szekely, J. "Problems in continuous steelmaking" *Heat Mass Transfer Process Met., Proc. Symp.*, 1966, pp. 115 – 139
13. United Nations, Economic Commission for Europe "The increasing use of continuous processes in the iron and steel industry and their techno-economic aspects" *United Nations Publication*, 1979, sales No. E.79.II.E.7, Chapter II "Development of continuous steelmaking processes: present situation and prospects" pp. 13 – 72
14. Domröse, W., Koch, K., Steimetz, E. "Metallurgy and process technology of continuous steelmaking" *Stahl und Eisen*, Vol. 96, No. 21, 21. October 1976, pp. 993 – 997
15. Houseman, D.H. "Continuous steelmaking processes" *Steel Times*, May 1978, Vol. 206, No. 5, pp. 457 – 462
16. Abildgaard, O., de Lassat, Y., Malgarini, G., Mirabile, M., Norgianni, C., Poos, A., Vannson, P., Steffen, R., Welbourn, B. "European direct steel feasibility study" 1997, *Office for Official Publications of the European Communities*
17. Fruehan, R.J. "Evaluation of steelmaking processes" *Topical Report for US Department of Energy, Office of Industrial Technology*, 1994
18. Fruehan, R.J., Nassaralla, C.L. "A critical review and evaluation of alternative steelmaking processes" *ISS Transactions, Iron & Steelmaker*, August 1998, pp. 59 – 68
19. Beteiligungs- und Patentverwaltungsgesellschaft m.b.H. "Continuous production of steel from pig iron" *Netherlands, NL patent No. 6604203*, 3. October 1966
20. Bigeev, A.M. "Continuous steelmaking processes" *Magnitogorsk Gornomet Inst*, 1972, No. 115, pp. 3 – 12

21. Kravchenko, V.F., Grigor'ev, V.P., Yavoiskii, V.I., Klyuev, M.P., Pankratov, O.S. "Basic features of continuous melting of steel in a bath-type unit" *MISiS*, 1973, No. 74, pp. 104 – 111
22. Paniotov, Y.S., Lysenko, I.V., Kravchenko, V.A., Dudinskii, B.Y., Sergeev, N.K., Piunovskii, A.M. "Scrap meltings in continuous steelmaking reactors" *Metallurgiya I Koksokhimiya*, 1975, Vo. 47, pp. 36 – 38
23. Kazakov, A.A. "Continuous Steelmaking Processes" *Metallurgiya*, Moscow, USSR, 1977
24. Brooks, G.A., Ross, N.G., Worner, H.K. "Continuous steelmaking: the balance between intensity and refining" *Ironmaking Conference Proceedings*, 1997, Vol. 56, pp. 695 – 701
25. Kai, T., Shibata, T. "Continuous steelmaking furnace" *US patent No. 3287006*, 22. November 1966
26. Alexandrovsky, G.B. "Continuous steelmaking The answer to rapid and economic steelmaking?" *Journal of Metals*, September 1963, Vol. 15, No. 9, pp. 651 – 653
27. Dastur, M.N., Ratnam, T.V.S. "Recent developments in oxygen steelmaking processes" *SEAIISI Quarterly*, January 1976, Vol. 5, No. 1, pp. 44 – 56
28. Ando, R., Kukushima, T. "Continuous process for steel production" *DE patent No. 1923596*, 29 January 1970
29. Klisiewicz, Z. "Development of a continuous steelmaking process" *Pol. Hutnik*, 1969, Vol. 36, No. 7-8, pp. 404 – 410
30. Gorjup, J. "Metallurgical furnace for continuously manufacturing metals, especially steel from pig iron" *DE patent No. 2013960*, 14. October 1971
31. Sibakin, J.G., Roeder, D.A., Hookins, P.H.H. "Preparing steel in a continuously charged electric furnace" *France patent No. 94429*, 14. August 1969
32. Engledow, D. "Method and apparatus for steel manufacture in a electric arc furnace" *German patent No. 22*. December 1977
33. Koenig, H., Rath, G. "Continuous steelmaking in the electric slag resistance furnace (ESW – process) charging sponge iron" *36th Electric Furnace Conference proceedings*, Vol. 36, Toronto Meeting, December 5-8, 1978, pp. 75 – 81
34. Kobe Steel, Ltd. "Continuous steelmaking process" *Japan patent No. 56041311*, 18. April 1981
35. Vallomy, J.A. "Continuous steelmaking via electric furnace: the Consteel process" *Electric Furnace Conference Proceedings*, 1985 (1984), Vol. 42, pp. 93 – 96
36. Harrington, T.H. "Electron-beam continuous hearth refining process and its products" *Canadian Metallurgical Quarterly*, 1971, Vol. 10, No. 2, pp. 137 – 145
37. Nafziger, R.H., Hundley, G.L., Jordan, R.R. "A two-stage electric arc-electroslag process for continuous steelmaking" *CIM bulletin*, Vol. 70, No. 785, September 1977, pp. 155 – 159
38. Radke, D., Wetzel, R.E. "Steel from finely divided iron ore" *DE patent No. 2401909*, 17. July 1975
39. Steinmetz, E., Kuhn, J. "Apparatus and method for continuous steel production" *DE patent No. 2418109*, 24. July 1975
40. Hawkes, D.A., Uemlianin, A., Lubanska, H. "Apparatus and method for manufacturing steel" *British patent No. 848562*, 16. March 1977
41. Rheinlander, P. "Reaction between iron and slag" *German patent No. 222.15*, 1523 November 1973
42. Umezawa, K., Katayama, H. "Control of carbon and phosphorus content in molten steel" *Japan patent No. 50144618*, 20 November 1975
43. Eketorp, S. "A proposal for a future steel plant and research program" *Transactions of the Iron and Steel Institute of Japan*, January 1976, Vol. 16, No. 1, pp. 1 – 10
44. Taguchi, C. "Continuous steel melting under a reduced pressure" *Japan patent No. 54006806*, 19. January 1979
45. McFeaters, L.B., Fruehan, R.J. "Desulfurization of bath smelter metal" *Metallurgical Transactions B*, June 1993, Vol. 24B, pp. 441 – 447

46. Abel, C.A., Fruehan, R.J., Vassilicos, A. "Physical modeling of bottom-blown continuous steelmaking, part I: The decarburization reaction model and water modeling results" *Iron & Steelmaker*, July 1995, Vol. 22, No. 7, pp. 47 – 56
47. Abel, C.A., Fruehan, R.J., Vassilicos, A. "Physical modeling of bottom-blown continuous steelmaking, part II: Development of mass transfer correlations and process feasibility" *Iron & Steelmaker*, August 1995, Vol. 22, No. 8, pp. 49 – 64
48. Kawasaki Steel Corp. "Apparatus for continuous steelmaking and casting" *Japan patent No. 58071323*, 28. April 1983
49. Fink, F. "Apparatus and method for continuous blowing and refining of pig iron to steel" *De patent No. 3615096*, 17 September 1987
50. Moon, I., Song, H.K. "A Development of a Continuous Steelmaking Process" *KAIST R&D Report, N167-2592-1*, Sept 1985
51. Warner, N.A. "Towards coal based continuous steelmaking part 1 – iron ore fines and scrap to low carbon steel via melt circulation" *Ironmaking and Steelmaking*, 2003, Vol. 30, No. 6, pp. 429 – 434
52. Fink, F. "Apparatus and method for continuous blowing and refining of pig iron to steel" *De patent No. 3615096*, 17 September 1987
53. Cignetti, N.P., Mortimer, J. H. "Micromill continuous steelmaking process" *US Patent No. 4836273*, 6. June 1989 (priority application 10. November 1986)
54. Volkov, A.E., Shalimov, A.G., Laktionov, A.V. "A method for continuous electroslag melting of non compact materials" *International Journal of Materials & Product Technology*, 1995, Vol. 10, No. 3-6, pp. 541 – 544
55. Spivey, P.B., Vallomy, J.A. "Operation and experience of the Consteel continuous steelmaking process at Nucor Steel" *Iron and Steelmaker*, 1988, Vol. 15, No. 4, pp. 18 – 22
56. Spada, A.T. "American Cast Iron Pipe Co" *Modern Casting*, August 2002, pp. 20 – 24
57. Yamaguchi, R., Mizukami, H., Maki, T., Ao, N. "Ecoarc technology" *58th Electric Furnace Conference proceedings*, November 2000, pp. 325 – 336
58. Kobeza, I.I., Dytchik, G.E., Loginov, V.I., Grinev, A.F., Grishchenko, S.G., Olearskaya, O.Y. "Development of novel thermal-engineering technique and equipment (BF converter) for direct continuous steelmaking, and for manufacture of a semifinished product" *Metallurgicheskaya I Gornorudnaya Promyshlennost*, 1998, No. 2, pp. 108 – 112
59. Fourie, L.J., Bhandari, M.M. "Contifur – A Continuous Induction Furnace" *AISE Steel Technology*, March 2003, pp. 48 – 52
60. Wallner, F., Fritz, E. "Fifty years of oxygen converter steelmaking" *MPT International*, June 2002, pp. 38 – 43
61. E. T. Turkdogan, "Equilibrium Data on Liquid Steel-Slag Reactions," *Fundamentals of Steelmaking*, The Institute of Materials, London, UK, 1996, pp. 182-183.
62. A. Haider and O. Levenspiel, "Drag Coefficient and Terminal Velocity of Spherical and Nonspherical Particles," *Powder Technology*, Vol. 58, 1989, pp.63-70.
63. S. T. Johansen and F. Boysan, "Fluid Dynamics in Bubble Stirred Ladles: Part II. Mathematical Modeling," *Metallurgical Transactions B*, Vol. 19B, October 1988, pp.755-764.
64. R. M. Wellek, A. K. Agrawal and A. H. P. Skelland, "Shape of Liquid Drops Moving in Liquid Media," *A. I. Ch. E. Journal*, Vol. 12, Issue 5, 1966, pp.854-862.
65. S. A. Morsi and A. J. Alexander, "An Investigation of Particle Trajectories in Two-Phase Flow Systems," *J. Fluid Mech.*, Vol. 55, Issue 2, 1972, pp. 193-208.
66. L. Zhang and F. Oeters, "Mathematical Modeling of Alloy Melting in Steel Melts," *Steel Research*, Vol. 70, Issue 4+5, 1999, pp. 128-134.

67. S. Whitaker, "Forced Convection Heat Transfer Correlations for Flow in Pipes, Past Flat Plates, Single Cylinders, Single Spheres, and for Flow in Packed Beds and Tube Bundles," *A. I. Ch. E. Journal*, Vol. 18, Issue 2, 1972, pp. 361-371.
68. FLUENT inc., Lebanon, NH.
69. Y. Xie and F. Oeters, "Experimental Studies on the Flow Velocity of Molten Metals in a Ladle Model at Centric Gas Blowing," *Steel Research*, Vol. 63, Issue 3, 1992, pp. 93-104.
70. Q. Yuan, B. G. Thomas and S. P. Vanka, "Study of Transient Flow and Particle Transport in Continuous Steel Caster Molds: Part I. Fluid Flow," *Metallurgical and Material Transactions B*, in press.
71. L. Zhang, B.G. Thomas, K. Cai, L. Zhu, J. Cui, "Inclusion Investigation during Clean Steel Production at Baosteel," in *ISSTech2003*, ISS, Warrendale, PA, 2003, 141-156.
72. Lachmund, H., Xie, Y., Buhles, T., Pluschkell, W. "Slag Emulsification during Liquid Steel Desulphurisation by Gas Injection into the Ladle" *steel research*, 2003, Vol. 74, No. 2, pp. 77-85.
73. Grip, C.E., Jonsson, L. "Physical Behavior of slag in a 107-tonne ladle: production scale experiments and theoretical simulation" *Scandinavian Journal of Metallurgy*, 2003, Vol 32, No. 3, pp. 113-122.
74. El-Kaddah, N., Szekely, J. "Mathematical model for desulphurization kinetics in argon-stirred ladles" *Iron and Steelmaking*, 1981, Vol. 8, No. 6, pp. 269 – 278.
75. Ghosh, A. "Secondary Steelmaking Principles and Applications" CRC Press, Boca Raton, London, New York, Washington DC, p. 203.
76. Qu, Y. "Mass transfer coefficients in metallurgical reactors" *Journal of University of Science and Technology Beijing*, April 2003, Vol. 10, No. 2, pp. 1-9.